Compressive Sensing for DoD Sensor Systems

Contact: Daniel McMorrow @ dmcmorrow@mitre.org

November 2012

JSR-12-104

REPORT DOCUMENTATION PAGE

Form Approved
OMB No. 0704-0188

Public reporting burden for this collection of information is estimated to average 1 hour per response, including the time for reviewing instructions, searching existing data sources, gathering and maintaining the data needed, and completing and reviewing this collection of information. Send comments regarding this burden estimate or any other aspect of this collection of information, including suggestions for reducing this burden to Department of Defense, Washington Headquarters Services, Directorate for Information Operations and Reports (0704-0188), 1215 Jefferson Davis Highway, Suite 1204, Arlington, VA 22202-4302. Respondents should be aware that notwithstanding any other provision of law, no person shall be subject to any penalty for failing to comply with a collection of information if it does not display a currently valid OMB control number. **PLEASE DO NOT RETURN YOUR FORM TO THE ABOVE ADDRESS.**

1. REPORT DATE *(DD-MM-YYYY)*	2. REPORT TYPE	3. DATES COVERED *(From - To)*
November 2012	Technical	

4. TITLE AND SUBTITLE

Compressive Sensing for DoD Sensor Systems

5a. CONTRACT NUMBER

5b. GRANT NUMBER

5c. PROGRAM ELEMENT NUMBER

6. AUTHOR(S)

Michael Gregg, et al.

5d. PROJECT NUMBER
13129022

5e. TASK NUMBER
PS

5f. WORK UNIT NUMBER

7. PERFORMING ORGANIZATION NAME(S) AND ADDRESS(ES)

The MITRE Corporation
JASON Program Office
7515 Colshire Drive
McLean, Virginia 22102

8. PERFORMING ORGANIZATION REPORT NUMBER

JSR-12-104

9. SPONSORING / MONITORING AGENCY NAME(S) AND ADDRESS(ES)
OSD
Radar Space Sensors Systems
4800 Mark Center Drive, Suite 17 E08
Alexandria, VA 22350-3600

10. SPONSOR/MONITOR'S ACRONYM(S)

11. SPONSOR/MONITOR'S REPORT NUMBER(S)

12. DISTRIBUTION / AVAILABILITY STATEMENT
Approved for public release

13. SUPPLEMENTARY NOTES

14. ABSTRACT

During its 2012 Summer Study, JASON was asked by ASDR&E (Assistant Secretary of Defense for Research and Engineering) to consider how compressed sensing may be applied to Department of Defense systems, emphasizing radar because installations on small platforms can have duty cycles limited by average transmit power.

15. SUBJECT TERMS

16. SECURITY CLASSIFICATION OF:			17. LIMITATION OF ABSTRACT	18. NUMBER OF PAGES	19a. NAME OF RESPONSIBLE PERSON
a. REPORT	b. ABSTRACT	c. THIS PAGE			Mr. John Novak
Unclassfied	Unclassified	Unclassified	UL		**19b. TELEPHONE NUMBER** *(include area code)* 571-372-6408

Standard Form 298 (Rev. 8-98)
Prescribed by ANSI Std. Z39.18

Contents

1 EXECUTIVE SUMMARY

1.1 Background

Finding efficient ways of dealing with signals having a low density of information is a problem that has been recognized and acted upon for decades, the most familiar example being JPEG (Joint Photographic Experts Group) compression algorithms for photographs, first issued in 1992. Going beyond data compression, Donoho [20] considered whether it is necessary to collect full data sets when only a small part will be retained, coining the term Compressed Sensing (CS) and starting exploration of the tradeoffs involved with sub-Nyquist sampling of compressible or sparse signals. Donoho [19] and Candés *et al.* [15] demonstrated a computationally feasible approach that also gives worst-case bounds for reconstruction errors and how much sampling is needed. This advance triggered thousands of papers designing improved sampling matrices, constructing more efficient reconstruction algorithms, and developing additional performance guarantees for different kinds of data and sensing.

During its 2012 Summer Study, JASON was asked by ASDR&E (Assistant Secretary of Defense for Research and Engineering) to consider how compressed sensing may be applied to Department of Defense systems, emphasizing radar because installations on small platforms can have duty cycles limited by average transmit power.

Assuming that the reader has some knowledge of the basic ideas of compressive sensing, at the level of Candés and Wakin [14], we review a few key definitions needed for the following discussion.

Sparse Signal: a signal of length N that can be exactly represented in a suitable basis or dictionary with at most K non-zero coefficients, where $K \ll N$.

Compressible Signal: a signal that can be represented accurately by its K largest coefficients on a suitable basis or dictionary. Few signals are truly sparse, but many are compressible.

Sparse Recovery (SR): finding the $K \ll N$ coefficients that are consistent with a set of $M < N$ measurements.

Compressive Sensing (CS): taking $M \ll N$ measurements using a scheme that allows sparse recovery. The term is often used loosely to include activities that are inspired by CS or involve only sparse recovery.

Compression Ratio: The ratio of the number of measurements, M to the length of the signal N, i.e. M/N. Some authors, however, define N/M as the compression ratio.

Sparse Illumination: Reduced scene illumination coupled with compressive sensing.

1.2 Principal Findings

1. In general, the sparsity or compressibility of scenes of interest to the DoD is not well studied. The CS literature often deals with idealized situations, e.g., a few bright objects against a dark background. Many scenes, however, have lesser contrasts, and it is not clear what fraction can be treated as sparse versus compressible.

2. The CS literature provides quantitative performance guarantees for a variety of sparse reconstruction techniques, stated in terms of the minimum number of data samples that are needed for successful reconstruction and the magnitude of the reconstruction errors. In addition, there has also been much practical work on the development of faster, more reliable reconstruction algorithms. Both the philosophy and specific algorithms are likely to benefit many DoD

programs, warranting reexamination of older deconvolution approaches as well as incorporation into new projects.

3. Compressive sensing is not a 'free lunch' but always involves a tradeoff; reduced data may save measurement resources, but it also means a lower signal-to-noise ratio (SNR) and possibly other artifacts, such as side lobes or false alarms. Less mature than sparse reconstruction, compressive sensing research is looking for 'sweet spots' where tradeoffs enable measurements that could not be made otherwise.

4. The single-pixel camera (Duarte *et al.*, [21]) trades signal-to-noise ratio (SNR) and sampling speed for cost, using a single, high-quality sensor in lieu of a more expensive focal plane array (FPA). Commercial infrared single-pixel cameras are being developed, but to date there is no independent evaluation to understand the tradeoffs that are being made.

5. Compressed sensing may be an attractive option for small remote systems with limited power and bandwidth, e.g., satellites, drones, and unmanned underwater vehicles (UUVs). Investigation of radar applications is at an early stage, and to date most studies are academic analyses of idealized cases that may not apply to DoD.

6. As an additional tradeoff factor, compressed sensing may increase flexibility in designing and operating radars, but other traditional approaches should also be investigated. In many cases, CS will be most effective as an option rather than a requirement.

7. CS research is fully international and could influence design and operation of systems by potential adversaries.

1.3 Principal Recommendations

1. DoD can and should play a major role in exploring where and how compressed sensing can be applied, particularly to radar and optical systems. These efforts should include applying new sparse reconstruction algorithms to old deconvolution problems as well exploring new systems.

2. To find where and how CS can benefit DoD radar applications, DoD should develop a strongly guided program of 6.1/6.2 research to:

   - Develop a sparsity library for important types of targets

   - Quantify how CS degrades target identification through Receiver Operating Characteristic (ROC) curves

   - Create performance metrics for evaluating reconstructed signals

   - Develop operational experience with CS-radar with test beds on different types of radars

   - Perform regular reviews and provide guidance from people experienced in military radars

3. If attractive CS radar applications are found, they should be developed in conjunction with software-defined, cognitive radars to provide the needed flexibility in choosing when and how sparse illumination is used.

4. Although this is not necessarily an example of compressed sensing, DoD should consider consolidating GMTI (Ground moving target indicator) and SAR (Synthetic aperture radar) functions in a 'Foveal Radar' that subdivides the coherent processing interval to obtain coarse identification of movers and then switches to full SAR for high-resolution images. Pulses are not skipped in this mode; nor is resolution compromised in the final images.

5. The use of compressed sensing for visible or infrared imaging, as in the single-pixel camera, involves tradeoffs between cost, sensitivity, resolution, and speed.

When commercial models of such cameras become available, we recommend than an independent investigator be tasked to evaluate these devices to assess these tradeoffs. In addition to assessing the utility of these devices for DoD, the information will be useful as a case study of pluses and minuses of compressed sensing.

1.4 Study Charge

Compressive or sparse sensing represents a conceptual approach for enhancing the capabilities of DoD sensor systems used for image generation. Many DoD sensor systems support multiple functions (e.g., multi-mode radar performing both surveillance and SAR) which often compete for the sensors resources (e.g., dwell times, beam positions). Other sensors generate huge volumes of data (e.g., airborne/overhead EO/IR) which can overwhelm communications links utilized to send this information to users at other facilities. In other instances, operators may want sensors with large physical apertures to achieve good angular resolution but cannot afford to fully populate the entire array with sensor elements due to cost, power and/or weight considerations. (In other words, compressive sensing can lead to improved array angular resolution performance whereby a larger array with the same number of elements as the original smaller physical aperture array are arranged in a pseudo-random pattern resulting in improved angular resolution with the application of compressed sensing.) All of these situations represent potential candidates for a relatively new technology approach known as compressive sensing. Compressive sensing involves intentionally under-sampling an object or image, typically in a random manner, and then using a companion process known as sparse reconstruction (SR) to recover the complete object or image information as if a fully populated array or fully satisfied Nyquist criteria were employed during the formation of the final end-product. Compressed sensing can conceivably lead to reductions in data link requirements, reductions in radar resources needed for radar image formation (thereby providing the radar

5

more resources for its other functions such as target detection, target tracking, and fire control), increased angular resolution without commensurate increases in array costs, and increased fields of view without degradation in resolution and without commensurate increases in focal plane array sizes. Factors such as the sparsity in the full image, the probability of acceptable image reconstruction, the level of noise in the sensor measurements, the amount of disparity between actual sensor parameter values and those programmed into the reconstruction algorithm utilized, and the stability of the measurement system all must be considered. Once a more complete understanding is obtained of the critical parameters that affect compressed sensing, then criteria can be developed to guide sensor design and operation about when to employ compressed sensing. In other words, what is needed is a more complete and holistic understanding of the critical parameters of CS versus classical approaches, and under what circumstances CS offers an operational or engineering advantage. Using such a criterion the DoD's technology investments could be planned to incorporate this technology into major sensor systems of the future guiding the sensor as to when CS can be advantageously utilized operationally. Critical questions that need to be answered for the development of a compressed sensing application guide (for sensors) include:

A . What is the processing load required to construct records from sparse data?

    1. How do computational requirements and under-sampling patterns vary with image sparsity as functions of various image characteristics and reconstruction options?

    2. What are the computational requirements associated with sparse reconstruction?

B . How much does collecting sparse data limit resolution compared to Nyquist sampling?

    1. What are appropriate design metrics for evaluating CS/SR algorithm per-

formance (e.g., image reconstruction quality, ability to support target recognition systems)?

2. How does the quality of the reconstructed image vary with the inherent sparsity in the image and the sensor sampling schemes?

C . How is data quality affected, including signal-to-noise ratios, and when does it matter?

1. How robust (or fragile) are CS/SR techniques to variations in clutter in the scene, noise levels, and sparsity levels in the actual image?

2. To what extent do variations in sensor performance (e.g., calibration, linearity) from the sensor parameters assumed within the CS/SR algorithms affect image reconstruction?

D . What are the system/operational benefits provided by CS?

1. What characteristics must the sensor possess to successfully implement CS?

2. What are the fundamental tradeoffs between CS and SR?

E . What are the appropriate design criteria for CS and SR?

1. What are the types of sensor functions where CS would prove most beneficial?

2. What are the criteria that indicate that sparse reconstruction techniques can be used successfully and how can these criteria be quantified in terms of sensing and imaging?

3. What are the performance/cost tradeoffs of using compressive techniques where cost accounts for both changes to receiver characteristics and also computational costs? For example, if a receiver requires greater sensitivity to detect a more complex signal than in non-CS application, what will be the increase in hardware costs?

4. What is the required sensitivity of the receivers? If compressive techniques require detection of signals that are more complex than in non-CS application, what dynamic range and sensitivity do the receivers require to detect such signals such that the processing is robust?

1.5 Briefers

Excellent briefings were held in La Jolla, CA on 28 and 29 June 2012, and we are grateful to the briefers for their time and insight.

Mark Davenport (Georgia Tech. Univ.)

Marco Duarte (Univ. Massachusetts, Dartmouth)

Azita Emami (California Institute of Technology)

Emre Ertin[1] (Ohio State Univ.)

Nathan Goodman (Univ. Oklahoma)

Kent Haspert (Institute for Defense Analysis)

Jarvis Haupt (Univ. Minnesota)

Robert Muise (Lockheed-Martin)

Lam Nguyen (Army Research Laboratory)

Lee Potter[1] (Ohio State Univ.)

Raghu Raj (Naval Research Laboratory)

Thomas Strohmer (Univ. California, Davis)

Michael Wakin (Colorado School of Mines)

Rebecca Willett (Duke Univ.)

---

[1]Teleconference

2 OVERVIEW OF SPARSE RECONSTRUCTION AND COMPRESSED SENSING

2.1 The Mathematical Paradigm of CS

One familiar setting for signal processing is compressible images. Recall that images consist of pixels (picture elements), each of which is represented by some number of bits, call it β; for example, $\beta = 1$ for a black-and-white image, and $\beta = 8$ or $\beta = 24$ for an image in "8-bit grayscale" or "24-bit color" respectively. Then an N-pixel image comprises βN bits. But in most images of interest those βN bits are redundant: they can be *compressed* to an encoded format such as JPEG that retains most or all the data ("lossy" or "lossless" compression respectively) but occupies much less than βN bits, and can thus be stored or transmitted much more efficiently. The example in Figure 1 demonstrates that an image containing one-tenth of the full set of coefficients can be indistinguishable from a full image in some representations.
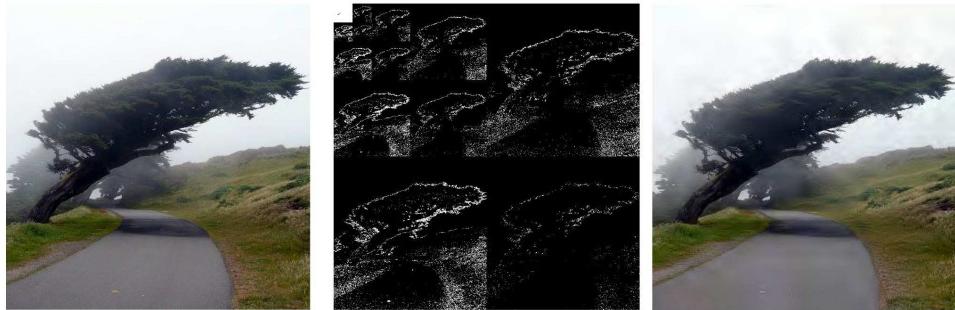
Figure 1: Uncompressed image (left) with some of its wavelet coefficients (center) and a JPEG-2000 version using only 10% of the wavelet coefficients (Davenport *et al.*, 2012). [18] The middle panel is a montage of wavelets computed over different length scales.

A compressed N-pixel image takes up much less space than the βN bits that it would take to write its contents one pixel at a time; but usually it still takes N observations, one per pixel, to *acquire* the image. Compressed sensing (a.k.a. compressive sensing, henceforth abbreviated "CS") is motivated by the following insight:

information theory suggests that if the image is compressible to only βM bits, with $M \ll N$, then it may be possible to acquire these bits in about M observations, thus exploiting the redundancy already in the sensing stage, not just in storing and transmitting the image. CS provides a mathematical model that gives definitions of "compressible image" and "measurement" that are general enough to apply to many real-world settings, and precise enough to allow for theorems and algorithms that realize many of the gains suggested by the information-theoretical motivating insight.

Even when CS is possible it incurs trade-offs: the image takes longer to compute, and is somewhat less accurate, than the image that would result from observing each pixel separately. For example, serious photographers save their images in raw format to provide maximum flexibility in retouching. The loss of information during compression rapidly becomes apparent during editing by comparing histograms of raw and JPEG forms of the same image. In each application these costs must be weighted against the benefits from the reduced number of measurements. The mathematical and algorithmic discipline of CS quantifies the costs in image quality and computing time, up to small factors that remain the topic of ongoing research both theoretical and empirical. Some of these ideas are useful even in contexts where the measurement protocol does not fully follow the CS model, or was already tantamount to CS before the term was introduced.

Radio astronomy and coastal radars provide two examples of sparse sensing and recovery that were developed decades before the formal development of compressed sensing. The overviews below illustrate the inherent attractiveness and the limitations of these techniques.

2.2 Radio Interferometry

The technique of multiple-telescope, aperture synthesis interferometry has been used for high-resolution imaging at radio wavelengths for over five decades, and provides the basis for the largest, most powerful radio astronomical instruments built to date. Interestingly, the basic measurement technique in radio interferometry is a form of compressed sensing. Radio interferometry therefore provides a very useful case study and illuminates the basic ingredients necessary for a highly successful application of the principles of compressive sensing.

Radio astronomy concerns wavelengths $\lambda \sim 1 - 30\,\text{cm}$ that are roughly five orders of magnitude longer than for the visible band. Consequently, the diffraction-limited angular resolution $\delta\theta \sim \lambda/D$ of even the largest individual radio telescopes (Fig. 2) is several orders of magnitude worse than the typical $0.1 - 1\,\text{arcsec}$ resolution achievable at visible wavelengths with ground-based or space telescopes. During the early development of radio astronomy in the 1950s, this angular resolution gap effectively prevented the optical study of compact objects (mostly galaxies) discovered in surveys of the radio sky. It was only through lunar occultations that the radio position of 3C 273, object number 273 in the 1959 Third Cambridge radio sky survey catalog, was determined with sufficient precision to allow its optical identification in 1963 (Hazard *et al.,* 1963) [26]. Measurement of the optical spectrum and determination of the redshift Schmidt (1963) [45] indicated a cosmologically distant, extremely luminous object, the first example of a quasar - an accretion-powered black hole at the center of a galaxy. Clearly, high angular resolution was essential for further progress in radio astronomy. Interferometry, the art of combining signals from widely separated telescopes that has roots in World War II radar (Kellerman and Moran, 2001) [31], would provide the solution.

Figure 2: Photograph of the 100 m Robert C. Byrd Green Bank Telescope (GBT) located at the National Radio Astronomy Observatory (NRAO) site in Green Bank, West Virginia. The GBT is the largest fully-steerable single-dish radio telescope built to date, and has a collecting aperture of $110 \times 100 \, \mathrm{m}$.

2.2.1 Fundamentals of aperture synthesis interferometry

Aperture synthesis interferometry is the technique of using an interferometer with multiple, movable radio telescopes, along with the rotation of the earth, to produce high-fidelity images that are comparable in angular resolution to that of a (hypothetical) single-dish telescope - the synthetic aperture - whose diameter is equal to the maximum antenna separation (baseline) of the interferometer. Interferometry saw rapid development in the 1960s (Kellerman and Moran, 2001) [31], especially at Cambridge University under the leadership of Martin Ryle, ultimately leading to the construction of the large-scale facilities shown in Fig. 3. In a synthesis array, the signal collected by each telescope is amplified, filtered, and sent to a common laboratory via optical fiber, allowing the signal correlations between all pairs of telescopes to be measured and recorded.

Imagine that an aperture synthesis array is being illuminated by a monochro-
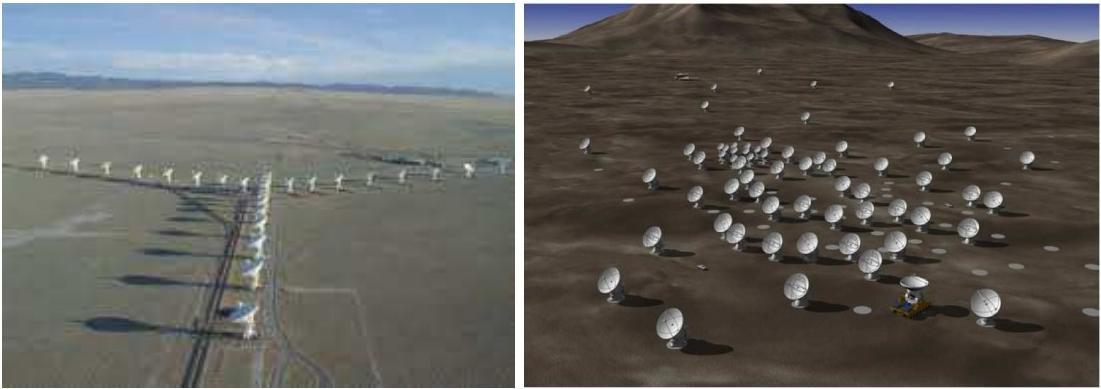
Figure 3: **Left**: The Karl G. Jansky Very Large Array (VLA), located at the NRAO site near Socorro NM, is an aperture synthesis array consisting of 27 radio telescopes, each 25 m diameter. The antennas are located along the arms of a "Y" defined by the rail tracks used to transport the antennas; the separations need not be regular. The maximum baseline is 36 km. The VLA operates over the wavelength range $\lambda = 0.7 - 400$ cm, and was constructed in the mid-1970s at a cost of roughly $\$\,0.5\,$B (2012 dollars). **Right**: The Atacama Large Millimeter/Submillimeter Array (ALMA), is an aperture-synthesis array of 50×12 m telescopes nearing completion on a high plateau in the Chilean Andes. ALMA is an international consortium including the U.S. through NRAO. The construction cost is estimated to be roughly $\$\,1.5\,$B (2012 dollars). The antenna configuration appears less regular than for the VLA; such configurations are feasible because a rubber-tired transporter is used to move the ALMA antennas instead of rails as for the VLA. ALMA will operate at wavelengths as short as $\lambda = 0.3$ mm and will have a maximum baseline of 16 km.

matic plane wave at frequency ω and with wave vector $\vec{k} = -(\omega/c)\hat{k}$, arriving from a direction on the sky indicated by the unit vector $\hat{k}$. The corresponding electric field is $\vec{E}(\vec{r},t) = \text{Re}\left[\vec{E}(\omega,\hat{k})e^{i\omega t}e^{-i\vec{k}\cdot\vec{r}}\right]$. This wave induces a time-harmonic voltage represented by the complex amplitude $V_i(\omega)$ at the output of telescope i in the array that is given by $V_i(\omega) = \vec{G}_i(\omega,\hat{k}) \cdot \vec{E}(\omega,\hat{k})e^{-i\vec{k}\cdot\vec{r}_i}$, where $\vec{G}_i(\omega,\hat{k})$ describes the angular and polarization response of the telescope at frequency ω, and $\vec{r}_i$ is the position of telescope i. By superposition, the response to an arbitrary illumination is given by an integral over the direction of arrival,

$$V_i(\omega) = \int d^2\hat{k}\, G_i(\omega,\hat{k})E(\omega,\hat{k})e^{-i\vec{k}\cdot\vec{r}_i} \ , \tag{2-1}$$

where for simplicity a single polarization is assumed.

An aperture synthesis interferometer operates by multiplying the output voltages of all telescopes in pairs and taking the time average, yielding correlations

$$
\begin{aligned}
C_{ij}(\omega,\omega') &= \left\langle V_i(\omega)V_j^*(\omega')\right\rangle \\
&= \int d^2\hat{k}d^2\hat{k}' G_i(\omega,\hat{k})G_j^*(\omega',\hat{k}')\left\langle E(\omega,\hat{k})E^*(\omega',\hat{k}')\right\rangle e^{i(\vec{k}\cdot\vec{r}_i-\vec{k}'\cdot\vec{r}_j)} \tag{2-2}
\end{aligned}
$$

where $\vec{r}_i$ and $\vec{r}_j$ are baseline vectors describing the separation of the two telescopes. Astronomical sources are spectrally and spatially incoherent, which means that the electric field correlation takes the form

$$\left\langle E(\omega,\hat{k})E^*(\omega',\hat{k}')\right\rangle = I(\omega,\hat{k})\,\delta(\hat{k}-\hat{k}')\delta(\omega-\omega') \ . \tag{2-3}$$

Thus, the measured correlation is given by:

$$C_{ij}(\omega,\omega') = \delta(\omega-\omega')\int d^2\hat{k}G_i(\omega,\hat{k})G_j^*(\omega,\hat{k})I(\omega,\hat{k})e^{-i\vec{k}\cdot\vec{B}_{ij}} \ , \tag{2-4}$$

where $\vec{B}_{ij} = \vec{r}_i - \vec{r}_j$. This is simplfy a component of the Fourier transform of the intensity pattern on the sky at frequency ω, $I(\omega,\hat{k})$, multiplied by the angular response functions or beam patterns of the individual telescopes, G_j and G_j. If the angular size of the astronomical source is small compared to the beam pattern of a

single telescope, the correlation simplifies to

$$C_{ij}(\omega, \omega') = \delta(\omega - \omega') \, G_i G_j^* \int d^2\hat{k} I(\omega, \hat{k}) e^{-i\vec{k}\cdot\vec{B}_{ij}} \ . \qquad (2\text{-}5)$$

Thus, each telescope pair provides one component of the spatial Fourier transform of the sky image $I(\omega, \hat{k})$. In practice, radio interferometers operate with finite spectral resolution $\Delta\omega$, so the actual result of the measurement is given by

$$\bar{C}_{ij} = G_i G_j^* \int d^2\hat{k} \int_{\Delta\omega} d\omega \, I(\omega, \hat{k}) e^{-i\vec{k}\cdot\vec{B}_{ij}} \ . \qquad (2\text{-}6)$$

2.2.2 Image reconstruction

An array of N telescopes has $N(N-1)/2$ distinct pairs, therefore the 27-element VLA can measusure 351 Fourier components of the image simultaneously. However, this is a small number compared to the number of resolution elements in the image, $(B_{\max}/D)^2 \sim 2\times10^3 - 2\times10^6$ depending on the antenna configuration. The antennas are transportable (see Fig. 3), so additional Fourier components may be obtained by using several configurations. The rotation of the earth is also useful in this regard since it causes the baseline vectors $\vec{B}_{ij}$ to rotate relative to the astronomical source. An example of the resulting coverage of the Fourier plane is illustrated in Fig. 4 (left). Note that although the coverage spans a wide range of baselines, the coverage is far from complete, as is visually apparent from the large amount of white space in the image. The incomplete Fourier-plane coverage causes the point-spread function (PSF), or "dirty beam" in radio astronomy parlance, to exhibit high sidelobe levels, as illustrated in Fig. 4 (right). Because $|\vec{k}| = \omega/c$, the phase factor $e^{i\vec{k}\cdot\vec{B}_{ij}}$ varies with frequency, so the fractional bandwidth must generally be restricted to $\delta\omega/\omega < B_{\max}/2\pi\lambda$. Splitting up a wide observing bandwidth into multiple narrow channels obeying this criterion provides additional coverage of the Fourier plane, a technique known as bandwidth synthesis that relies on the assumption that the sky image $I(\omega, \hat{k})$ is relatively constant with frequency.
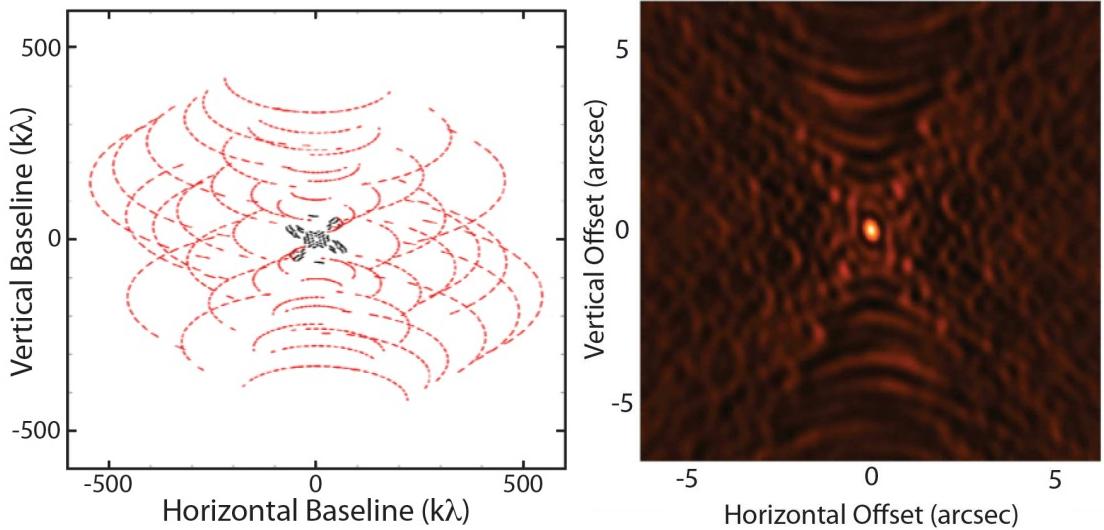
Figure 4: **Left**: The Fourier-plane coverage obtained with earth rotation synthesis with the 8-element Submillimeter Array (SMA) operating at $\lambda = 0.9$ mm. Each track corresponds to pair of telescopes. Two telescope configurations were used: the black points are for a compact configuration, and the red points are for a more extended configuration. **Right**: The Fourier transform of the Fourier-plane coverage gives the point-spread function (PSF) of the measurement, also known in radio astronomy as the "dirty beam". The dirty beam exhibits high-level sidelobes that result from the incomplete coverage of the Fourier plane. Credit: Wilner (2012) [52].

The simplest approach to image reconstruction is to apply a Fourier transform to the measured components, setting the unmeasured Fourier components to zero. As illustrated in Fig. 5, this results in a "dirty image", which is equal to the convolution of the true image with the point-spread function (dirty beam). The large sidelobe response of the dirty beam introduces artifacts in the image and makes it difficult to discern faint features or sources in the presence of brighter sources. These problems may be largely overcome by applying a better image reconstruction algorithm. The first such algorithm (Högbom, 1974) [28], known as CLEAN, was published in 1974 and is still very widely used today. CLEAN proceeds by finding the brightest peak in the dirty image, placing a point source with appropriate intensity at that position into the reconstructed image, subtracting the contribution of that point source (including the sidelobe response) from the dirty image, and repeating this process until a convergence criterion is satisfied. An example of a successful application of CLEAN
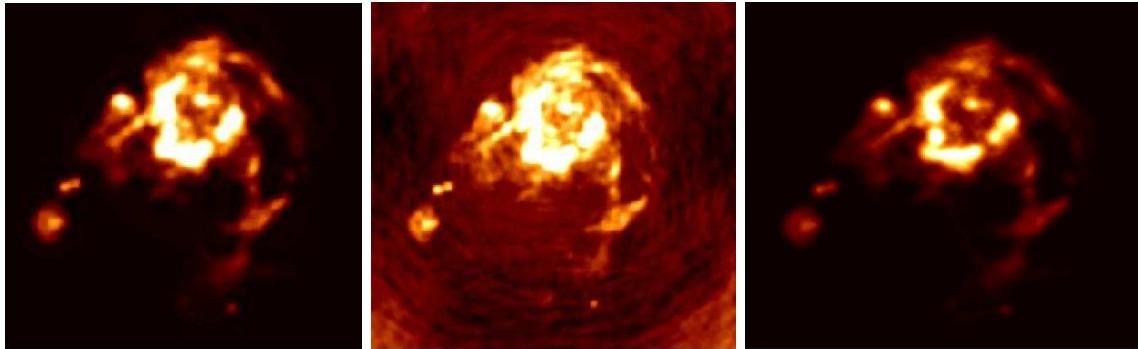
Figure 5: **Left**: Model image. **Center**: Dirty image, which is equal to the model image convolved with the dirty beam. The sidelobe response of the dirty beam reduces the apparent dynamic range of the image and introduces artifacts. **Right**: Deconvolved image, using the CLEAN algorithm. Credit: Bhatnagar (2006) [11].

is shown in Fig. 5. The final image is produced by convolving the set of point sources found by the CLEAN algorithm with a 'restoring' beam, typically a Gaussian free of side lobes and with angular size comparable to the diffraction-limited resolution of the array. In other words, super resolution - beating the standard diffraction limit - is rarely attempted.

2.2.3 Relation to compressed sensing

The paradigm for compressed sensing (Candes and Wakin, 2008) [16] involves several key ingredients:

- The quantity of interest is a signal x of dimension N that is K-sparse in a known basis.

- Information about x is provided by a data vector y which contains $M \sim O(K \log N) << N$ linear measurements of x, according to the measurement equation $y = Ax + n$, where A is the measurement matrix and n is the measurement noise vector.

17

- The rows of the measurement matrix A are incoherent with respect to the sparsifying basis.

- A nonlinear reconstruction technique is used to obtain a sparse solution x to the measurement equation.

Aperture-synthesis interferometry closely follows this paradigm:

- The signal vector x is a discretized or pixellated version of the sky image $I(\omega, \hat{k})$. In the most common case, the sky image is assumed to consist of a small number of point sources. Thus, the signal is taken to be sparse in the image or "pixel" basis.

- The measured correlations $\overline{C_{ij}}$ make up the elements of the data vector y. The rows of the measurement matrix A are the discretized Fourier coefficients $e^{i\vec{k} \cdot \vec{B}_{ij}}$. These quantities are related by the standard measurement equation $y = Ax + n$. Typically, there are far fewer measurements than there are resolution elements in the image, $M = \text{length}(y) << N = \text{length}(x)$, see Fig. 4.

- The Fourier basis used for the measurement is is maximally incoherent with respect to the pixel basis (Candes and Wakin, 2008) [16].

- The CLEAN algorithm contains a nonlinear step in every iteration, i.e. the determination of the peak of the residual dirty image. CLEAN is similar in spirit but predates the matching pursuit algorithms discussed in the compressive sensing literature (Tropp and Wright, 2010) [51].

That radio interferometry is a good example of compressed sensing has not gone unnoticed, and a number of journal papers have been published on this subject. Li *et al.* (2011) [34] give a recent, extensive discussion of this connection,

and demonstrate that a recent compressed-sensing sparse signal reconstruction algorithm, FISTA (Beck and Teboulle, 2009) [10], can be successfully applied to aperture synthesis data and significantly outperforms CLEAN in some cases. As a result, the FISTA reconstruction algorithm is being incorporated into a radio interferometry data analysis package (Li *et al.*, 2011) [34].

2.2.4 Discussion

Radio astronomical interferometry is a clear example of a case where the paradigm of compressed sensing has demonstrated obvious benefits. Billions of dollars have been spent building radio interferometers, and Martin Ryle was awarded the 1974 Nobel prize in physics for his pioneering work on aperture synthesis interferometry. It is therefore of great interest to look at this case closely, to identify the key ingredients that led to this success. Ryle's 1974 Nobel prize lecture contains the essence of the answer:

> "The method of aperture synthesis avoids the severe structural problems of building very large and accurate paraboloids or arrays, and allows both high resolving power and large effective collecting area to be obtained with a minimum of engineering structure and therefore cost."

In other words, practical engineering and financial constraints prevent construction of a filled-aperture instrument, one that would measure all Fourier components simultaneously. Inspection of Fig. 3 gives an immediate visual impression of the incompleteness of the measurement: the telescope array fills only a very small fraction of the land area that it occupies. An array that filled the land area would measure all Fourier components simultaneously, and would also collect much more energy than the sparse array. The filled array would therefore be far more sensitive: this illustrates the signal-to-noise penalty incurred in compressed sensing. However, the filled

array is financially unaffordable, while the sparse array with its compressed sensing paradigm provides the desired tradeoff between sensitivity and cost. This example suggests that compressed sensing should be considered in situations where a resource constraint prevents application of the standard full sampling (Nyquist limited) measurement approach, and a tradeoff between resource usage and signal-to-noise ratio is desired.

2.3 Sparse Installations of Coastal HF Radar and the MUSIC Recovery Algorithm

To illustrate how a compressive sensing (CS) technique can 'find a good home' in a radar application, we consider the coastal HF radars that map surface currents along large portions of the coastal ocean along the US coastline. We use this example to show how a sparse sensing technique works very nicely when the sensing situation is known, stable and sparse. The success of the application shown here has enabled surface current mapping along US coasts with applications in oceanography, coastal engineering, maritime awareness, coastal emergency response and air-sea rescue.

2.3.1 Surface current mapping by coastal HF radar stations

An interesting application of a sparse sensing (CS) technique occurs in the mapping of surface currents in the coastal ocean using HF (3-30 MHz) radar. Using HF radar to sense ocean surface currents began in the 1970s, but it was seriously hampered by a lack of azimuth resolution unless large (L $\sim$ 100 m) linear antenna arrays on the coast were used (Fig. 6, left). At a typical radar frequency of $\sim$ 12 MHz, such long arrays provide angular resolution in azimuth (perpendicular to the radial direction from the radar to the sensed area) of $\delta\theta \approx (\lambda/L) \sim 15^{\circ}$, or a transverse spatial resolution $ds = r\delta\theta > 5$ km for ranges > 20 km. This is satisfactory for mapping

Figure 6: Left: Long ($\approx$ 50 m) 8-element linear receiving array for Multifrequency Coastal Radar (MCR). Right: Compact ($\sim$ 5 m), 3-element, receiving antenna for Codar HF radar. Both antenna systems have mapped surface currents in Monterey Bay, California.

coastal currents but requires a large multi-element antenna array to use conventional beamforming. Siting 100-m-long arrays every $\sim$ 70 km along the shoreline proved to be very difficult. To make a surface current mapping network practical required both reducing the 100 m footprint by using compact 3-element antennas (Fig. 6, right), using an alternative approach to azimuth resolution, and a CS algorithm called MUSIC (Multiple Signal Classification, Schmidt, 1986). In our terminology, MUSIC is a sparse signal recovery algorithm, and Kim *et al.* (2012) [32] connected it to l_1 minimization algorithms in the CS literature.

Along the California coast there are some 42 HF radar stations in the Coastal Ocean Current Monitoring Program (COCMP – www.cocmp.org). These stations produce a comprehensive surface current map every hour, such as shown in Figure 7 below.

Understanding how CS made coastal radar successful can guide other CS radar applications. In this particular case, a small company, Codar Ocean Sensors (www.codar.com), understood the need for a compact HF antenna system and de-
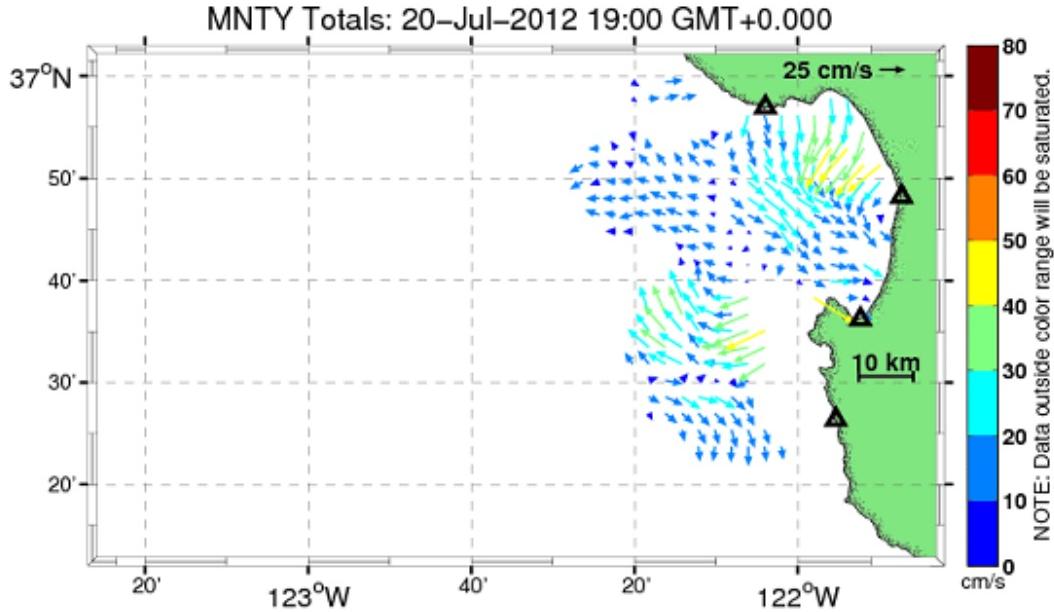
Figure 7: COCMP surface current map from July 20, 2012 for Monterey Bay and surrounding waters produced from radial current measurements at four radar stations as shown by triangles on the coastline. The current vectors are determined by combining the radial speeds from two or more radar sites. (Source www.cocmp.org)

veloped one using CS-type processing – the application of the MUSIC algorithm in the Codar radar systems is patented (US Patent 5,990,834). The success of the Codar HF systems attests to the effectiveness of using a sparse sensing algorithm when the circumstances call for it. A few hundred Codar systems have been deployed, a factor of ∼ ten greater than the nearest linear antenna HF radar system competitor (WERA in Germany).

2.3.2 Application of MUSIC algorithm to a three antenna, compact radar station

The application of MUSIC to compact HF radar stations depends on the existence of a sparse sensing situation. For the surface currents, radar echoes can be segmented into bins such that one expects to find only one or two radar "targets" in a single bin, i.e. a sparse sensing situation. Thus, the signal processing ahead of the CS
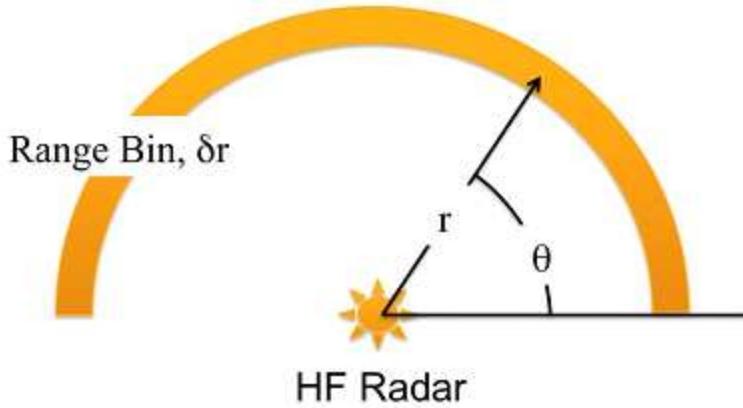
Figure 8: Schematic diagram of HF radar observational geometry. Since these systems are typically on a coast line, only a semicircular field of view is shown.

application (MUSIC) sets up the data in a format where a CS algorithm can be successful. Ocean echoes from HF radar exist in range, Doppler, azimuth space (r, f_d, θ). To segment the (r, f_d, θ) echo we first separate it into range bins according to the time delay of the echo. In this case the range bin is typically 1 to 3 km in depth. Thus, the echoes in a range bin are all from a semicircular annulus, as shown in Figure 8.

To measure surface currents, echoes from a given range bin are analyzed over a coherent integration time, T, to form the Doppler spectrum of the echoes in that range bin. The radial surface currents are estimated from very small (mHz) Doppler shifts in the echoes from the Bragg resonant ocean waves in a particular range bin (for reference see Barrick et al., 1994 or Oceanography, 1997). So now we have segmented the total radar echo into echoes from a given range and given Doppler shift. What is missing is determination of the angle of the patch of ocean from which the echo arises. From the range and Doppler shift we know the magnitude and sign of the radial current and its range and now need to determine θ. In the real ocean it is very unusual for a given range ring to have more than two range-Doppler shift resolution cells with the same radial current. Hence, we know that in the echo data

from a given range ring there will generally be only one or two angular resolution cells with a given radial surface current and its corresponding Doppler shift. We can now use the information from the three radar antennas to estimate the one or two directions with that surface current. Of course, there may be zero locations with a given radial surface current. This situation means that at most only one or two values of the azimuth angle will contain "targets" (patches of ocean with a given radial surface current), i.e. the target space is sparsely populated. This is where the MUSIC algorithm can use the very small amount of signal information gathered from the three antennas to correctly estimate the angular location of particular radial surface current values.

What are the requirements for the application of MUSIC direction finding and how does this radar application fit those requirements? MUSIC can be applied to this problem when:

1. The incoming observed signal can be modeled as a linear sum of sinusoidal signals at the radar frequency arriving from different azimuthal angles θ:

$$\mathbf{X} = \mathbf{AF} + \mathbf{W} \qquad (2\text{-}7)$$

where $\mathbf{X}$ is the vector of observed signals + noise (amplitude and phase at the three antennas), $\mathbf{F}$ is the vector of the incident signals (amplitude and phase) you are trying to find, $\mathbf{A}$ is the propagation matrix that computes (by complex multiplication) the amplitude and phase change of the incident signals after propagation from the source to the receiving antennas, and $\mathbf{W}$ is the noise vector that models the noise that is observed at each receiving antenna.

2. The number M of sensors in $\mathbf{X}$ must be greater than the number D of incident signals in $\mathbf{F}$, i.e. $M \geq D + 1$. Typically $M = 3$ (three antennas) and $D = 1$ (one azimuth resolution cell with a given radial current).

The sensors and emitters can be at arbitrary locations. These locations determine the matrix $\mathbf{A}$ that transforms the emitted signals into the observations $\mathbf{X}$ by knowing the phase and amplitude change that occurs during propagation over the distance from emitter to sensor. Here we focus on the phase change, although the source amplitudes can also be determined if the source loss is included in the propagation matrix A.

Equation (2-7) is the typical linear model that is frequently the basis of compressive sensing methods. The MUSIC algorithm is a type of modal analysis in the same class as least squares, principal components, and Prony's and pencil methods. Sharf (1990) reviews these methods, including MUSIC. MUSIC is a subspace method in which an n-dimensional vector space R^n contains a signal subspace and a noise subspace. Sharf (1990) and Vaseghi (1996) show how by doing an eigen-decomposition of the correlation matrix, R_{xx}, of the noisy signal $\mathbf{X}$, one can partition the noisy signal subspace into two disjoint subspaces, namely a signal subspace containing $\mathbf{F}$ and a noise subspace in which $\mathbf{W}$ resides. The partitioning is done by computing the eigenvalues of R_{xx} and putting them in decreasing order. The largest eigenvalues correspond to eigenvectors that span the signal subspace and the smallest eigenvalues correspond to eigenvectors that span the noise subspace. For the noiseless case the first D eigenvalues span the signal subspace and remaining $(M - D)$ eigenvalues span the noise subspace. When noise is added the partition is somewhat uncertain since each eigenvalue is determined only within an error corresponding to the noise power level. If one knows the number of signals D, then the partition is determined. In reality one typically obtains a maximum for D (sparseness assumption), but not a minimum and whether or not $D = 0$ (no signal present). Typically one sets a threshold for the value of smallest eigenvalue that is allowed to be in the signal subspace.

An important property of the signal and noise subspaces is that the eigenvectors that span the respective subspaces are orthogonal. We can use this orthogonality

condition to find the signal vectors since we know that they are constrained by the propagation based-matrix $\mathbf{A}$ and must be orthogonal to the noise subspace. These conditions lead to a function that has its zeros (or a minimum value if noise is present) at the values of θ that correspond to the directions of arrival of the emitters being sensed—this is what we need to find. Schmidt (1986) [46] visualizes this condition as a Euclidean distance

$$d^2 = a^* \mathbf{E_N} \ \mathbf{E_N}^* a$$

between a given vector and the signal subspace; d^2 can be calculated as the sum over the continuum of $a(\theta)$ components of $\mathbf{A}$, in terms of the eigenvectors of the noise subspace. With noise present, MUSIC makes use of the figure of merit $(1/d^2)$ plotted as a function of θ that will have peaks (rather than poles) when noise arrives from the same directions as the signals. Schmidt (1986) [46] writes this merit (estimator) function $P_{\mathrm{MU}}(\theta)$ as

$$P_{\mathrm{MU}}(\theta) = 1/[a(\theta)\mathbf{E}_N\mathbf{E}_N^*a(\theta)] \tag{2-8}$$

where $\mathbf{E}_N$ is the $M \times N$ matrix whose columns are the N noise eigenvectors from the partition into signal and noise subspaces, discussed above. He does an example case for a three-antenna system with two emitters $(D = 2)$. In addition he investigates the example case using both MUSIC and alternative techniques, namely conventional beamforming, maximum likelihood and maximum entropy.

Figure 9 shows this comparison and illustrates a very important aspect of evaluating the usefulness of a particular compressive sensing algorithm, to wit, comparison of the algorithm of interest with alternative methods applied to the same problem. We also point out the comment by Kay and Demeure (1984) that the sharpness of the peak in the MUSIC estimation function $P_{\mathrm{MU}}(\theta)$ can not be interpreted as an indication of the resolution of the method. Experience with the MUSIC method in the coastal HF radar application indicates that the resolution is of the order of a few degrees in azimuth angle.

26

The steps in the application of MUSIC in this case can be summarized as follows (following Schmidt, 1986):

1. Collect data and form the $M \times M$ cross correlation matrix S of observational data $\mathbf{X}$

2. Calculate the eigenstructure of $\mathbf{S}$ using the metric of the noise correlation matrix $\mathbf{S_o}$

3. Decide the number of signals present, D

4. Evaluate the estimator function $P_{\mathrm{MU}}(\theta)$ in Equation (2-8) vs. the direction of arrival θ signals

5. Pick D peaks of $P_{\mathrm{MU}}(\theta)$ to determine the directions of arrival

6. Calculate other parameters as needed, such as strengths and cross correlations, polarizations of incoming signals and strength of noise and/or interference.

2.3.3 Conclusions from this application regarding compressive sensing

What can we learn from this example about applying and evaluating CS algorithms for use in radar systems? The main points concern the requirements for successful application, evaluating the application, dealing with signals that are challenging or anomalous and lessons for using CS algorithms in radar systems.

The most basic requirements for MUSIC are as follows:

- There exists an autoregressive model for the signals one is seeking, e.g. a sum of sinusoidal signals at a given frequency from different angles of arrival

27
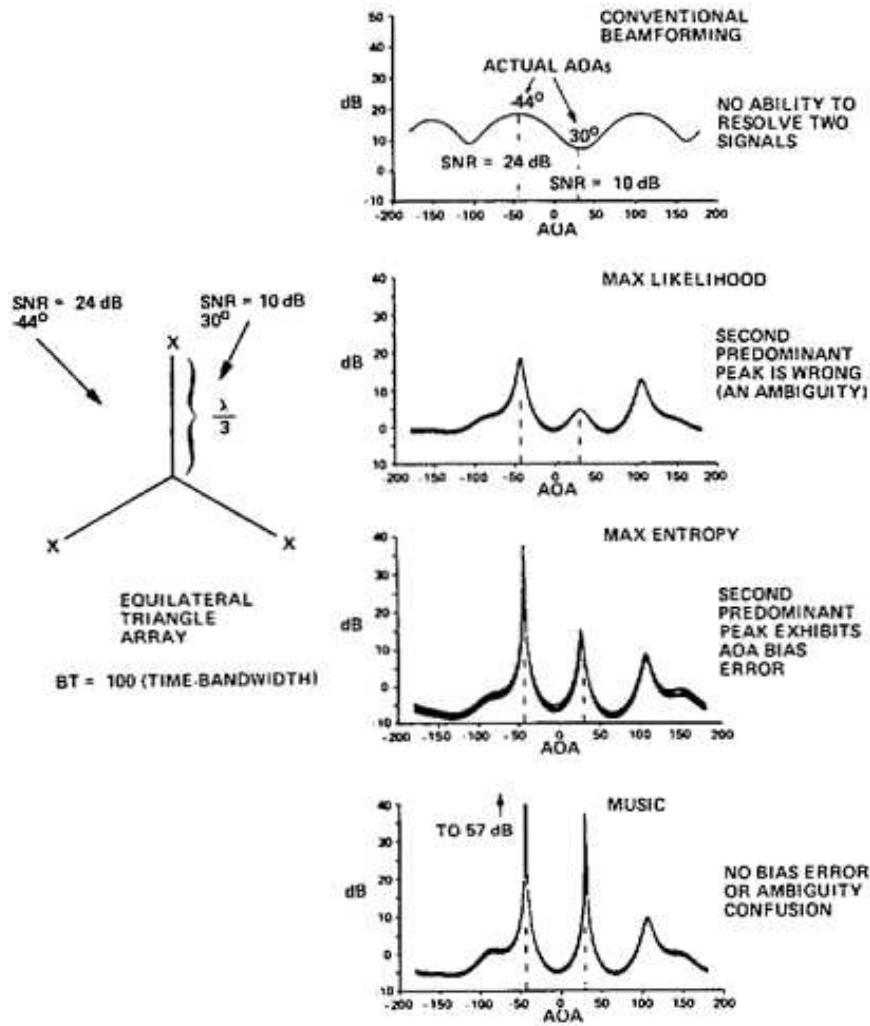
Figure 9: MUSIC estimation of angle of arrival of signals from 2 emitters, observed by 3 antennas arranged in a triangle as shown at left. Note the comments on the figure concerning the attributes of MUSIC and alternative techniques. After Schmidt (1986).

- The observations can be characterized by a linear model, e.g. of the form often used in CS investigations, namely $\mathbf{X} = \mathbf{AF} + \mathbf{W}$, as discussed in connection with Equation (2-7)

- The number of sensors must be larger than the number of signal sources by at least unity.

Further discussion of requirements is given by Schmidt (1986), Sharf (1990) and Vaseghi (1996).

Situations that are challenging for MUSIC include ones where the signal-to-noise ratios (SNR) are not large, there are more sources than allowed (targets are not as sparse as required), or the response to the sources is not strictly linear. Some of these difficulties are occasionally met in coastal HF radar applications. For example, as range is increased the SNR becomes smaller. In the example of Figure 9 the SNRs were 10 and 24 dB and the result was definitive. In cases where the maximum number of emitters may be present, i.e. $D \leq 2$, and the SNR is low, it may be difficult to estimate D since the principal (signal subspace) eigenvalues may not be clearly different from the noise eigenvalues, leading to an error in estimating D (either missing a signal detection or accepting a false alarm as genuine). In coastal HF radar there may be more signals present than $(M - 1)$. This situation can lead to errors by including a signal eigenvector in the noise subspace, making PMU produce erroneous peaks or suppressing valid ones. Non-Gaussian, e.g. impulsive, interference can lead to reduced performance even though the average SNR remains relatively high. Thus, the MUSIC estimate may not be unbiased as with Gaussian noise. Probably the most common problem is errors in the propagation matrix $\mathbf{A}$. This is usually caused by antenna patterns being incorrect due to use of ideal antenna patterns in non-ideal situations or changing circumstances after antenna pattern calibrations.

To correct errors produced by these situations, the approach is to first remove

all know causes of errors or compensate for them. This often determines site selection and careful and frequent antenna calibrations. However, even when best efforts are made there are errors in locating the azimuth direction(s) of particular Doppler shifts and hence an incorrect measurements of the radial currents at particular azimuths. These errors are overcome in several ways. One is to take advantage of averaging. In HF radar one often uses observation times of 4 minutes or less to get estimates that are averaged over an hour and the average result reported with the variance of the estimates in the average indicating the degree of confidence in the hourly estimate. A second error correction method concerns the use of radial current measurements at more than two sites to determine a surface current vector, i.e. further averaging over radar stations. Finally surface current maps, such as that of Figure 7 are subject to physical constraints, in particular the continuity equation for water flow. This means that the divergence of the surface currents over a small region must be zero or downwelling or upwelling currents must be present. There are limits to the size of such vertical currents; hence, surface currents that appear to exceed these limits are viewed with suspicion and omitted in quality checking of data.

In spite of some difficulties with errors in surface current fields obtained by HF radar the surface current results are of significant value in physical oceanography, ocean engineering and maritime situation awareness for spills and sea rescue. The proof of the usefulness of compact antenna systems using MUSIC direction determination is in the successful sales of the radar system using them, namely Codar SeaSonde radars. There are a few hundred Codar units deployed, a great deal more than the nearest competing system, the WERA systems requiring full arrays, such as shown in the left panel of Figure 6. In this case, the advantages of the compact antennas of the Codar systems outweighed the drawbacks of directional errors, discussed above.

2.4 Summary

2.4.1 Findings

1. Many elements of compressed sending have been used for decades, and benefits of using a CS approach in several application areas is clear. In some cases, e.g., JPEG photographic compression, elementary sparse reconstruction was used with simple algorithms, but other fields, such as radio astronomy and coastal radar, also applied sparse sampling and complex algorithms to overcome hardware limitations.

2. Compressed sensing always involves tradeoffs, most often accepting decreased SNR in exchange for maintaining resolution requirements despite limitations on measurement resources, or in exchange for a reduction in data volume.

2.4.2 Recommendations

1. Evaluation of CS algorithms proposed for radar should consider some or all of the following assessment methods suggested by the MUSIC case discussed here:

   (a) A candidate CS algorithm application must be shown to fulfill the basic requirements, such as illustrated above for MUSIC, for a sufficiently large portion of the operation time.

   (b) The CS algorithm must be needed for superior performance (e.g. probability of detection and false alarm rate) or by allowing superior implementation of a sensor concept, such as the MUSIC applications allows the use of compact radar sites.

   (c) The CS application algorithm must be compared comprehensively with alternative techniques, as shown in Figure 9.

(d) A candidate CS algorithm application must demonstrate the ability to cope with difficult and anomalous situations when requirements may not be strictly met.

3 COMPRESSED SENSING TUTORIAL

3.1 Sparse Images.

Various sources of compressibility appear in the literature. Most commonly, and most relevantly for us, an image is compressible because it is nearly sparse. We usually model an N-pixel image as a (column) vector in $\mathbf{R}^N$, with one coordinate per pixel.[1] Such a vector is said to be "sparse" *relative to the natural basis of unit vectors e_i of $\mathbf{R}^N$* if most of its coordinates are zero. Formally, we define the *sparsity* $\|x\|_0$ of a vector

$$x = (x_1, x_2, \ldots, x_N)^\mathsf{T} = x_1 e_1 + x_2 e_2 + \cdots + x_N e_N \tag{3-9}$$

to be the number of non-zero coordinates of x:

$$\|x\|_0 = \#\{i : 1 \le i \le N, x_i \ne 0\}. \tag{3-10}$$

[See below for the significance of the notation $\|\cdot\|_0$ and the properties of this function.] We say x is K-*sparse* if $\|x\|_0 \le K$. A typical example is a night sky with few bright spots against an entirely dark background. If we regard $\mathbf{R}^N$ geometrically as an N-dimensional space then the K-sparse vectors constitute the union of the

$$\binom{N}{K} = \frac{N!}{K!(N-K)!} = \frac{N}{K} \frac{N-1}{K-1} \frac{N-2}{K-2} \cdots \frac{N-K+1}{1} \tag{3-11}$$

coordinate subspaces of dimension K.

To specify a K-sparse image of length N, we must choose one of these subspaces and then a vector in one of them.[2] Given the subspace and β bits per word, it takes

---

[1] For color images each pixel may naturally correspond to more than one coordinate; for example, a 24-bit color pixel consists of three 8-bit picture elements, one for each primary color.

[2] This slightly overcounts the total of K-sparse images because an image of sparsity strictly less than K is counted multiple times. But this has a negligible effect on the final result, as can be seen by using the same technique to count for each $k \le K$ the images of sparsity exactly k, and then summing over k.

βK bits to specify its K pixels. The choice of subspace requires $\log_2 \binom{N}{K}$ bits. Each of the K factors in the formula (3-11) for $\binom{N}{K}$ is between N/K and N; hence

$$K \log_2 \frac{N}{K} \leq \log_2 \binom{N}{K} \leq K \log_2 N. \qquad (3\text{-}12)$$

We deduce that it takes at least

$$\left(\beta + \log_2 \frac{N}{K}\right) K \qquad (3\text{-}13)$$

bits to represent a K-sparse image. We must therefore acquire at least this many bits of information about the image to reconstruct it. CS will let us come within a small factor of this lower bound.

To be sure, very few images of interest are exactly K-sparse with K small enough for CS to exploit. But the linear-algebra framework of CS accommodates generalizations in two directions that together recover the most common and widely studied class of compressible images.

One necessary generalization is from exactly K-sparse to approximately K-sparse images, that is, images of the form $x = \tilde{x} + n$ where $\tilde{x}$ is K-sparse and n is a small "noise" vector. Noise is inescapable in any actual application, not just in the measurement but also in the image itself (even the night-sky background is not perfectly dark). In some applications the noise is modeled as coming from a Gaussian distribution, with small Euclidean (a.k.a. ℓ_2) norm

$$\|n\|_2 = \sqrt{n_1^2 + \cdots + n_N^2}. \qquad (3\text{-}14)$$

Another common model is a *power law*, where there are many point sources but their magnitude decays rapidly enough that the m-th largest coordinate is bounded by some multiple of $m^{-1/r}$ (with constant $r > 0$); then for each $\epsilon > 0$ there are only $O(\epsilon^{-r})$ coordinates satisfying $|x_i| > \epsilon$. If r is small enough, then the K-sparse vector that retains only the top K coordinates of x approximates x to within $O(K^{-\theta})$ for

some $\theta > 0$. For example, if we use the Euclidean norm, and $r < 2$, then the noise magnitude is bounded by a multiple of the convergent sum

$$\sqrt{\sum_{m>K} (m^{-1/r})^2} \sim \left(\int_{m=K}^{\infty} m^{-2/r} \, dm \right)^{1/2} = O(K^{\frac{1}{2}-\frac{1}{r}}), \qquad (3\text{-}15)$$

so $\theta = (1/r) - (1/2)$. Whatever the nature of the noise n, we are usually satisfied with recovering a sparse vector $\tilde{x}$ to within an error comparable with the size of n, and still regard x as compressible (this time with lossy compression).

The second generalization lets us replace the basis vectors $e_1, e_2, \ldots, e_N$ by an arbitrary set of N' typical image elements $v_1, v_2, \ldots, v_{N'}$, of which the image x is a K-sparse *linear* combination:

$$x = c_1 v_1 + c_2 v_2 + \cdots + c_{N'} v_{N'} \quad \text{with} \quad \|c\|_0 \le K. \qquad (3\text{-}16)$$

For example, $\{v_i\}$ might be a wavelet basis for $\mathbf{R}^N$, such as the one used for JPEG-2000. We write the expansion (3-16) in matrix form as

$$x = \Psi c, \qquad (3\text{-}17)$$

where Ψ is the matrix formed from the N' columns v_i, and $c = (c_1, c_2, \ldots, c_{N'})^\mathsf{T}$ is the coefficient vector. The CS framework does not require that the v_i be orthogonal, or even independent: any finite collection ("dictionary") of N' vectors will do. Usually these vectors linearly span $\mathbf{R}^N$, so that $N' \ge N$, but still N' will not exceed N by more than a small factor. For example, the dictionary might consist of both the unit vectors and a wavelet basis, in which case $N' = 2N$ and Ψ is the concatenation of the $N \times N$ identity matrix and the $N \times N$ orthogonal matrix corresponding to the wavelets.

Combining these two generalizations yields $x = \Psi \tilde{c} + n$, where $\tilde{c}$ is sparse, and n is a noise vector as above, possibly modeled by a Gaussian or the tail of a power law, or some combination of the two.

3.2 Linear Measurements

A camera measures each of the N coordinates (or pixels) x_i of an image x separately. CS replaces these N measurements with measurements of M linear combinations $y_j = \sum_{i=1}^{N} a_{i,j} x_i$ $(1 \le j \le M)$; in matrix form,

$$y = (y_1, \dots, y_M)^\mathsf{T} = Ax \tag{3-18}$$

where A is the matrix with M rows of length N, the j-th row consisting of the coefficients $a_{i,j}$ of the j-th measurement. If $M < N$ then we cannot solve the linear system (3-18) for x by inverting A, but this system might still determine x uniquely under the additional condition that x is K-sparse. Indeed this is the case for all K-sparse x precisely when the "spark" of A exceeds $2K$, that is, when any $2K$ columns of A are linearly dependent (Donoho, 2006b; Candé et $al.$, 2006) [20, 15]; equivalently when the kernel (column nullspace) of A contains no $2K$-sparse vectors other than 0.[3] If x is K-sparse with respect to the N' columns of some matrix Ψ, then our equation becomes

$$y = (y_1, \dots, y_M)^\mathsf{T} = A\Psi c, \tag{3-19}$$

to be solved for a K-sparse vector c of length N'; but this is a problem of the same form as (3-18) with (A, x) replaced by $(A\Psi, c)$, so the same analysis applies: the solution, if it exists, is always unique if and only if $A\Psi$ has spark $> 2K$.

---

[3]The reader familiar with the theory of error-correcting codes will recognize this "spark" criterion as the condition that $\ker A$ be a linear code of minimal distance $> 2K$, that is, a K-error-correcting linear code over $\mathbf{R}$. In this context $\|x\|_0$ is the Hamming weight of x. As in the coding-theory setting, the proof uses the fact that the Hamming weight, though not a vector-space norm (because $\|cx\|_0 = \|x\|_0$, for $c \ne 0$, not $|c| \cdot \|x\|_0$), does satisfy the triangle inequality $\|x + x'\|_0 \le \|x\|_0 + \|x'\|_0$, together with the property that every vector of weight $\le 2K$ can be written as the sum of two vectors of weight at most K. (This connection appears in Ackaya and Tarokh (2007) [4]).

3.3 Limitations of the Exact $y = Ax$ Mmodel

As it stands this $y = Ax$ model is not satisfactory for practical use, for several reasons:[4]

i) there is no efficient algorithm known for testing whether the spark of a given matrix (here A or $A\Psi$) exceeds $2K$;

ii) even if a sparse solution of $y = Ax$ is known to exist, there is no efficient algorithm known to find it (for example, it is wildly impractical to try all $\binom{N}{K}$ or $\binom{N'}{K}$ possible coordinate subspaces);

iii) Even if a solution exists it might not be numerically stable: a small change in y might move x to an entirely different subspace.[5] For that matter, the spark condition is itself not numerically stable, because the spark of a matrix A can drop drastically if A is perturbed.

This last difficulty is related with our earlier observation that real images and real-valued measurements are inevitably beset by noise: not only does x differ from a sparse vector $\tilde{x}$ by some noise vector n, but even our observation $A(\tilde{x} + n)$ is not exact, so we observe only a vector

$$y = A(\tilde{x} + n) + \Delta y = A\tilde{x} + A \cdot n + \Delta y, \qquad (3\text{-}20)$$

degraded by some further noise Δy (which may have various possible sources, ranging from thermal noise to inexact calibration to roundoff errors in digitization). Our task, then, is to approximately recover a K-sparse vector $\tilde{x}$ given that (3-20) holds for some

---

[4]When $N' = N$, the first two difficulties can be overcome by choosing A of a special form. For example, for $M > 2K$ one can use a Vandermonde matrix, with $a_{i,j} = \alpha_i^{j-1}$ for some distinct $\alpha_1, \ldots, \alpha_N$; then y_j is the T^{j-1} coefficient of the power series of a rational function $\sum_i x_i/(1 - \alpha_i T)$ of degree at most K, which can be recovered in time polynomial in K, as by the Berlekamp-Massey algorithm. (Again this corresponds to a classical construction in coding theory, here the Reed-Solomon codes.) But this approach is not available when $N' > N$ because each row of A must be in the row span of a given matrix Ψ).

[5]Indeed a generic matrix A satisfies the spark condition provided $M \geq 2K$, but this would contradict our lower bound (3-13) on the number of bits needed to encode a K-sparse vector unless β is large enough to absorb the $\log(N/K)$ penalty; this already suggests that the spark condition is not sufficient to achieve real-world CS.

known A and y (with y of length $M \ll N$) and some upper bounds on the size of the error vectors n and Δy.

In the CS literature, this task is typically performed as follows:

- The spark condition on A is replaced by a stronger condition, called the "restricted isometry property" (RIP), that is numerically stable and gives acceptable bounds on how far any solution of (3-20) can be from the desired $\tilde{x}$ when $\|\tilde{x}\|_0 \le K$.

- An even stronger condition on A (nearly orthogonal columns) is shown to imply RIP, and to hold for randomly chosen A provided that M exceeds a sufficiently large multiple of $K(1 + \log_2(N/K))$; moreover this condition can be tested in polynomial time (MN^2 multiplies, fewer if $A^\mathsf{T}A$ is computed using techniques for matrix multiplication).

- The solution of (3-20) is reduced, to within acceptable error, to optimization problems for which practical algorithms are known.

The vagueness of the phrasings "numerically stable", "acceptable", and "sufficiently large" is intentional. In each case there are proofs of inequalities with constants that at least in principle can be made explicit. *Actual implementation and evaluation of CS often requires more precision in these constants than the literature provides.* There are various sources for this imprecision: theoretical guarantees are by definition worst-case estimates that often understate practical performance; published results may be stated for a wide class of problems, making them weaker than necessary for a given case of interest; and finding the correct worst-case constant may be a difficult mathematical problem that is not yet fully understood. Still, in some cases it can be shown that the known estimates are not too far from the truth; for instance, the guaranteed M might exceed $K + \beta^{-1} \log_2(N/K)$ by a larger factor than necessary, but it can never fall below $K + \beta^{-1} \log_2(N/K)$.

Likewise "practical algorithms" means algorithms that are not much worse than the algorithms used for traditional signal processing, but again "not much worse" is a vague phrase that leaves open the question of just how much more effort CS processing requires. This is still the topic of ongoing research, and may involve tradeoffs against the choice of approximation to the true $\tilde{x}$.

3.4   The Restricted Isometry Property

Recall that a linear map $A : \mathbf{R}^N {\to} \mathbf{R}^N$ is an "isometry" if it preserves Euclidean distances; equivalently, if $\|Ax\|_2 = \|x\|_2$ for every x in $\mathbf{R}^N$. In particular, such a map has zero kernel (that is, $Ax \neq 0$ unless $x = 0$), and Ax cannot be close to Ax' unless x is close to x'. For these properties, it would be enough for A to satisfy

$$(1 - \delta)\|x\|_2 \leq \|Ax\|_2 \leq (1 + \delta)\|x\|_2 \tag{3-21}$$

for some positive $\delta < 1$, as happens for instance when A is a diagonal matrix each of whose diagonal entries is in the interval $[1 - \delta, 1 + \delta]$. We might call such A an "approximate isometry" with parameter δ. If $M < N$ then even approximate isometries from $\mathbf{R}^N$ to $\mathbf{R}^M$ cannot exist, because every linear map $\mathbf{R}^N {\to} \mathbf{R}^M$ has nonzero kernel. However, there *are* linear maps $A : \mathbf{R}^N {\to} \mathbf{R}^M$ that satisfy (3-21) for all *sparse* vectors x.

More precisely, we say A satisfies the *restricted isometry property* (abbreviated RIP) of order k if there exists some $\delta_k < 1$ such that

$$(1 - \delta_k)\|x\|_2^2 \leq \|Ax\|_2^2 \leq (1 + \delta_k)\|x\|_2^2 \tag{3-22}$$

holds for all k-sparse vectors x. In particular, if $x \neq 0$ then $Ax \neq 0$, so this property implies that the spark of A exceeds k. In our setting we take $k = 2K$ and deduce that *if A satisfies the RIP of order $2K$ then $y = Ax$ has at most one K-sparse*

solution x.[6] Moreover, unlike the "spark" approach, the RIP criterion is numerically stable: even if Ax' does not exactly equal Ax we still have

$$\|x - x'\|_2^2 \leq \frac{1}{1 - \delta_{2K}}\|Ax - Ax'\|_2^2. \tag{3-23}$$

Thus, if we observe $y = A\tilde{x} + \Delta y$ with $\|\Delta y\|_2 < \nu$, and find some K-sparse x with $\|y - Ax\|_2 < \nu$, then $\|A(x - \tilde{x})\|_2$ is

$$\|Ax - A\tilde{x}\|_2 = \|(y - A\tilde{x}) - (y - Ax)\|_2 \leq \|y - A\tilde{x}\|_2 + \|y - Ax\|_2 < 2\nu$$

(using the triangle inequality in the penultimate step), so from (3-23) we deduce — provided $\tilde{x}$ is also K-sparse as expected — that

$$\|x - \tilde{x}\| < \frac{2}{(1 - \delta_{2K})^{1/2}}\nu. \tag{3-24}$$

The other side of the inequality in the RIP definition (3-22) then yields

$$\frac{\|x - \tilde{x}\|_2}{\|\tilde{x}\|_2} < \frac{2}{(1 - \delta_{2K})^{1/2}}\frac{\nu}{\|\tilde{x}\|_2} \leq 2\sqrt{\frac{1 + \delta_{2K}}{1 - \delta_{2K}}}\frac{\nu}{\|A\tilde{x}\|_2}, \tag{3-25}$$

which bounds the SNR (signal-to-noise ratio) in the recovered x in terms of the bound $\nu/\|A\tilde{x}\|_2$ on the SNR of the observation.

This leads us to ask:

1. Given N, k, and δ_k, how small can M be for a matrix A that satisfies the RIP of order k?

2. How to construct such A?

3. Given A, how to find a sparse approximate solution of $Ax = y$?

4. How is the accuracy affected by noise in the image, rather than the observation (n rather than Δy in (3-20))?

---

[6]Proof: if x and x' are K-sparse vectors with $Ax = Ax'$ then $A(x - x') = 0$ with $\|x - x'\|_0 \leq 2K$, so $x - x' = 0$ and $x = x'$ as claimed.

The answers are known to within constant factors:

1) Provided $k \leq N/2$, the minimal M is between $ck \log_2(N/k)$ and $Ck \log_2(N/k)$, for some positive constants c, C depending only on δ_k. The expression $k \log_2(N/k)$ arises, as in (3-13), from the number of hyperplanes that must be distinguished. The best values of c, C are not yet known in most cases.

2,3) Explicit constructions are hard but not necessary: provided C is large enough, a *random* matrix will almost certainly satisfy the desired RIP.[7] Assuming this RIP, several practical approximation algorithms are known. Improvements are again a topic of ongoing research. We give further details below.

4) CS is much more sensitive to random (as opposed to sparse) noise in x than in Ax: the RIP bound (3-22) controls the size of $\|Ax\|_2/\|x\|_2$ only for sparse x; if x is allowed to vary randomly over $\mathbf{R}^N$, the ratio is typically of order $\sqrt{N/M}$, so CS incurs a degradation of N/M in the SNR ratio of the image (Arias-Castro and Eldar, 2011) [6].

3.5 Finding RIP Matrices with Small M

Recall that if A satisfies the RIP of order k then $M > ck \log(N/k)$, and we want such matrices with $M < Ck \log(N/k)$. The problem of explicitly constructing such matrices remains unsolved. Fortunately it is not necessary to give a formula for A: we can choose its entries randomly; and indeed this approach is the only known way to attain M as small as some multiple of $\log(N/K)$. The CS literature contains various results along these lines, depending on what probability distribution is used.

---

[7]This is again reminiscent of the theory of error-correcting codes: for some parameter ranges, the best existence result known is the Gilbert-Varshamov (GV) bound, obtained by analyzing the behavior of random codes.

Most easily, each entry can be $+1/\sqrt{M}$ or $-1/\sqrt{M}$ with equal probability. More generally, the columns can be independently chosen from the uniform distribution on the unit sphere;[8] or the rows can be chosen from the uniform distribution on the sphere of radius $\sqrt{N/M}$. More generally yet, the rows or columns can be chosen from any "subgaussian isotropic distribution": a probability distribution on $\mathbf{R}^M$ or $\mathbf{R}^N$ whose coordinates have zero pairwise correlations and for which the probability of a vector of norm $> T$ is smaller than $\frac{1}{2}e^{-BT^2}$ for some $B > 0$ (that is, with tails bounded by some Gaussian distribution). In each case the resulting matrix is known to satisfy the RIP of order k and parameter δ with probability at least

$$1 - 2\exp(-c\delta^2 M) \tag{3-26}$$

provided that

$$M \geq C\delta^{-2}k(1 + \log(N/k)). \tag{3-27}$$

Here c, C are positive constants depending only on B. Thus, once these constants are known it is enough to make M a large enough multiple of $K\log(N/K)$ for the random matrix A to almost certainly satisfy the needed RIP. Again the known proofs provide explicit constants c, C in (3-26,3-27), but the best constants are not known, and might depend on how much is known or assumed about the probability distributions used to generate A.

3.6 Sparse Recovery (SR)

When A satisfies the RIP of order $2K$ with a small enough δ (for example $\delta = 0.3$), it is feasible to recover a K-sparse vector $\tilde{x}$ exactly from an exact measurement $A\tilde{x}$, and approximately from an approximate measurement $A\tilde{x} + \Delta y$. This is done by finding, in the set $\mathcal{B}$ of all x consistent with the measurement, the one that minimizes

---

[8]A standard trick for doing that is to first choose each of M real numbers $a_1, \ldots, a_M$ from the same Gaussian distribution centered at 0, and then divide the resulting vector $(a_1, \ldots, a_M)$ by its ℓ_2 norm.

the ℓ_1 norm[9]

$$\|x\|_1 = \sum_{i=1}^{N} |x_i| = |x_1| + \cdots + |x_N|. \tag{3-28}$$

In the case of an exact measurement, this minimization problem is known as "basis pursuit". The feasible set $\mathcal{B}$ is defined by linear conditions on the variables, and the minimization is equivalent to minimizing $\sum_{i=1}^{n} \xi_i$ where the extra variables ξ_i are constrained by the inequalities $\xi_i \leq x_i$ and $\xi_i \geq -x_i$; thus basis pursuit is a special case of the linear programming (LP) problem, which is known to be solvable in polynomial time (and in this special case alternative algorithms are available that may outperform generic LP solvers). When $\delta_{2K} < \sqrt{2} - 1 \approx 0.414$ it is known that this solution recovers $\tilde{x}$ exactly. If each coordinate y_i of $A\tilde{x}$ is known to within an error of at most ϵ, then the ℓ_1 minimization problem is again an instance of linear programming, this one called the "Dantzig selector". The solution approximates $\tilde{x}$ with an ℓ_2 error bounded by a constant multiple of $\sqrt{k} \cdot \epsilon$, again under the same assumption $\delta_{2K} < \sqrt{2} - 1$. (Note that the ℓ_2 bound on the error is $\sqrt{M} \cdot \epsilon$ which grows somewhat faster than $\sqrt{k} \cdot \epsilon$.) Finally, if we have an ℓ_2 bound on $\Delta y = y - A\tilde{x}$, or seek to minimize some positive linear combination $\|x\|_1 + \lambda \|y - A\tilde{x}\|_2$, then the solution approximates $\tilde{x}$ with an ℓ_2 error bounded by some multiple of $\|y - A\tilde{x}\|_2$. Here this solution can be computed by convex quadratic optimization, or by algorithms designed for this special case ("basis pursuit denoising").

Orthogonal matching pursuit, an alternative approach to recovering sparse signals, is considered by its proponents to be fast and easy to implement (Tropp and Gilbert, 2007a) [49]. The approach is iterative, at each step finding the column of the measurement matrix, A in (3-18), that is most correlated with the remaining part of

---

[9]In general for $p \geq 1$ the "ℓ_p norm" of a vector x is defined by $\|x\|_p = (x_1^p + \cdots + x_N^p)^{1/p}$. For $p = 2$ this recovers the familiar Euclidean norm (3-14); for $p = 1$ it gives the norm (3-28) associated to the "taxicab metric" on $\mathbf{R}^N$. The condition $p \geq 1$ is imposed to ensure the triangle inequality $\|x + x'\| \leq \|x\| + \|x'\|$ for this norm (which for arbitrary $p \geq 1$ is provided by the Minkowski inequality): for $0 < p < 1$ the triangle inequality fails, because the homogeneity property $\|cx\| = |c| \|x\|$ still holds but the unit ball $\{x : \|x\|_p \leq 1\}$ is not convex. As $p \to 0$, this unit ball shrinks to the set of 1-sparse vectors of size at most 1; this suggests the definition of $\|x\|_0$ for arbitrary x, which satisfies the triangle inequality but not the homogeneity required for a norm.
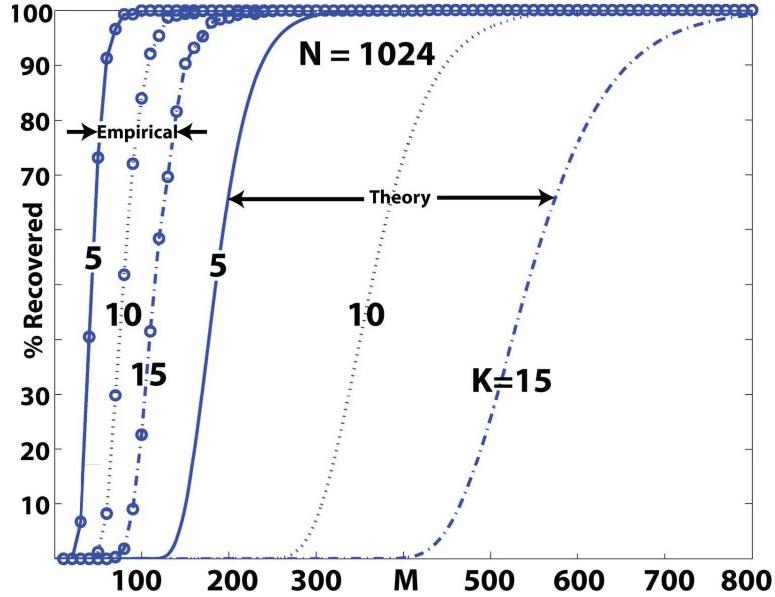
Figure 10: Percent of signals with sparsity K recovered) versus the number of measurements, M, recovered orthogonal matching pursuit (Adapted from Tropp and Gilbert (2007a) [49]). The dimension of the signal space was $N = 1024$. Empirical recoveries are much more efficient than the theoretical guarantee (Tropp and Gilber, 2007b) [50].

the signal, x. The contribution of that column to x is subtracted before proceeding to the next iteration. Numerical simulations to test the recovery guarantee in Tropp and Gilbert (2007b) [50] used normalized, independent Gaussians for columns of A and determined how many measurements, M, were in fact needed to recover arbitrary random signals x of dimension N and sparsity K. As in other sparse recovery cases, many fewer measurements are needed than the worst case guarantee (Fig. 10). For instance, with $K = 5$ about 130 measurements are needed to recover the first signal element and ≈ 280 are needed to get them all, according to the guarantee. In practice, these numbers decrease to $M \approx 10$ and $M \approx 70$. That is, even for this algorithm, full recovery required 15 times more measurements than the sparsity.

3.7 Noisy Images

CS is more sensitive to random noise in the image $\tilde{x}$ than in the measurements that constitute Ax. The phrase "random noise" is intended to exclude the case that $\tilde{x}$ is not sparse but its nonzero coordinates are distributed according to a power law. In the power-law case, $\tilde{x}$ is not K-sparse but is increasingly close to K'-sparse vectors as K' increases. In this case A likely still has RIP of order $2K'$ for K' somewhat greater than K, albeit with worse (i.e. larger) parameters $\delta_{2K'}$; so the SR algorithms can still approximate the K'-sparse approximations to $\tilde{x}$, and thus come reasonably close to $\tilde{x}$ itself.

But when the noise n is not concentrated in K' coordinates but spread evenly throughout the image, the SR techniques cannot adapt as well. Indeed, an RIP matrix A typically takes n to a vector whose ℓ_2 norm $\|A \cdot n\|_2$ exceeds $\|n\|_2$ by a factor of about $\sqrt{N/M}$.[10] If we can tolerate the resulting degradation of the signal-to-noise ratio by a factor of N/M, then we can simply include this $A \cdot n$ term in Δy and recover an approximate $\tilde{x}$ as before. But if the SNR of the image is already too small, then we must scale back the compression ratio of N/M, and with it our ambitions for using CS to reduce the costs of acquiring an N-pixel image.

After noting that most CS literature does not consider noise and those that do assume only measurements noise, Arias-Castro and Eldar (2011) [6] analyze the most realistic situation, sensor, n_s, and measurement, n_m, noise,

$$y = A(x + n_s) + n_m \quad .\tag{3-29}$$

If A is an $M \times N$ matrix, they show that an equivalent statement is

$$\tilde{y} = Bx + n_1 \tag{3-30}$$

---

[10]A typical entry of $A \cdot n$ has contributions of size about $M^{-1/2}\|n\|_2$ from all N coordinates, not just K of them. Since the RIP guarantees that $\|Ax\|_2$ is comparable with $\|x\|_2$ for K-sparse x, this suggests a ratio $\|A \cdot n\|_2/\|n\|_2$ of about N/K, which is roughly consistent with the actual $\sqrt{N/M}$ estimate because M is within logarithmic factors of K.

where the noise variance of n_1 is $\sigma_1^2 = (\sigma_m^2 + (N/M)\sigma_s^2$, where σ_m^2 is the measurement noise variance and σ_s^2 is the sensor noise variance. If σ_s is comparable to σ_m, sensor noise will degrade the signal-to-noise ratio (SNR), severely so, when $M \ll N$. This result illustrates the fundamental tradeoff between measurement effort and SNR inherent in most applications of CS.

3.8 Two Examples of Compressed Sensing

The first example applies CS techniques to identify rare alleles efficiently, and the second uses sparse reconstruction to estimate the cosmic microwave background where it is obscured by our galaxy. The first appears to be on a useful path. Though the second is questionable, the underlying approach should be kept in mind for possible DoD applications.

3.8.1 Identification of rare alleles

Here we outline a simple example of compressed sensing, inspired by the paper "Identification of rare alleles and their carriers using compressed sensing" (Shental *et al.*, 2010) [47]. The authors consider the problem of identifying members of a population who have a rare genetic variant. One method for finding these individuals is to sequence the entire population, and then by brute force identify those with the rare alleles. But this is expensive. It has long been known that if you are instead interested in simply analyzing the frequency of occurrence of the rare allele, this can be done by pooling all of the DNA from the population, and measuring the frequency of the rare allele (See Norton *et al.* (2002) [35]). But with such a measurement, one has no way of figuring out precisely which individuals possess the rare alleles.

To do this, Shental *et al.* (2010) [47] argue that we should proceed as follows. Let us denote the genotypes of the population by $\mathbf{x}$, which is a vector of length N,

where the ith component, x_i, gives the genotype of the population, and N is the size of the population. Denote the common allele by A and the rare allele by B. Each person has either $0, 1$ or 2 copies of the rare allele. Since the allele in question is rare, by construction the vector $\mathbf{x}$ is sparse–only a small fraction of its entries are nonzero. In fact, the more rare the allele, the more sparse the entries will be.

Now, we would like to determine which members of the population have the rare allele; we will do this by breaking the population into pools, and measuring the frequency of the rare allele in each pool. To represent this in mathematical form we construct the sensing matrix M: each entry m_{ij} is equal to one if the jth individual is in the ith pool, and it is zero otherwise. For each pool, we measure the frequency f_i of the rare allele. Thus, we have arrived at the mathematical problem

$$\mathbf{f} = M\mathbf{x}$$

where $\mathbf{f}$ is the vector of frequencies that are measured in the different pools.

The theory of compressed sensing requires that for the solution $\mathbf{x}$ to be unique, the matrix M must be sufficiently sparse and obey the restricted isometry property (RIP). To require this, we demand that M be a Bernoulli matrix, whose entries are either $0, 1$ with probability 0.5. Such a matrix obeys the RIP (Donoho, 2006b) [20]. Other designs of the sensing matrix are possible, which might be more economical[11], but this example demonstrates that the pooling idea is theoretically possible.

The idea of using compressed sensing to find the individuals with rare alleles is a beautiful one, but as always the devil is in the details. To understand whether it can actually work it is necessary to consider the noise in the measurements. There are several different sources of noise that are discussed in the Shental paper that could be significant:

---

[11]For example the Shental paper discusses a matrix with only $O(\sqrt{N})$ nonzero entries per row and argues that this also works.

1. First, when pooling the DNA, it is assumed that an equal amount of DNA is taken from each person. If there were variability in this amount it would significantly contaminate the measurements.

2. Sequencing requires PCR amplification of the different individuals, and it is assumed that PCR affects every individual in the same way. If not, the amplified pools will contain different amounts of the allele in accordance with an individual's amplification propensity, which will contaminate the formalism. It has been previously shown that the number of reads of a given genetic region can depend on factors like the GC content of that region, and can depend on experimental conditions. The distribution of read length has been previously modeled as a Gamma distribution (rightly or wrongly!) (Prabhu and Pe'er, 2009) [40].

3. The frequency of each pool is obtained by computing the ratio of the number of reads of the are allele to the total number of reads in that pool. In reality, if a specific locus contains a small enough number of reads the frequency will itself have an uncertainty associated with it due to sampling noise. Additionally, the sequencer will itself introduce sequencing errors.

The authors deal with these uncertainties by formulating a compressed sensing problem with noise–instead of demanding an exact solution to $\mathbf{f} = M\mathbf{x}$, they require an approximate one where the error is suitably bounded according to the noise levels in question. Under suitable conditions for the size of the different noise factors, they show through simulations that the compressed sensing framework does allow determination of the rare allele individuals. Of course whether or not this works in practice depends on the actual sources of noise in an actual experiment, both the read errors in the sequencer, as well as the sampling errors in extracting DNA from each individual. Additionally, the method using the Bernoulli matrix as the sensing matrix requires that each pool contains of order 1/2 the people in the entire

population. This might be difficult to carry out in practice.

3.8.2   Inpainting the cosmic microwave background

We survey an application of CS/SR-inspired ideas to the Cosmic Microwave Background (CMB) measurement problem which in turn led to yet another series of mathematical results. The application is from Abrial *et al.*(2008) [3] and concerns the Wilkinson Microwave Anisotropy Probe (WMAP) data.

The CMB *inpainting* problem is to render an accurate full-sky temperature anisotropy map, $\Delta T(\phi, \theta)$, of the universe as observed from Earth in all directions where

$$T(\phi, \theta) = T_0 + \Delta T(\phi, \theta).$$

The difficulty is that the measured data incorporates "voids" arising from the interference from "nearby" sources as well as from our own galaxy which effectively prevent direct measurements in a substantial "equatorial" region (Fig. 11). With the new data sets coming in from the Planck Mission, solving the inpainting problem is seen as an important step in determining fundamental constants from the experimental data.

Under the assumption that $\Delta T = \Delta T(\phi, \theta)$ is well approximated by a *sparse* function when expanded relative to the basis of spherical harmonics, CS/SR inspired ideas have been used to fill in the voids. The approach is to view the inpainting problem as an instance of the following abstract problem.

Suppose that $L^2(\nu)$ is the Hilbert space of square-integrable functions (real or complex valued) over a probability measure space (M, ν). Suppose $\langle \phi_i : i \in \mathbb{N} \rangle$ is an orthonormal basis, $N \in \mathbb{N}$ and

$$f : M \to \mathbb{C}$$
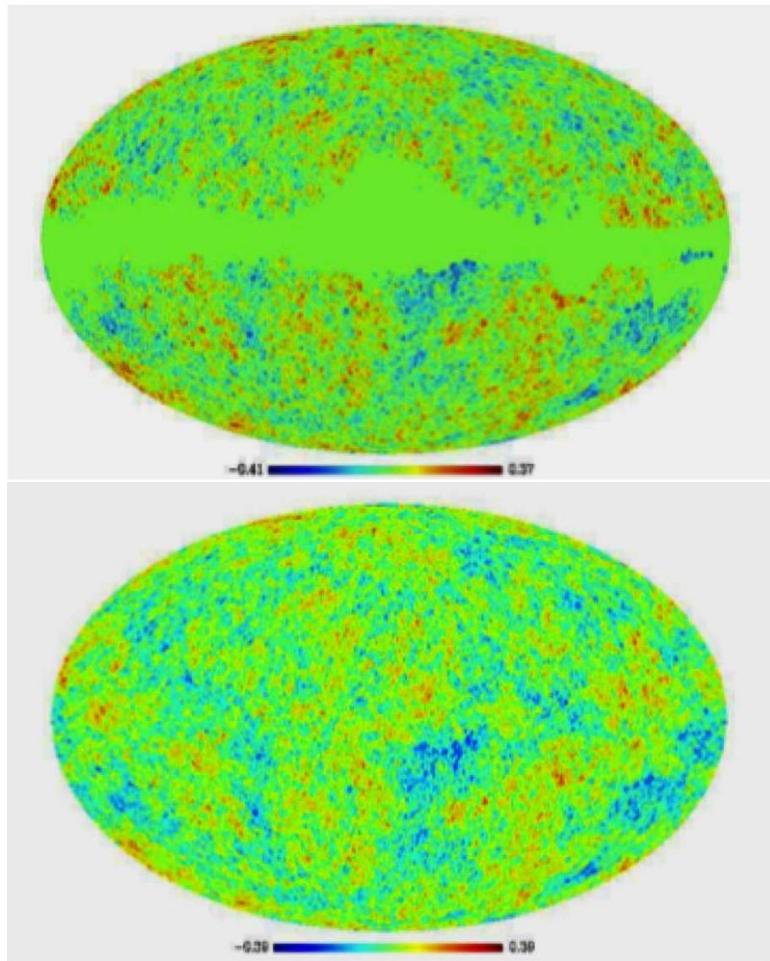
Figure 11: WMAP observations of the CMB (top) showing the broad equatorial zone masked by nearby structure, principally in our galaxy. The effect of inpainting is shown below (Abrial *et al.* 2008) [3]. The color scale shows fluctuations in degrees K about the average background temperature of ≈ 2.7 K.

is function in $L^2(\nu)$. For a given $s < N$, f is s-sparse and N band-limited relative to the given basis if

$$f = \Sigma_{k=1}^{N} c_i \phi_i$$

and the set of c_i such that $c_i \neq 0$ has size at most s. The problem is to recover f by sampling f at points chosen at random. If B bounds the values $|\phi_i(x)|$ for all $x \in M$ and $i \leq N$ (these are the L^∞-norm bounds), then choosing m points at random where

$$m \geq s \cdot B^2 \cdot \log^4 N$$

makes recovery provably possible with high probability. The connection with the conventional CS/SR schemes is that the $m \times N$ matrix $(\phi_j(x_i))$, given by evaluating the j-th basis element at the i-th point, is proved with high probability to have the required instance of the *Restricted Isometry Property* (RIP), [R]. The remarkable fact is that as a consequence of the RIP property, f, is the only s-sparse solution to the under-determined linear system:

$$A \cdot \vec{X} = \vec{y}$$

where A is the $m \times N$-matrix $(\phi_j(x_i))$ and $\vec{y} = (f(x_i))$; moreover it is the unique vector of minimum l_1-norm among all possible solutions (sparse or not) to this equation (Candés *et al.*, 2006) [15]. Thus, the recovery of f is a linear programming problem which can be efficiently solved.

More generally, if g is a function which is well-approximated by an s-sparse, N band-limited, function f, then the same methodology works to recover a good approximation to g.

One can also use a weight, $w(x)$ (with $w(x) \geq 0$ and $\int w(x)d\nu = 1$), provided the induced measure preserves orthogonality of the basis functions. Then the original bound B is replaced by

$$\sup\{|\phi_i(x)/[w(x)]^{1/2}| : i \leq N, x \in M\}.$$

51

In the CMB context, the space of functions is $L^2(\mathbb{S}^2)$ of functions defined on the unit sphere in 3-dimensions with the uniform measure, and the basis is that given by the (normalized) spherical harmonic functions, Y_l^m where m and l are integers with $l \geq 1$ and $|m| \leq l$. Thus

$$\Delta T(\phi, \theta) = \Sigma_{l=0}^{\infty} \Sigma_{m=-l}^{l} a_{l,m} Y_l^m(\phi, \theta)$$

The function ΔT has an associated power spectrum

$$S_{\Delta T}(l) = \Sigma_{m=-l}^{l} |a_{l,m}|^2$$

which is important in evaluating cosmological models and for determining key cosmological parameters.

Sparsity up to the m-degeneracy is independent of the choice of polar axis (choice of "north"). Even assuming the predicted "approximate l-sparsity" is such that the function ΔT is in theory well approximated by sparse functions relative to any choice of the axis for θ, the requisite bound B is useless. However one can replace the uniform measure by a weighted measure (preserving the orthogonality of the basis functions).

In angular coordinates the uniform measure is $(1/4\pi) \sin \theta d\theta d\phi$, where θ, is the polar angle. The uniform measure in the angular coordinates, $(1/2\pi^2)d\theta d\phi$, is still an orthogonalization measure for the original basis, and, further, the (non-trivial) estimate

$$(\sin \theta)^{1/2} |Y_l^m(\phi, \theta)| \leq l^{1/4}$$

gives (by the methodology described above) a sampling requirement,

$$m \geq s N^{1/4} \log^4 N \quad ,$$

for exact recovery (with high probability) for an s-sparse function f (Rauhut and Ward, 2011) [42].

By a fortunate coincidence randomly choosing points relative to this measure concentrates points at the poles and *away* from the equator, matching the general character of the data sets (so here one is specifying "north" so that the Milky Way occupies the equatorial field of view).

In Burq *et al.*(2011) [13] a substantial additional improvement is obtained by changing the weighted orthogonalization measure to $[\tan\theta]^{1/3}d\theta d\phi$ and proving the requisite bound which now converts to the sampling requirement of

$$m \geq sN^{1/6}\log^4 N$$

for exact recovery (with high probability) for an s-sparse function f.

Choosing points with this measure concentrates points at the poles and the equator , apparently not very useful for the inpainting problem. But, the rather sophisticated techniques used to establish bounds yielding improvement, specifically in proving the kinds of sufficient L^∞-norm estimates as indicated above, generalize to the much more abstract setting given by functions defined on surface of a convex solid of revolution (Burq *et al.*, 2011) [13].

But is this really an instance of CS/SR? If one looks at the actual numbers, the pixel resolution of the WMAP data ranges from about .3 to .5 degrees depending on the measured frequency. This gives a maximum pixel count of around $5 \cdot 10^5$. Viewing the pixels as corresponding to the sampling points in the above schemes then

$$5 \cdot 10^5 \geq s \cdot N^{1/6}\log^4 N$$

using the most optimistic estimate from Burq *et al.* (2011) [13] and ignoring that the corresponding sampling measure in this case concentrates the points at the poles and equatorial region (the equatorial region is where the data are masked by noise). The recovered multipole spectrum has nontrivial support uniformly in the interval ranging from $l = 100$ to $l = 1000$ and so $N \geq 10^6$ (and the CS/SR idealization would

require that $N > m$ where m is the number of sampling points anyway). Thus

$$5 \cdot 10^5 \geq s \cdot (10^6)^{1/6} \log^4(10^6) \geq s \cdot 15 \cdot 10^5$$

which is impossible since $s \geq 1$. Further, a sparsity of $s \leq 100$ is completely inconsistent with the recovered multipole spectrum even assuming the expansion in spherical harmonics is such that only one basis basis function for each l-value is used (so that sparsity in l corresponds to actual sparsity). Given the physical symmeties of the problem there should be no preferred orientation and so the amplification of the sparsity parameter given by the m-degeneracy very likely makes the situation much worse.

In summary, the CS/SR idealization of the inpainting problem for the CMB data from the WMAP mission seems very possibly to be so idealized as to be totally irrelevant. This, however, does not mean that inpainting may not have use for some DoD applications.

4 THE SINGLE-PIXEL CAMERA

One prominent application of CS is the single-pixel camera developed by Kelly and Baraniuk of Rice University. Duarte *et al.* (2008) [21] describe the prototype, and a startup company, InView, is marketing several versions of single-pixel infrared cameras (http://www. inviewcorp.com). To avoid using expensive focal plane arrays, each pixel of which must detect infrared light, these devices use pseudo-random selections of micro mirrors to reflect light from an imaging system onto a single detector that is cheaper and of higher performance than the focal plane arrays. Figure 12 shows the concept schematically. InView is marketing their first models at prices 3 to 10 times less than those of comparable 'market leaders,' which sell for \$40,000 to \$50,000. We also were told that Lockheed Corp. is optimistic that it can develop an infrared camera that will increase capability and decrease costs for DoD.

Duarte *et al.* (2008) [21] discuss theoretical tradeoffs, comparing the CS single-pixel approach with a conventional multi-pixel array and a raster scan. Typically, a CS image is formed by taking $M = \mathcal{O}(KP\log_2(\mathrm{N/K}))$ measurements, where K is the image sparsity, and $N \gg M$ is the number of elements in the equivalent multi-pixel array and raster scan. If 0 to D is the dynamic range of a pixel in a focal plane array, Duarte *et al.* give $ND/2$ as the required dynamic range of the single-pixel camera, assuming that the weakest signal occurs when only one of the $N/2$ mirrors directed at the detector is illuminated and the strongest signal results from all $N/2$ mirrors being illuminated. For $N = 1 \times 10^6$, or more, this is a very stiff requirement, i.e. that the single detector have a dynamic range 5×10^5 times that of a single pixel in a mega-pixel focal plane array. On the other hand, if the light intensety is relatively uniform across the image, they dynamic range required is around $D\sqrt{N}$, or $\sim 10^3$, higher than for the FPA. For a sample duration of T seconds, the mean square counting error for the array is P/T, where P is the number of photons per
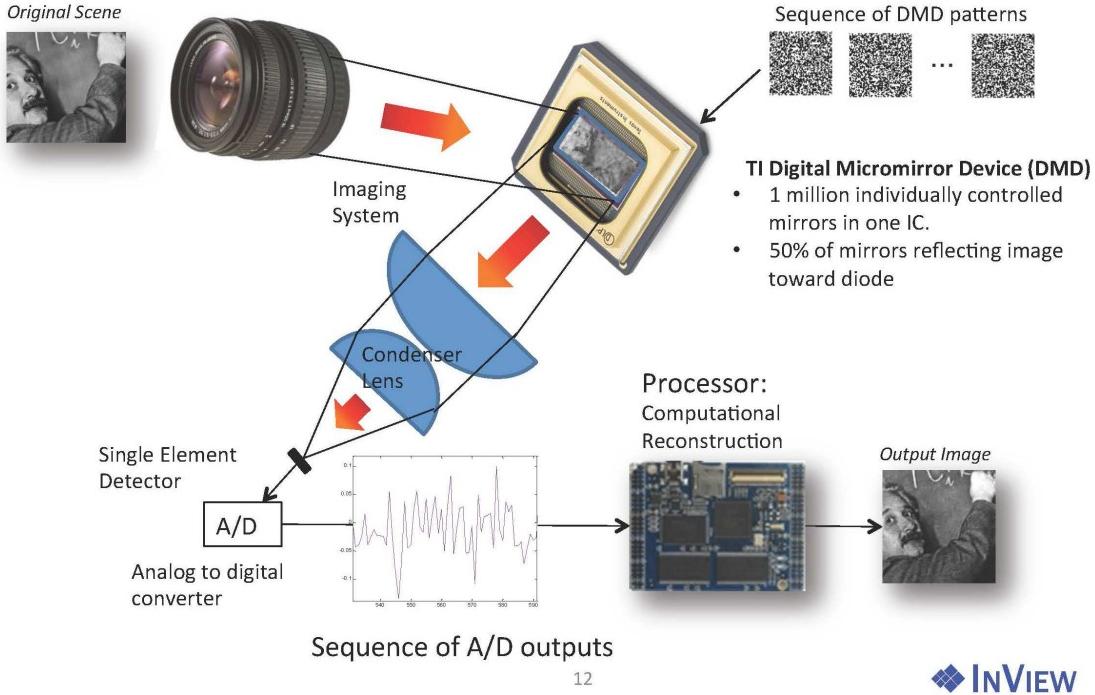
Figure 12: Schematic of single-pixel cameras developed by InView. The imaging system focuses on a digital micromirror device (DMD) consisting of a million micron-sized mirrors that are randomly selected so half reflect photons onto a single-element infrared detector, the output of which is sampled by an analog-to-digital (A/D) converter. Successive frames are formed different combinations of mirrors.

second on a pixel. This rises to NP/T for the raster scan and $(3N-2)P/T$ for a basis scan. For CS, Duarte et al. obtain $3C_N^2 MP/T$, where C_N is the noise amplification factor after reconstruction, implying that the CS measurement scheme would have lower noise than the simple raster scale if $M < N/3C_N^2$.

Because these estimates are central to understanding the benefits and liabilities of the single-pixel approach, below we present an alternate analysis that assumes the scene of interest is relatively uniformly illuminated, as was also assumed by Duarte et al. (2008) [21].

4.1 Focal-plane Array

Suppose the image consists of a set of N pixels with mean intensity (photons per second) μ_i, where $i = 1, ..., N$ indexes the pixels. Let y_i represent the actual number of photons collected by a pixel in a focal-plane over a measurement time T, and let $\delta y_i = y_i - \langle y_i \rangle$ represent the fluctuation of y_i. This is a Poisson random variable satisfying

$$\langle y_i \rangle = \langle \delta y_i^2 \rangle = \mu_i T \ . \tag{4-31}$$

Using δy and μ to denote the associated column vectors, we may write the covariance matrix as

$$C_y = \langle \delta y \, \delta y^T \rangle = \mathrm{diag}(\mu) \, T \ . \tag{4-32}$$

This equation expresses the fact that the photon counts are uncorrelated. We may estimate the image in the obvious way,

$$\hat{\mu} = \frac{y}{T} \tag{4-33}$$

and this estimator has a covariance

$$\langle \delta \hat{\mu} \, \delta \hat{\mu}^T \rangle = \frac{1}{T} \mathrm{diag}(\mu) \ , \tag{4-34}$$

indicating that our measurement uncertainty improves as the square-root of the measurement time. This result agrees with Duarte *et al.*, with the identification of the quantity $P = \mu$.

4.2 Raster Scan

Now suppose that a single detector is used to form an image by sequentially scanning through the N pixels in raster fashion. The measurements y_i obtained in this way have mean and variance

$$\langle y_i \rangle = \langle \delta y_i^2 \rangle = \mu_i \frac{T}{N} \tag{4-35}$$

because the total measurement time T is subdivided into N measurement periods. We now estimate the image using

$$\hat{\mu} = \frac{N}{T} y \qquad (4\text{-}36)$$

and the estimated image has covariance

$$\left\langle \delta\hat{\mu}\, \delta\hat{\mu}^T \right\rangle = \frac{N^2}{T^2} \left\langle \delta y\, \delta y^T \right\rangle = \frac{N}{T}\text{diag}(\mu) \;, \qquad (4\text{-}37)$$

Thus, compared to the N-pixel focal plane array, the measurement sensitivity has degraded by $\sqrt{N}$. This is obvious, because we are collecting photons at an average rate which is N times lower. This result also agrees with Duarte *et al.* (2008).

4.3   Basis Scan

In this case, the image is passed through a programmable mask (e.g., a DMD) which may either pass or block the light for a particular pixel, before sending all of the transmitted light to a single detector. A sequence of N masks is used to allow image reconstruction without making any assumptions regarding sparsity. The measurements are described by N independent Poisson random variables y_i arranged into a column vector y,

$$y = \frac{T}{N}\Phi\mu + \delta y \qquad (4\text{-}38)$$

where the fluctuation vector $\delta y = y - \langle y \rangle$ has a covariance of

$$\left\langle \delta y\, \delta y^T \right\rangle = \frac{T}{N}\, \text{diag}(\Phi\mu) \;. \qquad (4\text{-}39)$$

Here, the elements of the measurement matrix $\Phi_{ij} = 0$ or 1 represent the mask value for pixel j during measurement i. Again, the N in the denominator arises from subdividing the measurement time N ways. Duarte *et al.* take Φ to be

$$\Phi_{ij} = \frac{1}{2}(W_{ij} + 1) \qquad (4\text{-}40)$$

or

$$\Phi = \frac{1}{2}(W + O) \tag{4-41}$$

where O is a matrix filled with ones and $W_{ij} = \pm 1$ is the orthogonal Walsh or Hadamard matrix, satisfying

$$W^T W = NI \tag{4-42}$$

where I is the identity matrix. For example, the Walsh matrix for $N = 4$ is

$$W = W^T = \begin{bmatrix} 1 & 1 & 1 & 1 \\ 1 & -1 & 1 & -1 \\ 1 & 1 & -1 & -1 \\ 1 & -1 & -1 & 1 \end{bmatrix} \tag{4-43}$$

and the measurement matrix is

$$\Phi = \Phi^T = \begin{bmatrix} 1 & 1 & 1 & 1 \\ 1 & 0 & 1 & 0 \\ 1 & 1 & 0 & 0 \\ 1 & 0 & 0 & 1 \end{bmatrix} . \tag{4-44}$$

Note that there is a small peculiarity in that pixel 1 is singled out for special treatment in this scheme, since its light is always allowed to fall on the detector.

For this case of N measurements and N unknowns, the measurement equation is invertible, so we estimate the image using the unbiased linear estimator

$$\hat{\mu} = \frac{N}{T}\Phi^{-1}y \tag{4-45}$$

which has a covariance of

$$\begin{aligned} \langle \delta\hat{\mu}\,\delta\hat{\mu}^T \rangle &= \frac{N^2}{T^2}\Phi^{-1}\langle \delta y\,\delta y^T \rangle (\Phi^{-1})^T \\ &= \frac{N}{T}\Phi^{-1}\mathrm{diag}(\Phi\mu)\Phi^{-1}. \end{aligned} \tag{4-46}$$

Note that if we set $\Phi = I$, which is equivalent to a raster scan, we reproduce eqn. 4-37.

The inverse of the Walsh-derived measurement matrix may be shown to be

$$(\Phi^{-1})_{ij} = \frac{2}{N}W_{ij} - \delta_{i1}\delta_{1j} . \tag{4-47}$$

For a quick estimate of the covariance matrix, we assume the image is uniform enough so that

$$\sum_j \Phi_{ij} \mu_j \approx \frac{N}{2} \bar{\mu}(1 + \delta_{i1}) \ . \tag{4-48}$$

This is exactly correct if the image is perfectly uniform, $\mu_i = \bar{\mu}$ for all i. However our assumption is not particularly restrictive since each mask collects light from half of the pixels, and the brightness variations across the image will tend to average out. This gives

$$
\begin{aligned}
\left\langle \delta\hat{\mu}\,\delta\hat{\mu}^T \right\rangle_{ij} &= \frac{N}{T} \sum_{k=1}^{N} \left(\frac{2}{N} W_{ik} - \delta_{i1}\delta_{1k} \right) \frac{N}{2}\bar{\mu}(1 + \delta_{k1}) \left(\frac{2}{N} W_{kj} - \delta_{k1}\delta_{1j} \right) \\
&= \frac{2N}{T}\bar{\mu}\delta_{ij} - \frac{N}{T}\bar{\mu}\delta_{1j} + \frac{2}{T}\bar{\mu} - \frac{N}{T}\bar{\mu}\delta_{1j} \\
&\quad - \frac{N}{T}\bar{\mu}\delta_{i1} + \frac{N^2}{2T}\bar{\mu}\delta_{i1}\delta_{1j} - \frac{N}{T}\bar{\mu}\delta_{i1} + \frac{N^2}{2T}\bar{\mu}\delta_{i1}\delta_{1j} \\
&= \frac{2N}{T}\bar{\mu} \left[\delta_{ij} + \frac{1}{N} - \delta_{i1} - \delta_{1j} + \frac{N}{2}\delta_{i1}\delta_{1j} \right] \ . \tag{4-49}
\end{aligned}
$$

Thus, apart from the expected peculiar behavior of pixel 1 (it is never turned off in this measurement scheme, which makes it more difficult to determine its intensity), we see that the sensitivity relative to a focal plane array has been degraded by the factor $\sqrt{2N+2}$, or approximately $\sqrt{2N}$ for large N. Note that this result is also worse than that for a raster scan with a single pixel, by the factor of $\sqrt{2}$. This loss presumably results from the DMD throwing half the photons away. Note also that in the case of the raster scan, the noise of pixel i depends on the intensity of only that pixel, rather than the average intensity in the image. In other words, the variance for the raster scan is $N\mu_i/T$, rather than $2N\bar{\mu}/T$ for the basis scan. This detail is significant in the case that the image has a large contrast: the noise of the raster-scan image will be lower in the dark regions, exactly where you would like to have lower noise.

This result of $2N\bar{\mu}/T$ disagrees with that stated by Duarte *et al.*, who give a variance of $(3N - 2)\bar{\mu}/T$.

4.4 Compressive Sampling

We now examine the case in which we pick $M << N$ rows of the Walsh-Hadamard measurement matrix Φ at random, and spend an equal time T/M performing measurements for each of these rows. Thus we have

$$y = \frac{T}{M}\Phi\mu + \delta y \qquad (4\text{-}50)$$

except that Φ is now an $M \times N$ matrix and y is the measurement vector of length M. We make the assumption that the signal is K-sparse in the pixel basis, although any other basis that is also incoherent with respect to the measurement basis could be used equally well. To be more precise, we assume that the image is perfectly uniform with the exception of K pixels, whose intensities are only slightly different than the rest. If the k-th such pixel, located at position $p(k)$, has an intensity of x_k, we may write

$$\mu_i = \bar{\mu}\left[1 - \sum_{k=1}^{K}\delta_{i,p(k)}\right] + \sum_{k=1}^{K}x_k\delta_{i,p(k)}. \qquad (4\text{-}51)$$

In this form, the signal vector μ is the sum of a set of $K+1$ orthogonal basis vectors which are incoherent with respect to the measurement basis; this is the standard setup for CS. For simplicity, we will assume that $x_k - \bar{\mu}$ is small. This is essentially the case analyzed by Duarte *et al.* (2008).

4.4.1 Cramér-Rao bound

The average photon count for each measurement is given by

$$\lambda_m \equiv \langle y_m \rangle = \frac{T}{M}\sum_{i=1}^{N}\Phi_{mi}\mu_i \approx \frac{T}{M}\sum_{i=1}^{N}\Phi_{mi}\bar{\mu} \approx \frac{NT}{2M}\bar{\mu} \ . \qquad (4\text{-}52)$$

Here we have made use of the fact that that for each measurement, light is collected from about half of the pixels in the image. We also note that

$$\frac{\partial\lambda_m}{\partial x_k} = \frac{T}{M}\Phi_{m,p(k)} \equiv \chi_{mk} \ . \qquad (4\text{-}53)$$

The photon counts follow a Poisson distribution,

$$f(y|\lambda) = \prod_{m=1}^{M} \frac{(\lambda_m)^{y_m}}{y_m!} \exp(-\lambda_m) . \tag{4-54}$$

Therefore

$$\frac{\partial \ln f}{\partial x_k} = \sum_{m=1}^{M} \left(\frac{y_m \chi_{mk}}{\lambda_m} - \chi_{mk} \right) . \tag{4-55}$$

The Fisher information matrix for measurement of x is given by

$$
\begin{aligned}
F_{kl} &= \left\langle \frac{\partial \ln f}{\partial x_k} \frac{\partial \ln f}{\partial x_l} \right\rangle \\
&= \sum_{m,m'=1}^{M} \left\langle \left(\frac{y_m \chi_{mk}}{\lambda_m} - \chi_{mk} \right) \left(\frac{y_{m'} \chi_{m'l}}{\lambda_{m'}} - \chi_{m'l} \right) \right\rangle \\
&= \sum_{m,m'=1}^{M} \frac{\chi_{mk} \chi_{m'l}}{\lambda_m \lambda_{m'}} \langle y_m y_{m'} \rangle - \chi_{mk} \chi_{m'l} \\
&= \sum_{m,m'=1}^{M} \frac{\chi_{mk} \chi_{m'l}}{\lambda_m \lambda_{m'}} (\lambda_m \lambda_{m'} + \lambda_m \delta_{mm'}) - \chi_{mk} \chi_{m'l} \\
&= \sum_{m=1}^{M} \frac{\chi_{mk} \chi_{ml}}{\lambda_m} = \frac{T^2}{M^2} \sum_{m=1}^{M} \frac{\Phi_{m,p(k)} \Phi_{m,p(l)}}{\lambda_m} . \tag{4-56}
\end{aligned}
$$

Using $\lambda = (T/M)\Phi\mu$, we may write

$$F_{kl} = \frac{T}{M} \left[\Phi \operatorname{diag}(\Phi\mu)^{-1} \Phi \right]_{p(k),p(l)} . \tag{4-57}$$

The Crámer-Rao bound tells us that the inverse of the Fisher information matrix provides a lower bound for the covariance matrix of our measurement,

$$\left\langle \delta x \delta x^T \right\rangle \geq F^{-1} . \tag{4-58}$$

In the limit of full image reconstruction, $M = N$, and by comparing eqns. (4-46) and (4-57), we see that the Crámer-Rao bound reproduces our earlier result for the basis scan. This confirms the choice of estimator used for the analysis of the performance of the basis scan.

Using our approximation $\lambda_m \approx NT\bar{\mu}/2M$,

$$F_{kl} \approx \frac{2T}{MN\bar{\mu}} \sum_{m=1}^{M} \Phi_{m,p(k)}\Phi_{m,p(l)} \ . \tag{4-59}$$

Remembering that Φ is a matrix that is (randomly) filled with zeros and ones, we see that if $k = l$, the sum will be $M/2$, on average, whereas if $k \neq l$, we will get $M/4$ on average. Thus,

$$F \approx \frac{2T}{MN\bar{\mu}}\frac{M}{4}(I + O) = \frac{T}{2N\bar{\mu}}(I + O) \ . \tag{4-60}$$

Here O is a $K \times K$ matrix filled with ones. We thus arrive at a lower bound for the covariance matrix of our measurement,

$$\langle \delta x \delta x^T \rangle \geq F^{-1} = \frac{2N\bar{\mu}}{T}(I + O)^{-1} = \frac{2N\bar{\mu}}{T}\left(I - \frac{1}{K+1}O\right) \ . \tag{4-61}$$

Thus, for the case $K >> 1$, we arrive at an approximate **lower bound** for the noise in the K pixels we are interested in,

$$\sigma_k^2 = \langle \delta x_k^2 \rangle \geq \frac{2N\bar{\mu}}{T} \ . \tag{4-62}$$

Note that for the special case $M = K = N$, this result agrees with eqn. 4-49.

4.4.2 Discussion

The sensitivity for the CS measurement scheme in this case is no better than for the raster scan or the basis scan; in fact it is worse than a simple raster scan by $\sqrt{2}$, presumably because half of the photons are being thrown away. Compared to a focal-plane array, the loss in sensitivity is $\sqrt{2N}$, and the penalty in measurement speed is $2N$. Equation 4-62 is again in disagreement with Duarte *et al.* (2008), who give a formula of $3C_N^2 M\bar{\mu}/T$.

These analyses are applicable for the case that the measurement sensitivity is limited by photon Poisson noise. If the sensitivity is limited by other factors, e.g.

detector noise, the conclusions will be different. This appears to be the situation for the experimental results shown in the Duarte *et al.* paper, in which the shot noise of the detector dark current appears to be significant. This is not a surprise, because a detector used in a single pixel camera must necessarily have a much larger area than that of a pixel in a focal plane, because the etendue (the $A\Omega/\lambda^2$ product) is conserved in an optical imaging system. Generally speaking, dark current scales with detector area.

4.5   Comparison with CS Performance Bounds

Here the results are compared to the CS performance bounds for the case of Poisson noise obtained by Raginsky *et al.* (2010) [41]. It is difficult to make a rigorous comparison because of differences in the underlying assumptions and differences in the performance metrics that are used.

The Raginsky *et al.* paper assumes that the measurement matrix is random, consisting of 0 or $1/M$. This is equivalent to our choice of 0 or 1, with the total measurement time divided M ways. (Note that the definitions of N and M are reversed in that paper compared to our usage; We have undone this in order to stay with a consistent notation.) The Raginsky paper provides bounds for the performance of a specific reconstruction technique, or image estimator. The estimator is not based on the usual l_1-minimization prevalent in the CS literature; rather it is the maximum (Poisson) likelihood estimator with a prior term added to allow solution of the underdetermined problem. In this case the prior, or penalty function, basically measures the number of bits needed to encode the reconstructed signal. A smaller number of bits corresponds to a vector that is more sparse.

The performance guarantee is in the form of an upper bound on the average mean square error between the true image f^* and the reconstructed image $\hat{f}$. These

images are in photon units, and can be translated to our notation using $f^* = \mu T$ and $\hat{f} = \hat{\mu}T$. The bound reads

$$\frac{1}{I^2}\left\langle ||\hat{f} - f^*||_2^2 \right\rangle \leq CM \left(\frac{\log N}{I}\right)^{2\alpha/2\alpha+1} + \frac{\log(N/M)}{M} \ . \qquad (4\text{-}63)$$

Here, I represents the total number of photons; $I = \bar{\mu}NT$ in our notation. The parameter α appearing in the exponent is a measure of the compressibility of the image; basically, if we approximate the image as a K-sparse vector, we expect the l_2-norm of the approximation error to decay as $K^{-\alpha}$. Translating to our notation, this bound reads

$$\frac{T^2}{\bar{\mu}^2 N^2 T^2}\left\langle ||\hat{\mu} - \mu||_2^2 \right\rangle \leq CM \left(\frac{\log N}{N\bar{\mu}T}\right)^{2\alpha/2\alpha+1} + \frac{\log(N/M)}{M} \ . \qquad (4\text{-}64)$$

The assumption of a compressible signal instead of a sparse signal causes a bit of trouble in this comparison. We would like to see the mean square error decrease as $1/T$, but that requires $\alpha \to \infty$. For finite α, the mean square error decreases more slowly than $1/T$. Our intuition is that this has to do with the 'support' of the reconstructed signal changing as the SNR builds with increasing measurement time, because the signal is only compressible and not truly sparse. It would therefore seem that $\alpha \to \infty$ is the right limit to take if we have truly sparse signals. If this guess is correct, we have

$$\left\langle ||\hat{\mu} - \mu||_2^2 \right\rangle \leq CM \frac{N\bar{\mu}}{T}\log N + \frac{\log(N/M)}{M} \ . \qquad (4\text{-}65)$$

This is now starting to resemble the previous results. However, it is stated as a mean square error for the entire image, whereas we are interested in the mean square error on per-pixel basis. Here is where things get tricky again. Suppose that we represent the image in the sparsifying basis, $\mu = W\theta$, where W is the orthonormal matrix that transforms from the sparsifying basis to the pixel basis, and θ is the coefficient vector in the sparsifying basis. The norm is preserved by this transformation, $||\hat{\mu} - \mu||_2^2 = ||\hat{\theta} - \theta||_2^2$. However, under the assumption that the signal is truly sparse, and the reconstruction method recovers K coefficients, with decent SNR there will be only

K nonzero contributions to the difference norm in the θ basis so we may write $||\hat{\theta} - \theta||_2^2 = K\sigma_\theta^2$, where σ_θ^2 is the mean square error for a reconstructed signal coefficient in the sparsifying basis. This yields

$$\sigma_\theta^2 \leq C\frac{M}{K}\frac{N\bar{\mu}}{T}\log N + \frac{\log(N/M)}{MK} \quad . \tag{4-66}$$

Admittedly, the entire argument is not exactly a shining example of mathematical rigor, but it at least appears fairly plausible that the Raginsky *et al.* bound does not contradict the results obtained with far more pedestrian means because the factors multiplying $N\bar{\mu}/T$ in the bound substantially exceed unity (in particular, $M/K > 1$ is required for reconstruction).

It is interesting to note that the Raginsky bound contains an explicit factor of M, the number of measurements (or masks), suggesting that perhaps performance improves for the compressed sensing case vs. the basis scan case. However, the numerical experiments performed by Raginsky *et al.* and shown in Figure 13 do not seem to indicate much dependence for large M.

4.6 Summary

4.6.1 Findings

1. The single-pixel camera is an intriguing concept that could reduce costs of imaging sensors for some DoD applications. Because commercial developments are well underway, independent development by DoD is not needed at the present time.

2. Data are not available to evaluate the performance estimates discussed here.
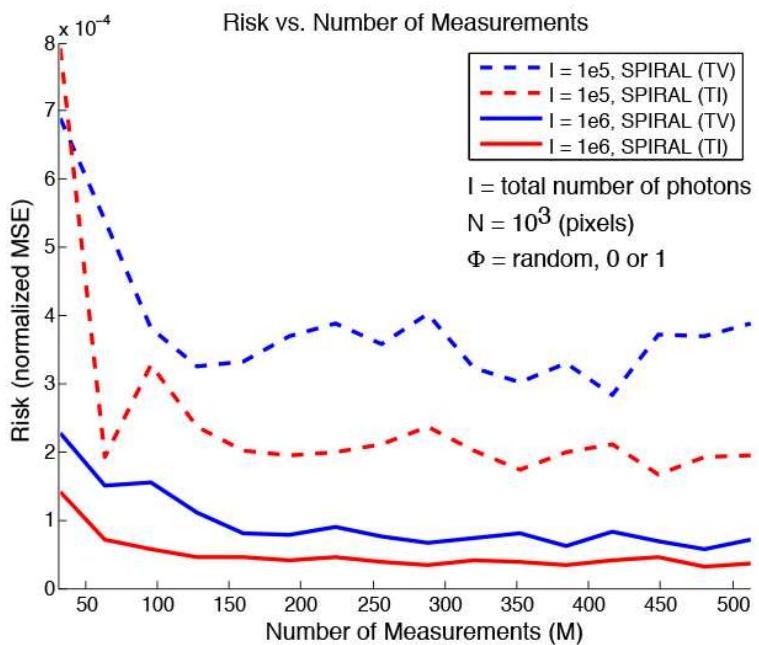
Figure 13: Mean square reconstruction error in numerical experiments, from Raginsky *et al.* (2010). The TI and TV labels indicate two somewhat different reconstruction methods, the TI version favors smoother reconstructions. Note that the MSE for both appears to be fairly flat for $M \geq 150$.

4.6.2 Recommendations

1. When commercial single-pixel infrared cameras are available, DoD should fund a thorough independent evaluation to compare performance with theoretical estimates. In addition to evaluating the potential of these devices, the results should provide valuable practical experience with the CS approach.

5 PULSED RANGE-DOPPLER RADAR

5.1 Introduction

A major use of radar is to find the location and velocity of individual targets. In pulsed range-Doppler (P-RD) radar, the range to the target is given by $r = c\tau/2$ where τ is the elapsed time of the pulse return and c is the speed of light. Velocity, v, (along the line of sight) is found from the Doppler shift of the radar frequency f, given by $f_v = -2vf/c = -2v/\lambda$, with λ the radar wavelength. When the transmitted radar pulse, $s_T(t)$, is reflected by a single target it produces a received radar signal $s_R(t) = \alpha s_T(t - \tau)e^{2\pi i f t}$, where α is the target reflectivity, and we ignore attenuation. Additional targets are represented by separate terms with the (τ, α, f_v) values for each target. Cross-range location is determined in the case of monostatic radar by the elevation and azimuth of the line of sight, while for multistatic radar, the cross-range location can be found in part by the phase change of the signal at the detection antenna. A useful multistatic arrangement is MIMO radar (multiple-input and multiple-output), utilizing multiple antennas at both the transmitter and receiver. For simplicity, we will focus on monostatic range-Doppler radar along a single line of sight. Extension to cross-range measurement is conceptually straightforward.

In the following subsections, after reviewing conventional pulsed range-Doppler radar, we will turn to applications of compressed sensing (CS) to this problem, then offer a comparison of various conventional and CS approaches, and conclude with findings and recommendations.

5.2 Conventional Pulsed Range-Doppler Radar

Pulsed range-Doppler radar is one of several modes widely used in military radars, e.g. on aircraft (Fig 14) and surface platforms, to gain critical situational awareness about locations and trajectories of nearby objects. A P-RD radar returns target
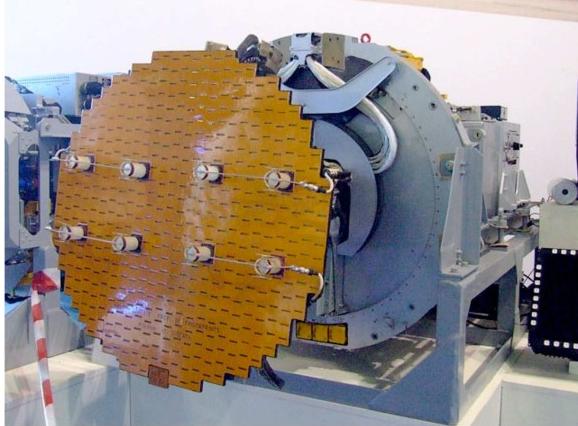

Figure 14: Russian MAKS - 2007 'Zhuk' X-band, P-DR tested for the MIG 23 and 29. (Source: Wikipedia entry on Zhuk radar).

detection and speed for each range and azimuth resolution cell, shown schematically in Figure 15. The frequency spectrum of the return signal is displayed. The left and right endpoints show the repetition of the spectrum at integer intervals of the pulse repetition frequency, PRF (Ch. 3 of Skolnik (2008) [48]). To avoid aliasing, the target must have a Doppler shift less than the $PRF/2$, and hence a radial velocity between $\pm(\lambda * PRF/4)$. This example shows the spectrum for an aircraft flying horizontally. The 'altitude return' is the echo from the ground directly below the aircraft which has zero radial velocity with respect to the aircraft, $V_r = 0$. Main-beam clutter refers the ground echo arriving in the radar's main antenna beam. Sidelobe clutter refers to ground echoes arriving in the radar antenna sidelobes. Note how clutter appears near zero Doppler and at its aliases at both ends of Figure 15. Target and clutter echoes with radial speeds greater than $\pm(\lambda * PRF/4)$ will be aliased to appear within the Doppler spectrum, but with incorrect radial speeds. For effective

operation, target echoes must be distinguished from clutter echoes to prevent false alarms.

Using N pulses, a given PRF and bandwidth W over a time $\mathcal{T}$ allows a conventional P-RD radar to resolve $M = \mathcal{T}W$ targets with Doppler resolution $\delta f_D = 1/\mathcal{T}$ and range resolution $\delta_r = c/(2W)$, where T is the time between pulses, $T = 1/PRF$ and $\mathcal{T}W$ is the time-bandwidth product.
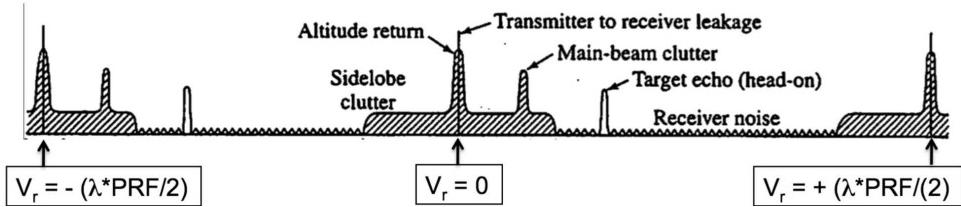

Figure 15: Schematic diagram of a P-RD spectrum. For each range and angle resolution cell, conventional P-RD radar produces a Doppler shift spectrum that corresponds to the radial velocities of targets in that cell (After Skolnik (2008)[48]).

An important part of traditional P-RD radar is the use of a matched filter to detect the return signal. As the name implies, the matched filter correlates the received signal with the waveform of the transmitted pulse, thus passing the desired signal together with that part of the noise and clutter that matches the filter. The result of the matched filter is given by:

$$\chi(\tau, \omega_v) = \int_{-\infty}^{\infty} s_T(t) s_R^*(t) \, \mathrm{d}t = \alpha \int_{-\infty}^{\infty} s_T(t) s_T^*(t - \tau) e^{-i\omega_v t} \, \mathrm{d}t = \alpha A(\tau, \omega_v)$$

with obvious extensions for multiple targets. Here $\omega = 2\pi f$. $A(T, \omega)$ is known as the *ambiguity function*. (The properties of $A(T, \omega)$, much studied in the radar literature, indicate that no signal $s_T(t)$ can yield simultaneously fine resolution in both delay and in Doppler.)

It is worthwhile to mention some forms of $s_T(t)$ being used, because they illustrate the lengths to which current radar designers go to obtain adequate signal/noise (S/N). In addition, they serve as a warning that if only a part of the standard radar

signal is retained in CS there may be a large penalty in S/N when dealing with real data. Transmitted signals can be simple waveforms, such as Gaussians, with the time width approximately the inverse of the frequency bandwidth. More commonly in current radars, signals and filters achieve *pulse compression* (not to be confused with compressed sensing, which we will be discussing later). Pulse compression gets around the following dilemma. For better range resolution, one wants to shorten the pulse. However, to maintain pulse energy for adequate S/N one would then need to increase the peak power, and at some point the high voltage supplies become too bulky and costly. The solution is pulse compression: transmit a long pulse that is rapidly modulated or coded at a bandwidth corresponding to a short pulse, with sufficient integrated energy for adequate S/N; the correct matched filter then collapses the radar return signal to a short pulse. For example a long, frequency-chirped transmitted signal yields with the matched filter a very short detected pulse with a time width given by the inverse of the frequency change of the chirp. A coded pulse or a pseudo-noise (PN) sequence will work as well. Note that the receiver must sample at the Nyquist rate of the full bandwidth to effect the pulse compression and obtain the desired S/N. In CS, as we will see, it may be possible to identify a sparse distribution of targets by sub-sampling, but there may be a cost in S/N compared to standard radar.

5.2.1 Illustration of conventional P-RD radar using two targets

This is the baseline case, in which Haspert (2012) [25] considered two targets in a two-dimensional range-Doppler space (r, f_D) with the following parameters:

Bandwidth: $W = 0.1$ GHz (1.5 m resolution)

PRF: 20 kHz

Coherent integration time: $\mathcal{T} = 0.1$ sec (10 Hz Doppler resolution)

Total number of pulses: $N = \mathcal{T} \times PRF = 2000$

SNR: 30 dB

Targets: two, differing in range and speed

Haspert used conventional Fourier transform processing to resolve the two targets, as shown in Figure 16. With SNR = 30 dB, the targets are resolved very well in range and radial speed (Doppler shift).

5.2.2 Thinned P-RD radar example using two targets

This case differs from the baseline case by using only 1/10 of the full pulse train, selected randomly. The parameters that differ are thus:

Total number of pulses: $N = 0.1\mathcal{T} \times PDF = 2000$
SNR: 20 dB

Missing signals were simulated by being set to zero before Fourier processing. Because SNR remained large, dropping only to 20 dB, the targets are still well-resolved in range and Doppler (Fig. 16). The impact of thinning is not worrisome in this simulation because the SNR of the thinned case was quite adequate to resolve the targets in range and Doppler, in spite of the elevated side lobes. This, however, will be a serious concern for lower SNR, say from small targets, when false alarms would be significant.

5.3 Application of Compressed Sensing to P-RD Radar

Compressed sensing (CS) encompasses a wide variety of techniques, many of which have been applied to radar (Parker *et al.*, 2012) [36]. In recent years, there have been many proposals for applying CS methods to the range-Doppler problem when there
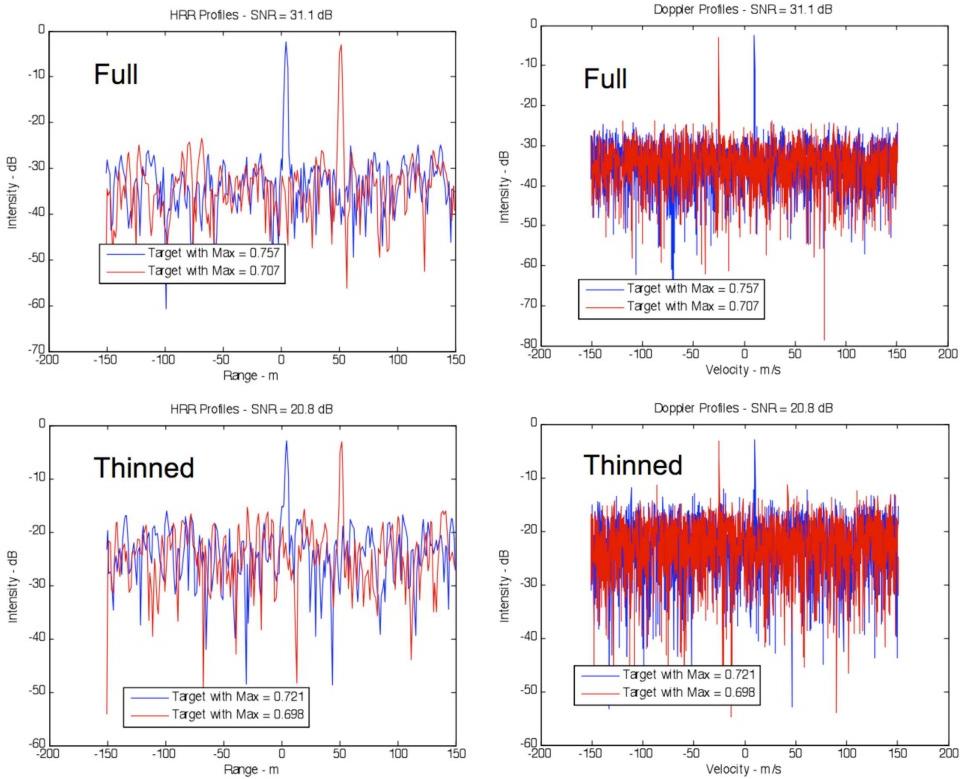
Figure 16: Left) Horizontal range (HRR) profile for conventional and thinned pulse bursts. Note the increased width of the primary peaks and the higher side lobes for the thinned case. Right) Radial speed profiles. Note the increased side lobes and lower SNR for the thinned case. (After Haspert [25]).

are few enough targets to satisfy relevant sparsity constraints for a given number of transmitted pulses. These proposals point to the following possible advantages of CS over standard radar methods: transmitting fewer pulses, sampling at lower rates, avoiding the complications of a matched filter in the receiver, and obtaining better resolution of targets closely spaced in range-Doppler. Note, however, that P-RD radar is a well-honed field, just as are other areas of radar, and current radar systems already have many features designed to get at such problems as range-Doppler ambiguity. Furthermore, many CS proposals have been tested by simulations, but not in the field with real systems and real data.

Here we give a brief summary of the general CS theory applied to the range-

Doppler problem, using just the range part for simplicity. We employ the notation of Baraniuk and Steeghs (2007) [8] who were among the first to apply recent compressive sensing approaches to radar. Suppose we probe for target locations within a range interval corresponding to a spread in time delays $\Delta\tau = T$, using a transmitted signal of this same total length T but containing a sequence of N pieces of length $\Delta T = T/N$. The range resolution is of order $c\Delta T$. We assume that we have K targets located at K positions, or delay times τ_i with $i = 1, 2...K$. If $K \ll N$, then the targets are K-sparse and we may not need to sample the return signal at the rate $1/\Delta T$. In fact if proper pieces are chosen for the transmitted sequence we can make $M \ll N$ measurements of return signals and extract the locations of the K targets. We do this by making M non-adaptive, linear observations in the form of $y = \Phi x$ where Φ is a dictionary of size $M \times N$. Here, x is a vector of length N and represents the N possible time delays τ, only K of which are non-zero, and y is the length M vector giving the results of the M samples. Φ is called the measurement matrix and if it is sufficiently "incoherent" then the information of x will be embedded in y such that it can be perfectly recovered with high probability provided that $M = O(Klog(N/K))$. Using, for example, a pseudo-random string for s_T is sufficient to guarantee sufficient incoherence. As an example, Baraniuk and Steeghs (2007) [8] shows the results of a simulation with $K = 20$ targets probed by a pseudo-noise (PN) signal generated from a length-$N = 240$ random Bernoulli ± 1 vector $p(n)$ via $s_T(t) = p([t/\Delta T])$. The 20 targets are recovered exactly using an OMP greedy algorithm and a sparsity frame combining delta spikes and Haar wavelets. These results are shown in Fig. 17.

Basically, rather than sample at the Nyquist rate with a matched filter, as in standard radar, no matched filter has been used, and far fewer samples have been taken, but the targets have been identified clearly. This procedure is typical of most CS applications to this kind of radar problem - no matched filter and far fewer samples are used when the targets are sparse. However, note that no noise has been
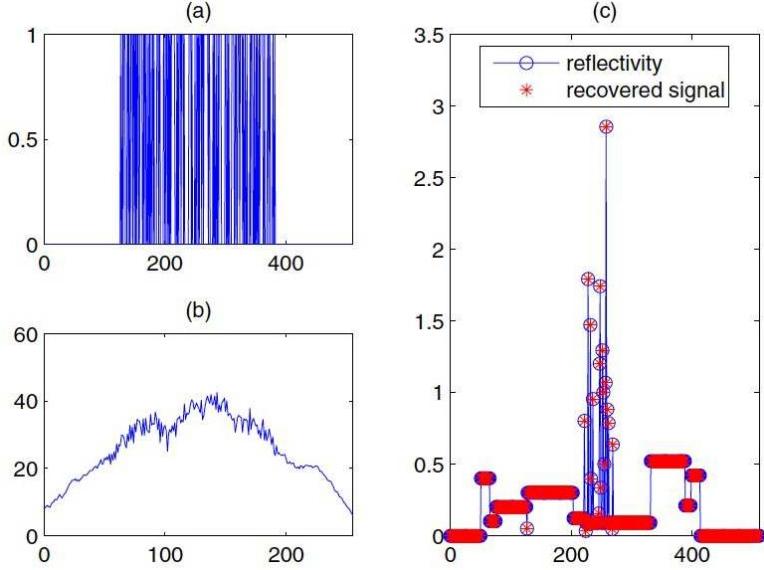
Figure 17: CS radar range example described in text and taken from Baraniuk and Steeghs (2007) [8]. (a) Transmitted PN pulse $s_T(t)$, (b) low-rate measurement y, and (c) true and recovered reflectivity profiles u(t).

introduced in this simulation, and there should be an S/N penalty because not all the signal energy was utilized.

5.4 Compressed Sensing using a Range-Doppler Grid

Here we will include target velocities and consider the range-doppler problem, using a method that locates the targets and their velocities on a discrete grid in delay-Doppler (τ, ω_v) space (Herman and Strohmer, 2009) [27]. As we will see, this method can work well except it suffers from a serious problem referred to as grid-mismatch (Chi *et al.*, 2011) [17]: when the actual targets do not fall close to the grid points, their locations and velocities have projections (often called *leakage*) onto neighboring grid points that can violate the sparsity condition.

5.4.1 The CS grid method

We present the range-Doppler CS method introduced by Herman and Strohmer (2009) [27]. As in the previous subsection, assume that the transmitter signal consists of a sequence of N pieces, each of time length ΔT, lasting a total time $T = N\Delta T$. The receiver can detect range delays τ with resolution ΔT and Doppler shifts with resolution $1/T$. Herman and Strohmer introduce a time-frequency (τ, ω) grid on which to locate the radar targets as shown in Fig. 18; the natural individual grid size corresponds to the resolution limits above, and thus has dimensions ΔT and $1/T$ along the τ and ω axes respectively. Suppose there are K targets located on this $N \times N$ grid. These targets can be considered sparse if they are few compared to the total number N^2 of possible delay *and* Doppler measurement values, i.e. the N^2 grid points available. We assume then that $K \ll N^2$. A similar CS formalism can be used here as was introduced in the previous subsection: $y = \Phi x$. Here y is a length-N vector giving the results of the N radar receiver measurements, Φ is the $N \times N^2$ measurement matrix, and x is a length-N^2 vector representing the range-Doppler locations on the grid, only K of which are non-zero. We must use a length-N sequence for s_T that gives the necessary incoherence to Φ, in which case K targets can be located using Basis Pursuit, provided that $1 \leq K \leq N/(2\log N)$. In Herman and Strohmer (2009) [27], the Alltop sequence was chosen, a chirp-type function given by the sequence of elements $f_n = e^{2\pi i n^3/N}/\sqrt{N}$ with n taking on the integer values from 0 to $N-1$, for some prime $N \geq 5$. The results of a simulation with $K = 8$ and $N = 47$ are shown in Fig. 18. It is seen that targets on adjacent grid points are identified correctly, well within the range-Doppler resolution implied by the bandwidth $\times$ time width product $T/\Delta T = N$. The effect of noise (included via $y = \Phi x + N$) is also shown in the figure. Noise does indeed degrade the signal.

There are many good features of this CS approach. It provides a means of using the smallest pulse length N for a given number of targets, and also it seems to
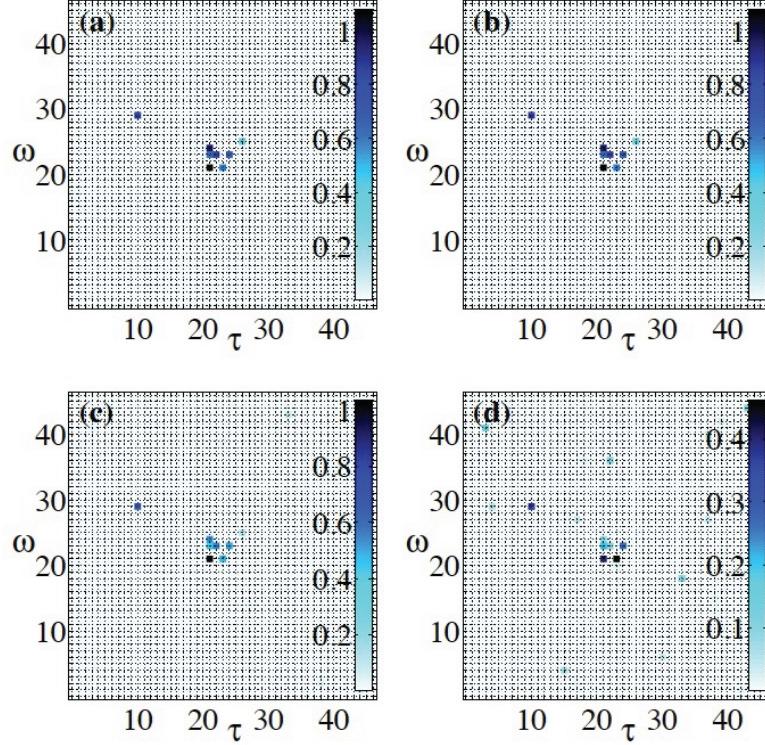
Figure 18: Radar simulation with K = 8 targets on a 47 x 47 time-frequency grid, shown in Herman and Strohmer (2009) [27]. (a) Original target scene. Compressed sensing reconstruction of original target scene with S/N: (b) ∞ dB, (c) 15 dB, (d) 5 dB. Notice in (b) that compressed sensing perfectly recovers (a) in the case of no noise.

resolve targets that would overlap each other in range-doppler making them difficult to resolve by standard radar. There, however, is a major difficulty: actual targets will not all fit precisely at the vertices of a single grid; some of their locations will project onto nearby grids leading to the problem of grid leakage, which can be so severe as to destroy the sparsity. This problem is treated in the next subsection.

5.4.2   Grid mismatch issues

Difficulties due to grid mismatch are discussed in Bajwa *et al.* (2011) [7] and elsewhere. Here, we will follow the discussion of Chi *et al.* (2011)[17], who argue there there are two main principles for inverting the kinds of images that are measured in

radar and other fields. The first principle is matched filtering as we discussed in connection with standard radar. The second is one of *parameter estimation wherein a sparse modal representation for the target is posited and estimates of parameters (for instance, delay and Doppler) are extracted.* Recent advances in CS have shown that the latter method has manageable consequences for image inversion, provided that the image is sparse in an apriori known basis, usually taken to be a Digital Fourier Transform (DFT) basis constructed for resolution of $2\pi/N$, with N a pulse-to-pulse processing length. It is natural then to consider the use of CS when the targets are taken to be on a regular grid in delay and Doppler, as was done in the previous subsection.

Chi *et al.* (2011) [17] point out that no matter how large the size of the grid, the actual field will not place its sources on the center of the grid points in frequency-wavenumber, or in delay-Doppler-wavenumber space. This means that the image is actually not sparse in the basis defined by the grid. In fact, any target lying between two cells of a discretely-resolved range-Doppler plane or frequency-wavenumber plane will spill non-zero values into all cells, with the amplitude of the spillage following a Dirichlet kernel, decaying as $1/x$. This spillage can turn a sparse representation into an incompressible one. These observations raise the following question: What is the sensitivity of compressed sensing for image inversion to mismatch between the assumed basis for sparsity and the actual basis in which the image is sparse?

Using our previous notation, there are two models for y, the measured "image" of the targets. In the mathematical model assumed for CS, as in the previous subsection, $y = \Phi_0 x$, where the basis Φ_0 is known and is typically a gridded matrix, and x is a sparse or compressible vector. But, in reality, the image is $y = \Phi_1 \theta$, where the basis Φ_1 is determined by a point spread function, a Greens function, or an impulse response, and the vector θ in this basis is sparse. Typically Φ_1 is determined by parameters that are unknown apriori and that do not lie exactly on the gridding points of Φ_0, so $\Phi_1 \neq \Phi_0$. Chi *et al.* call this *basis mismatch* and claim

that it is present in all imaging problems, no matter how fine-grained the gridding procedure is. The question raised in Chi *et al.* (2011) [17] is *'what is the consequence of assuming that x is sparse in Φ_0, when in fact it is only sparse in an unknown basis, which is determined by the mismatch between Φ_0 and Φ_1?'*

Their analysis shows that, in the presence of basis mismatch, exact or near-exact (within noise levels) recovery cannot be guaranteed, and suggests that the recovery using basis pursuit (or greedy algorithms) "*may* suffer large errors." Their numerical examples demonstrate a considerable performance degradation in recovering x from compressed sensing measurements, when the assumed basis for sparsity is a DFT basis but the actual sparsity basis does not align with the DFT basis. Numerical results for range estimation are shown in Fig. 19. A $N = 512$ point grid is assumed. The inaccuracy in target reconstruction persists even when the number K of compressed sensing measurements is increased to the full image dimension N. Chi et all say that their comparisons show that classical image inversion approaches, such as reduced rank linear prediction, can provide more reliable reconstructions of the image than basis pursuit with a similar number of measurements in the presence of basis mismatch.

Chi *et al.* do not claim flat out that gridded methods of CS must fail in practical cases. They say that *extra care may be needed to account for the effects of basis mismatch.* Perhaps the best observation at this stage is that how to get around basis mismatch is an active area of current study.

In the next subsection we introduce a method of implementing CS (Bajwa *et al.*, 2011) [7] which avoids the quantization of the delay-Doppler space by treating the problem directly in the analog domain.
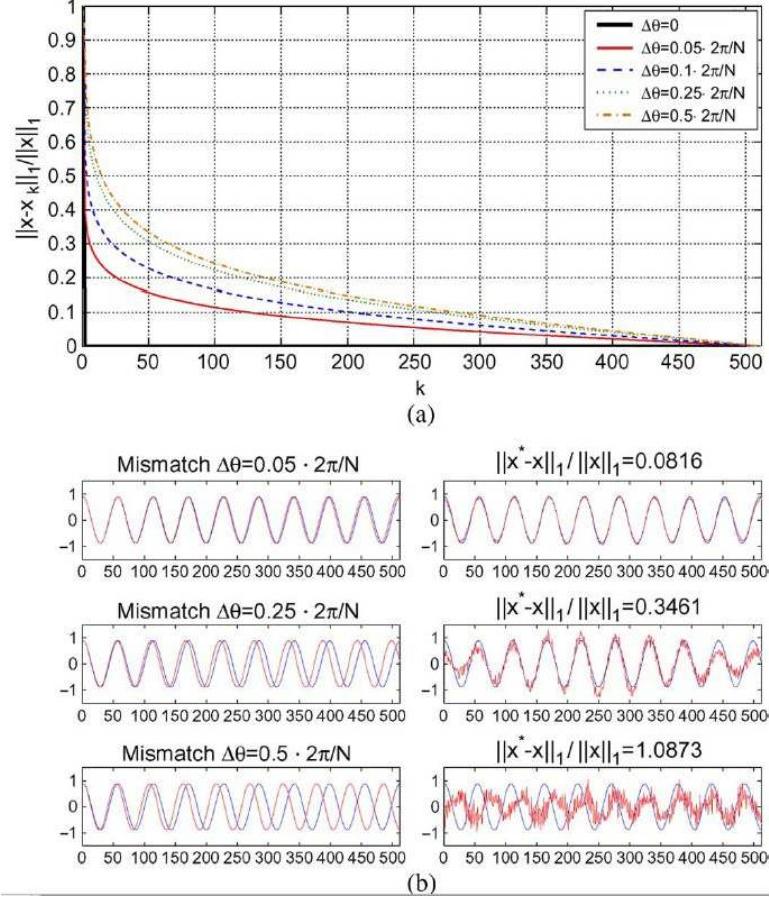
Figure 19: Taken from Chi *et al.*(2011) [17]. (a) The effect of grid mismatch as a function of k, the number of CS measurements, up to the $N = 512$ points in the grid. (b) Left column: the actual tone (blue) superimposed on the closest DFT tone; Right column: the reconstructed tone (red) superimposed on the actual tone (blue). The frequency mismatch is 0.05 for the plots in the top row, 0.25 for the plots in the middle row, and 0.5 for the plots in the bottom row.
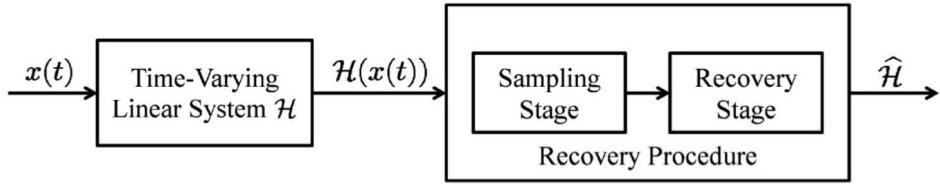
Figure 20: Schematic system identification approach to P-RD radar. The response $(\mathcal{H}(x,t))$ to a known probing pulse, $x(t)$, allows identification of the time-varying linear system, $\mathcal{H}$. The probing pulse is the radar pulse, and the response $\mathcal{H}(x(t))$ is the radar echo. Identifying (characterizing) H allows determination of the pulse time delay (or radar range), and the time-varying phase change (or Doppler shift). (After Bajwa *et al.* (2011) [7]).

5.5 Compressive Sensing using a System Identification Approach

For this example, we consider work by Bajwa *et al.*(2011) [7] in which they take a system identification approach to processing data from a P-RD radar. Figure 20 shows a schematic of this approach, in which a known probing signal, i.e. a radar pulse, passes through a time-varying linear system, $\mathcal{H}$. The output of $\mathcal{H}$ is characterized in terms of time delay and phase shift. As the radar target moves, variations in $\mathcal{H}$ change the time delay and hence phases in Fourier space, creating a Doppler shift corresponding to the target's radial speed.

The system response $\mathcal{H}$ can be formulated as

$$\mathcal{H}(x(t)) = \sum_{i=1}^{K_r} \sum_{j=1}^{K_{v,i}} \alpha_{ij} x(t - \tau_i) e^{j2\pi\nu_{ij}t}$$

where the response components correspond to individual radar targets. Note how there can be targets with more than one speed associated with a discrete time delay, i.e. radar range.

The system identification process of Bajwa *et al.* (2011) [7] is a combination of several previous techniques, as shown in Figure 21. These techniques are as follows:

82
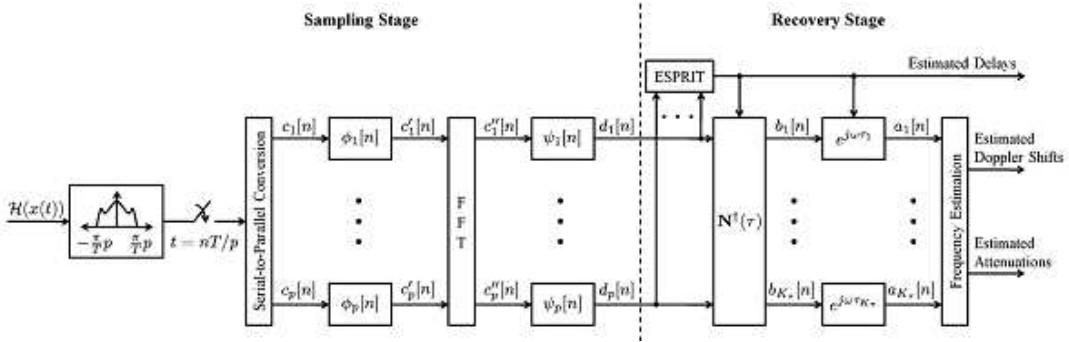
Figure 21: Schematic block diagram of the recovery procedure for identification of radar signal time delays and Doppler shifts. After Bajwa *et al.* (2011) [7].

1. The sampling stage uses the sub-Nyquist time delay estimation technique of Gedalhayu and Eldar (2010) [24].

2. The recovery stage makes use of the ESPRIT technique of Roy and Kailath (1989) [43].

3. Other sub-space signal processing methods are also used in the recovery procedure (Krim and Vigberg, 1996) [33].

The radar echo signal $\mathcal{H}(x(t))$ is first low-pass filtered over frequencies determined by the inter-pulse spacing time T and a factor p, where the output of the low pass filter is sampled at times $t = nT/p$ and $T = 1/\mathrm{PRF}$. Thus, there are p samples over the inter-pulse spacing time T. These p samples are used in turn to construct p data streams as shown in Figure 21. These p data streams are then Fourier transformed and otherwise processed as shown schematically in Figure 21 and described in detail by Bajwa *et al.* (2011) [7]. We point out that the ESPRIT method is a modal method with similarities to the MUSIC algorithm described in more detail in connection with HF radar elsewhere in this report.

Bajwa et al. (2011) specify conditions required to apply this method. We summarize these conditions in practical terms as follows:

1. The system must be underspread, i.e. occupy a region in delay-Doppler space with an area $\tau_{\max}\nu_{\max} \leq 1$, where $\tau_{\max}$ is the maximum time delay and $\nu_{\max}$ is the maximum Doppler shift.

2. The product of the coherent integration time $\mathcal{T}$ and the bandwidth W must satisfy $\mathcal{T}W \geq 8\pi K_\tau K_\nu^{\max}$, where K_τ = number of distinct target delays and $K_\nu^{\max}$ is the maximum number of Doppler shifts associated with any one of the distinct target delays. The $\mathcal{T}W$ condition above is satisfied so long as $\mathcal{T}W \geq 2\pi(K+1)^2$, where K is the total number of targets.

3. The bandwidth W of the radar transmissions must satisfy $W \geq (2p\pi/T)$.

In a conventional P-RD radar, the total number of pulses in a burst that last one coherent integration time would be $N = \mathcal{T}W =$ time-bandwidth product. Further, the coherent integration time, $\mathcal{T}$, specifies the frequency resolution of the Doppler shift, namely $\delta f_D = 1/\mathcal{T}$, and the bandwidth, W, specifies the time delay resolution and hence the range resolution, $\delta r = c/(2W)$. Conventional radars typically maximize the time-bandwidth product, not so much to accommodate a large number of targets, but to provide high range and speed resolution as well as the capability to detect small targets using coherent integration. In this CS method, the emphasis is on using a small time-bandwidth product fitted to a sparse target space. In addition, the CS method offers the opportunity for obtaining "super resolution", i.e. resolution better than the conventional radar resolution mentioned above. It is obtained in the same way as with the MUSIC Algorithm discussed elsewhere in this report.

Probably the best way to illustrate the advantages and disadvantages of applying CS algorithms to radar is to use an example case. After the example, we will proceed with our comparison of the three methods of processing P-RD radar signals. Bajwa *et al.* (2011) [7] provide a useful numerical experiment and assess its performance in terms of noise, truncation of digital filters, finite number of samples, choice of

probing sequence $\{x_n\}$, and model-order mismatch. We will limit our illustration to consideration of SNR, but the other assessments are contained in their article.

This example has six targets at two discrete locations ($K_\tau = 2$) with three target speeds associated with each location ($K_{\nu,2} = 3$). The maximum time delay is taken to be $\tau_{\max} = 10\mu s$, and the maximum Doppler shift is $\nu_{\max} = 10$ kHz. Values of these parameters are known a priori and influence the design of the probing pulses and analysis. To implement the CS algorithm, Bajwa et al. make the following parameter choices:

1. The prototype pulse is thus taken to be constant over the working spectral band $\pm(\pi \text{ p/T})$, with $p = 4$ and $T = 10\mu s$, yielding bandwidth is $W = \pm 1.256$ MHz.

2. The pulse burst is a random binary (± 1) sequence with $N = 30$ pulses, leading to $\mathcal{T}W = 240\pi = 754$, about 5 times greater than the minimum quoted above, $8\pi K_\tau K_\nu^{\max} = 48\pi$.

The processing method for recovering the time delays and Doppler shifts is that of Figure 21 with the input low-pass filter (LPF) taken to have a flat frequency response over the prescribed bandwidth. As shown in the figure, the ESPRIT algorithm was used to recover time delays, and a matrix-pencil method Hua and Sakar, 1990) [29] recovered Doppler shifts. Both ESPRIT and matrix-pencil are modal methods, as is the MUSIC algorithm (Scharf, 1991) [44].

Figure 22 shows the results for the example case from Bajwa *et al.* (2011) [7]. All targets were successfully identified. Estimation of the ranges and speeds was accomplished using only 30 pulses with a time-bandwidth product of about 750. In a conventional radar one would use a PRF > 20 kHz, and if we specify a Doppler resolution of $\delta f_d = 50$ Hz, more than 400 pulses would be needed to accomplish the same target detection and measurement. So we see the advantage of using a CS
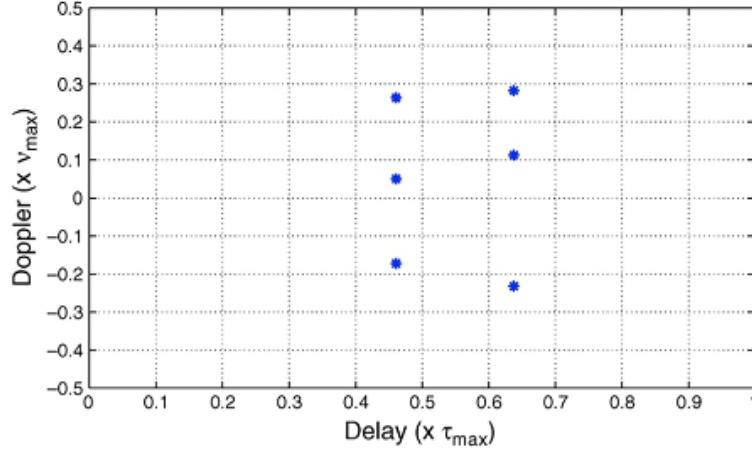
Figure 22: Six targets identified by using the system identification approach to P-D radar operation. A 30-pulse burst was used to recover these six targets. After Bajwa et al. (2011).

technique to operate in a target environment known to be sparse.

The next step is to see how errors in estimating time delays and Doppler shifts vary with SNR and the choice of processing parameters, e.g. the number of taps and digital filters, the number of samples collected, and different probing sequences. The item of most interest here is the error as a function of SNR (Fig. 23).

Noting that the error is normalized by the maximum value of the variable, we see in Figure 23 that the Doppler shift errors become very large for SNR < 20 dB, so one needs signal-to-noise ratios at least $\sim$ 30 dB for successful operation in this example. Bajwa et al show that mean square error variations with the number of taps on digital filters and the number of samples collected have an impact mainly at high SNR for realistic parameter choices. However, the error variation with different probing sequences does change somewhat for SNR less than 30 dB.
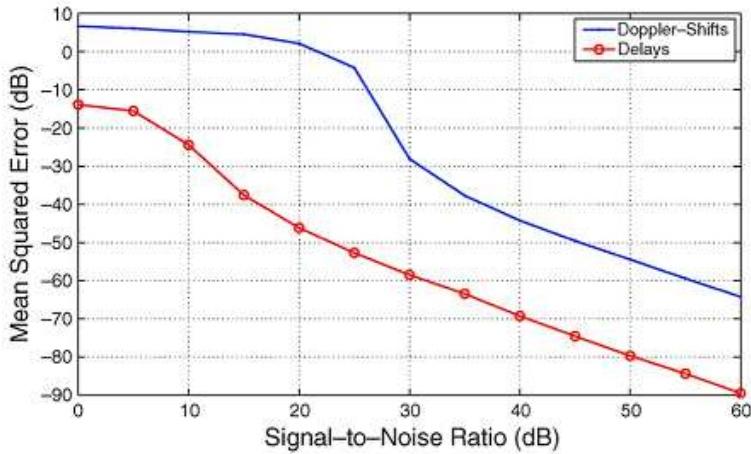
Figure 23: Mean Square error is a function of signal to noise ratio for the example case given by Bajwa *et al.* (2011) [7]. Note that the error is normalized by the maximum value of the variable.

5.6 Comparison of Methods for Pulse-Doppler Radar Operation

The objective of this section is to compare three methods for performing the function of a P-RD radar to illustrate how CS techniques can be used to enhance performance, what drawbacks they may have, and what metrics are relevant in evaluating their performance. Put another way, how can a given number of radar pulses be used most effectively?

There are a large variety of compressive sensing methods and many may be applied to radar. For these CS methods to be successful, we need to find the right niche for CS application and the right CS technique to use. We discussed the application of MUSIC to coastal HF radars in which the algorithm has made a strong contribution to the HF radar network that senses large sections of the U.S. coastline. For a useful comparison of methods one must have relevant metrics and we suggest a list of such metrics as summarized below:

- Error in target parameter estimation (range and speed) as a function of SNR

87

Table 1: Method Comparison Table

Metric/Method	Full N pulses	Thinned pulses	CS pulses
Number of pulses	N	$N_{\text{thin}} = N/10$	$N_{\text{CS}} > 2K_v^{\max}$
SNR for samples	Nominal 30 dB	20 dB	Nominal SNR $\times$ (N_{CS}/N)
Sidelobes	-25 dB	-10 dB	Unassessed, but see Figure 22
Processing Load	Nominal Compute Time=Tc	Tc to Tc/10	> 10 Tc
Search Time	$N_{\text{nominal}} = 1$ s	$> N_{\text{nominal}}/10 = 0.1$ s	$N_{\text{nominal}} \times (N_{\text{CS}}/N)$

- ROC curves (probability of detection vs SNR for a given false alarm rate)

- Search rate

- Sidelobe levels and locations

- Response to excess targets ($> K$)

- Response to excess radial speed targets

- Processing load.

While comprehensive assessment of CS algorithms for pulse-Doppler radar is beyond the scope of the study, we present a limited illustrative example of how such an assessment can be accomplished. We have presented results from Haspert (2012) [25] in the introduction and Bajwa *et al.* (2011) [7] in the previous subsection illustrating three distinctively different approaches to P-RD radar operation: conventional full Nyquist pulse burst, random thinning of the full pulse burst and the system identification CS approach of Bajwa et al. (Here we omit specific results of the gridded CS approach to avoid issues of grid mismatch, but many of our comments about CS apply to this CS approach as well.) Table 1 gives a brief comparison of these methods.

By reducing the number of pulses, both thinning and CS methods decrease search time, reducing transmit power or allowing time to search other regions of

target space, e.g. other azimuth angles. For high SNR, greater than about 30 dB, it is likely that CS can achieve better resolution, especially in time delay than can full Nyquist or thinned-pulse techniques. The *relative disadvantages* of the thinned-pulse burst technique are lower SNR and higher sidelobes, particularly for measuring Doppler shifts. For CS, the *relative disadvantages* are the lower SNR and larger processing load. We were unable to assess the side lobe levels for CS, but note that the sharpness of a peak marking the estimate of time delay or Doppler shift is not an indication of the resolution of the technique as pointed out by Kay and Demeure (1984) [30].

5.7 Summary

As should be apparent from this discussion, not enough work has been done to reach hard conclusions about the role of compressed sensing in P-RD radar. Potential benefits could be large, but the threshold for improvements is very high, owing to highly optimized techniques being used.

5.7.1 Findings

1. Overall, it is likely that CS algorithms can find useful radar applications when the target space is know to be sparse and stable. Before recent CS developments, both radio astronomy and coastal radars demonstrated successful applications of compressed sensing, and similar results should be possible with military radars, under at least some conditions.

2. Thinned conventional P-RD and CS can reduce transmit power, decrease search time, and possibly processing time. This could be a strong advantage for power-limited radars on isolated platforms, such as drones and satellites. In both cases, reduced SNR is the principal disadvantage, which may be severe

for weak targets.

3. CS carries an additional disadvantage, increased processing time. In addition, there are issues about how sparse signals really are, as demonstrated by simulations with off-grid targets.

4. With most results coming from theory or simulations, application of CS to P-RD radar is at a very early stage of development, precluding firm conclusions. These studies, however, show where work is needed to better understand the possibilities.

5. Owing to the significant disadvantages, CS algorithms are likely going to be successful only when targets are sparse. Consequently, CS algorithms should be considered as supplements to optimized techniques developed for difficult targets.

5.7.2   Recommendations

1. Potential benefits warrant further research to determine when CS can benefit military P-RD radars. This work should be closely tied to observations with real systems, which can begin with software modifications rather than designing new hardware.

2. Because sparsity is the central issue in applying CS, development should begin with situations known to be sparse, such as a few aircraft against the sky, and proceed to more complicated situations.

6 SOME ISSUES IN COMPRESSIVE SENSING FOR SAR

6.1 Introduction

Synthetic aperture radar (SAR)[12] is an imaging technology with two main differences from electro-optical and infrared (EO/IR) applications of CS: First, it has to supply its own power, and second, it depends critically on coherent processing and coherent gains of up to 10^9 to get a useful signal-to-noise ratio (SNR). This turns out to mean that certain CS applications exact significant penalties in the signal to noise ratio.

Although both SAR and CS have long histories, the combination of the two is relatively new, and most publications are quite recent (Ender, 2010; Potter *et al.*, 2010) [23, 39] In new applications of CS to SAR, many of the algorithms have long been known and used. There are certainly cases where CS or CS-like algorithms are useful for SAR, and we give some examples. There are also examples of how a SAR can be used with the cooperation of those being illuminated, so as to get some of the advantages of CS without actually having to use CS techniques. We also discuss a 'foveal' SAR that can combine a wide-area ground moving-target indicator (GMTI) having poor resolution of movers with high-resolution SAR imaging of these movers, as long as there are not too many of them. Although this SAR does not explicitly use CS algorithms, it might profit from their introduction.

For purposes of this section, we take it that CS implies that the problem of retrieving a SAR image from the data is underdetermined for some reason, perhaps sub-Nyquist sampling, and that this underdetermination is an essential part of the problem. How well CS works depends on the sparsity of the illuminated SAR scene

---

[12]A SAR is a high-resolution sparse antenna formed in a particular way. There are other ways to do this, for example with multistatic radar, and some of the remarks we make about SAR are also applicable to the multistatic radar array.

and the degree to which CS reduces identification of targets. More work is needed to quantify the sparsity of common SAR scenarios. For example, what is the sparsity of the the tanks shown in Figure 24, and how does it change with image resolution? Many of the algorithms (basis pursuit, matching pursuit, ...) used in CS have a heritage predating CS itself, and so one finds that certain techniques widely-used in CS have been used in different ways in SAR without any reference to the sparsity of the scenes.
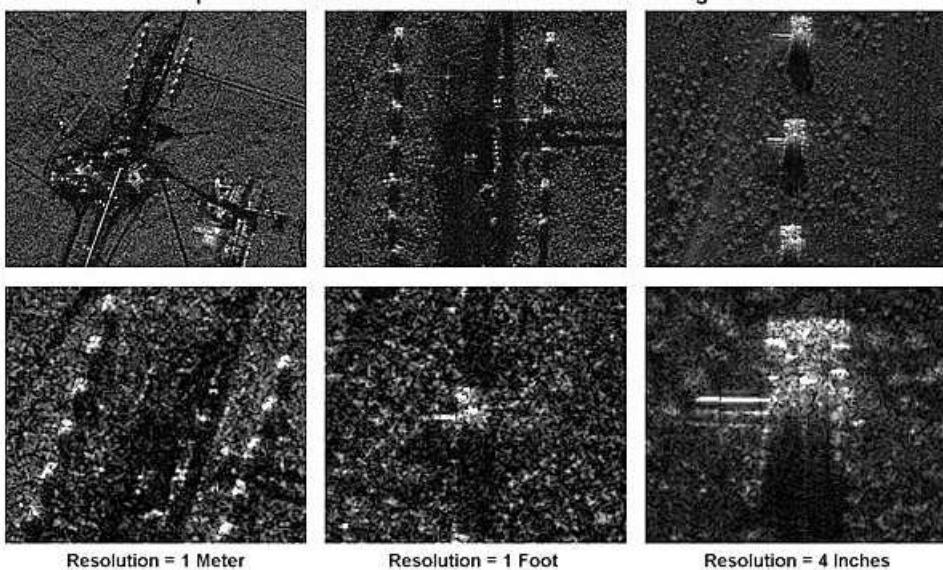
Figure 24: Images from an airborne Lynx SAR posted at http://www.sandia.gov/radar/images/lynx_tanks.jpg in an online library posted by Sandia Natl. Lab. From left to right, images have resolution of 1 m, 1 foot, and 4 inches. Those in the bottom row are 4x enlargements of portions of those in the top row. From left to right, the images show increasing detail of two rows of M-47 tanks.

There are a number of areas in which CS can enable a better SAR, both in hardware and in software. In general, CS software and processing improvements require a more flexible SAR, capable of, for example, putting out essentially arbitrary waveforms and doing a lot of processing onboard. We suggest that the best way to think of the CS-enabled SAR is as a *software-defined SAR* that has this flexibility and processing power built in. A software-defined SAR should be able to apply CS

as an option, and not as a requirement. Consequently it should be built for good SNR with Nyquist-rate sampling.

Some benefits expected from CS come from faster sampling, e.g., A/D converters that extend the physical bandwidth by compressive sampling of sparse signals at a factor of ~ 10 compression (Azita Emami briefing to JASON on 29 June 2012). As with the radar example of the next subsection, there is an SNR penalty in proportion to the subsampling ratio. However, if the sparse signal is known except for a few parameters that characterize it, one might be able to live with this SNR penalty. An example is forming chirped range pulses, where the transmitted waveform is not only sparse but completely known. After compression, the only useful information in the range pulse is its complex amplitude and time of arrival. Suppose that before compression the range pulse is a frequency-hopping signal. It turns out that such locally Fourier sparse (LFS) waveforms are particularly well-adapted to CS techniques for fast broad-band A/D converters used in forming the range pulses. (LFS waveforms are divided into sequences of short time intervals, in each of which the Fourier spectrum is restricted to a narrow band. Which band is active depends on the time interval.) Hardware improvements go along with CS to make a better SAR. One example is the A/D converter mentioned above, and there are doubtless others in the processing chain. Below consider other approaches, such as a 'foveal' SAR and an analog of the single-pixel camera.

To use CS effectively with SAR imagery one has to have a good idea of the expected sparsity. In at least one case, this is fairly apparent, as long as the SAR resolution is not as small as a few radar wavelengths. Man-made targets such as trucks or tanks often appear as if outlined by a series of glint points, a number of points quite a bit smaller than the actual number of pixels needed for the target. So these SAR images are naturally sparse. (In this case, higher resolution is the enemy of sparsity; as the number of pixels in a given target image increases, sparsity decreases as more background glint points appear in the image, e.g., Fig. 24.) Coherent change

detection is another example, where a background scene is imaged on one SAR pass and stored; on another pass (on very nearly the same trajectory) onboard CS processing might enable only the detected changes to be transmitted—a sparse signal compared to the already-known background scene. But there seems to be no general characterization of potential SAR images, except in broad statistical terms. In a later section we argue for wide-ranging sparsity studies whose results might well be couched in the framework of a NIIRS (National Image Interpretation Rating Scale).

There is, however, no free lunch for CS-SAR, and one must be aware of various penalties for using CS with SAR. These could be a poor SNR (unless peak power is significantly increased and duty factor decreased); poor resolution; speckle problems that get worse with undersampling; the need for quite long CS processing times compared to the gold standard of a matched filter; or even failure of CS because the scenes are much denser than the assumed sparsity would suggest. The issue is whether the new combinations of ingredients of CS applied to SAR bring advantages that outweigh the penalties that must necessarily be paid.

On the other hand, there may be occasions when CS applications that use less radar power through subsampling (with a consequent decrease in SNR) may free up the unused radar power for other applications, e.g., enabling search while tracking. This can happen when certain targets would have an SNR large enough to allow for this subsampling.

6.2 Conventional SAR

To begin with, we consider an aircraft- or space-based SAR operating conventionally, which means that the SAR transmits at the Nyquist rate a series of identical chirped range pulses at regular intervals and processes the returns with a matched filter. SAR parameters are defined as:

- P = peak radar power

- R = instantaneous range to target

- h = (constant) height above the ground plane

- v = velocity of SAR relative to ground (we take this velocity along the x-axis)

- λ = radar central wavelength

- B = bandwidth of range pulses

- D = aperture diameter

- PRF = pulse repetition frequency

- T_p = time duration of a pulse

- $R_c = BT_p$ = time-bandwidth product, or pulse compression ratio (for linear FM chirp)

- T_I = coherent processing interval

- σ_0 = average ground reflectivity per unit area

The radar's duty factor DF is given by $DF = (PRF)T_p$, and the average power is $P_{av} = P(PRF)T_p$.

In what follows we ignore various trigonometric factors. The range and azimuth resolutions are:

$$\Delta R = \frac{c}{2B}, \ \Delta x = \frac{\lambda R}{2vT_I}, \tag{6-67}$$

where c is the speed of light. Usually the idea of CS is to compress the data while preserving resolution, in which case these formulas must be obeyed whatever else is done. For conventional SAR operation the radar equation for the signal-to-noise ratio (SNR) is:

$$SNR = P\sigma_0 \Delta x \Delta R \left(\frac{D}{\lambda R}\right)^2 \frac{1}{4\pi R^2} \frac{D^2}{k_B T B}(PRF)\, T_I R_c. \tag{6-68}$$

The factor $(PRF)T_I$ is the total number of range pulses and can be many thousands. *coherent* processing gives this SNR as the gain factor over noise. With standard matched-filter processing at the Nyquist rate one requires that the PRF is at least

95

twice the Doppler bandwidth of about $2v/D$. The number of azimuthal pixels is the illuminated scene width of $\lambda R/D$ divided by Δx which equals $2vT_I/D$, so one easily calculates that $(PRF)T_I$ is at least twice the number of azimuthal pixels for Nyquist or super-Nyquist sampling.

It is crucial to note that if the peak power and resolution are fixed, there is a direct connection between the number of sampled azimuthal pixels and the SNR. Reducing one reduces the other in direct proportion. So it may be that CS can preserve the resolution of Eq.$\widetilde{(6\text{-}67)}$ even with subsampling, but if so it must reduce the SNR, all other parameters being unchanged. *There is no free lunch.*

6.3   Noise Sensitivity

Most CS literature examines noiseless signals, but this is not realistic for radar, particularly SAR, where the combination of under-sampling and noise can be severe. To examine this, Patel *et al.* (2010) [37] under sampled archived SAR data taken in spotlight mode. Under sampling was applied in the cross-range (slow-time) direction in two ways, by randomly omitting received pulses, and by jittering arrival times of full sets of recorded pulses. For an operational SAR, this would correspond to alterations of the pulse repetition frequency (PRF). One set of cases was run with no noise. Measurement noise, n noise was added to the other set as $y = Ax + n$ to produce a signal-to-noise ratio (SNR) of 20 db.

For a given compressibility ratio, M/N, recovery changed very rapidly from 100% success to failure as the sparsity ratio, K/M increased, as shown by the phase transition diagrams in Figure 25. Without noise, $M/N > 0.2$ is needed to begin recovery for minimal sparsity. Jittered under-sampling reduced recovery compared to random under-sampling as M/N tended toward 1, so that K/M did not exceed ≈ 0.4 even at full sampling, i.e. $M/N = 1$. Adding noise produced the largest effect;
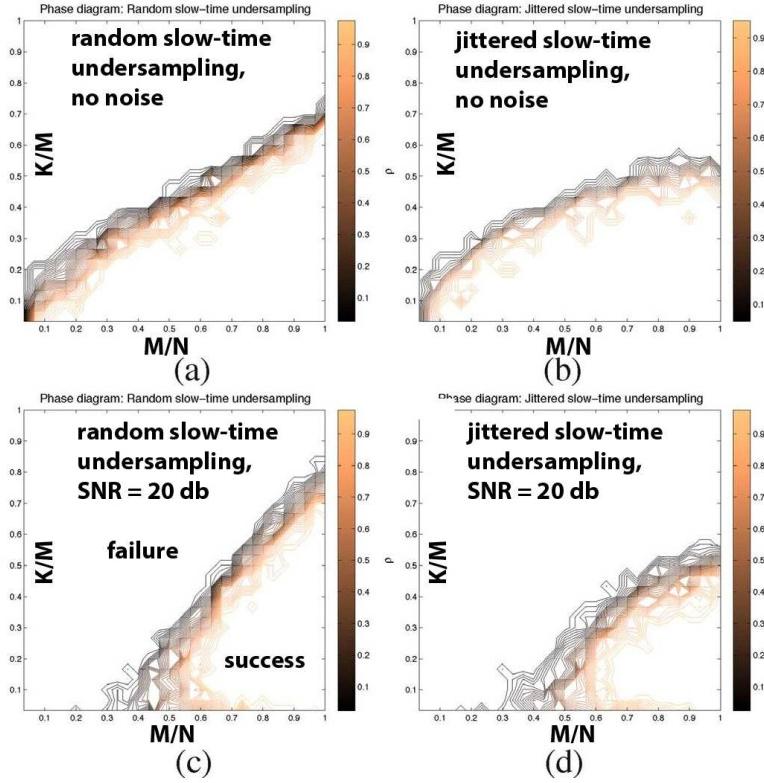
Figure 25: Effect of under-sampling and noise on recovering archived SAR data (adapted from Patel *et al.*(2010) [37]). These phase transition diagrams show recovery success, indicated by the color of the curves, versus the ratio of sparsity, K, to the number of measurements, M on the y-axis and the ratio of M to the dimension of the signal, N, on the x-axis. The curves are colored by the fraction of successful recovery, with full success below and failure above. Images were under sampled either randomly omitting recorded pulses (left column) or by randomly jittering arrival times (right column). Comparing top and bottom rows reveals the effect of noise, specified by a signal-to-noise (SNR) of 20 db.

increasing the minimum M/N to about 0.5, implying that power savings applying CS to SAR are likely to be less than twofold. The impact on jittered slow-time sampling was even greater, reducing the maximum sparsity ratio that could be recovered.

6.4   Toward a Software-defined SAR

A software-defined radar (Deb, 2010) [1] is one that has both hardware and software onboard powerful enough to give the radar extreme flexibility in transmitted waveforms and to do significant signal processing onboard. CS for SAR can be most useful for a radar that is in essence a software-defined radar. (Of course, a software-defined radar can be extremely useful even if true CS is not used with it.) Software-defined radar enables so-called cognitive radar, a radar using intelligent signal processing with feedback from receiver to transmitter, and capable of detection through tracking.

To understand an important point about software-defined radar, we write the radar equation in a different way, assuming that the SAR can transmit an arbitrary waveform within the constraints of the bandwidth and coherent processing interval. By expressing the total energy transmitted in time T_I as:

$$\int_0^{T_I} dt\, P(t) = PT_p \times (PRF)T_I \qquad (6\text{-}69)$$

the radar equation becomes:

$$SNR = \int_0^{T_I} dt\, P(t) \frac{\sigma_0 \Delta x \Delta R D^4}{4\pi \lambda^2 R^4 k_B T}. \qquad (6\text{-}70)$$

We see here that the SNR equation is not really a ratio of powers, but a ratio of energies. The total radiated radar energy is the integral in this equation, and so if it, and the resolution, are held constant one need not necessarily lose SNR by subsampling. But if fewer pulses will be used, then each must be of higher energy to preserve resolution and SNR, and the overall duty factor will decrease. This may not

be effective or even possible with modern radars. One could, of course, sub-sample simply by using a conventional pulse protocol and then throwing away some of the pulses, but this would only be attractive if there is an alternate use for the power that would otherwise be wasted, as we mentioned above. In the foveal radar discussed below sub-sampling is an important factor, but all pulses, gathered at the Nyquist rate, are saved for further adaptive processing.

In this form of the radar equation, an arbitrary power profile in time $P(t)$ can be inserted. What this profile might be depends on circumstances, and not just on the (assumed) sparsity of the scene. For example, a low probability of intercept (LPI radar) might use a pseudo-random profile. The profile has the full bandwidth, B, and will have to be chirp-compressible for full range accuracy; it must also be coded so that returns from different ranges can be distinguished. Of course, the code need not run over the entire timespan T_I; it can repeat after a time interval sufficient to avoid range ambiguity. This interval scales as $2R\lambda/cD$. In conventional radar operation there must be a dead time between pulses so that the returns can be received without interference from the vastly stronger transmissions. It is possible to do this with continuous transmission of power if transmissions are divided into two group, one above the radar center frequency and one below, each with a bandwidth $B/2$. We see that the SNR is directly proportional to the total amount of energy transmitted, whatever the profile. In fact, this form of the radar equation shows that for fixed scene, parameters, and resolution, the only thing at the disposal of the radar is this total amount of energy.

The general conclusion, in the spirit of "There is no free lunch", is that resolution-preserving CS must keep the integrated energy fixed to preserve the SNR. If fewer pulses are used (sub-Nyquist sampling), the energy per pulse must increase proportionately to preserve the SNR. But if resolution can be given up, there are other tradeoffs that could make CS useful. We give an example below.

6.5 A Foveal SAR and its Relation to CS

In the human eye the fovea is a small central area capable of sharp vision, while the rest of the eye takes in a much larger scene but at lower resolution. We describe here a space-based or air-based foveal SAR that capable of simultaneous GMTI and SAR operation;[13] A numerical example will be given for the space-based SAR. The SAR mode is analogous to using the fovea for high-resolution vision.

Usually a wideband GMTI radar can search for movers over a wide area, but it can see them at high resolution only in range (see Eq. (6-67)), with no azimuth resolution. For example, if the needed GMTI azimuthal resolution is 5 m, a conventional X-band GMTI radar in low-earth orbit (LEO) would need a 6 km antenna. In conventional practice, "images" of movers in GMTI are thin arcs hundreds of m or more long. The SAR can produce high-resolution images even of moving targets but has a much smaller search rate.[14]

The foveal radar in GMTI mode makes SAR-like sub-images at coherent processing times, T_G, small compared to the SAR processing time, T_I, such that a mover at ground speed u will shift about one pixel in time T_G. The idea is that the mover will move from one pixel to a contiguous one on successive sub-images, allowing for mover recovery by what amounts to change detection. For the azimuthal coordinate the requirement of about one pixel movement in time T_G leads to:

$$T_G^2 \approx \frac{\lambda R}{2uv}. \tag{6-71}$$

---

[13]The JSTARS radar aircraft has a SAR-like radar that can be used in either SAR or in GMTI mode, but not in both modes simultaneously.

[14]There are other ways for a SAR to capture movers, such as looking for a disconnect between a moving target's image and its shadow, due to the azimuthal translation of a mover in a SAR image. But using the SAR in SAR mode means a small search rate, and even then movers may be blurred because of the long coherent processing time. For SARs on slow-moving, low-altitude aircraft, a mover even at a velocity of a few m/s may, by this azimuthal translation, be shifted out of the Doppler band used for the stationary scene. Then the mover will be revealed on a dark (noise-only) background, although possibly blurred.

(In this section we use the definitions given in the table of Sec. 6.2 and ignore trigonometric factors.) Degrading range resolution is simply done by reducing the bandwidth.

As a strawman, take an X-band space-based SAR at range $R = 1000$ km, moving at velocity $v = 7$ km/s, and searching for movers having speeds $u \sim 2 - 20$ m/s. This leads to processing times of 1.0–0.3 sec and cross-range resolution of 2-7 m (just about right to hold one typical ground mover, such as a tank).

The next step is to compare the GMTI and SAR parameters with the radar sized for good SNR in full SAR mode, as described by Eqs. (6-67,6-68). As an example, take the parameter values (in addition to those already given):

1. P=500 W
2. $\sigma_0 = 0.05$
3. $B = 500$ MHz
4. $D = 5$ m
5. $PRF = 10$ kHz
6. $R_c = 2.5 \times 10^4$
7. $T_I \equiv$ coherent processing time for SAR function $= 5$ s

These parameters yield a SNR of about 20 dB, with range and azimuth resolutions of order 30 cm. Note that T_G is small compared to T_I.

In stripmap mode, this SAR covers an azimuthal strip of about 6 km and has an area rate of about 40 km^2/s, which is not at all good a GMTI. To get reasonable wide-area coverage in GMTI mode, one way is to split the antenna, assumed to be an electronically-scanned array (ESA), into F independent phase centers, where F is a number of order 2 to 10, that cover abutting swaths in azimuth. Each sub-antenna has an azimuthal coverage of $\lambda F R/D$ instead of the usual $\lambda R/D$, and there are F

of them, so the scan width and area search rate are increased by a factor of F^2. For $F = 4$ this increases the area scan rate to 640 km^2/s.

Of course, this leads to a loss of SNR in GMTI mode relative to SAR mode. However, we can recover most or all of this SNR, by observing that in GMTI we would like a degraded range resolution to capture the mover. This is easy to do by reducing the bandwidth by a factor of G, where we need (as will soon be shown) $G > F$. The easiest way to think of the problem is to imagine that we now have F individual radars, each working on a separate frequency band of bandwidth B/G, necessarily less than B/F. For simplicity, assume that each of the separate phase centers receives only in its own frequency band during GMTI operation (this assumption can be relaxed). Then, because each sub-antenna has an aperture in the cross-track direction reduced by a factor of F, the total loss of SNR from division into sub-antennas is a factor of F^3. But because of the increase in ΔR and the decrease in the noise bandwidth, there is a factor of G^2 gained back. In all then,

$$SNR_{GMTI} = \frac{G^2}{F^3} SNR_{SAR}. \tag{6-72}$$

The SNRs in the two modes can be made equal by requiring $G^2 = F^3$; for example, $F = 4$, $G = 8$.

In GMTI mode movers are detected by dynamical imaging, sometimes known as subaperture processing, meaning that the full coherent time T_I is divided into $N = T_I/T_G$ intervals and an image is made for each of these N intervals. The radar makes the first mover detection by coherent differencing of the first two or three subsamples. Differencing removes, at some level, the stationary background, but the mover stands out because it has moved about a pixel between subsamples. This processing gives a crude idea of the mover's velocity and position.[15] This first crude estimate is refined by differencing and processing later subsamples, until finally the

---

[15]Modulo the azimuthal offset due to the mover's velocity; this will not be large for a space-based SAR.

resolution can be improved in principle all the way to the highest SAR resolution the radar allows, because the more subimages that are coherently added the finer the resolution becomes.

How well this all works depends on, among many other things, how well the differencing that removes the stationary background can be done. For example, suppose the GMTI pixel is 7 m by 7 m, and the moving target radar cross-section is 1 m^2. At $\sigma_0 = 0.05$, the background scene has a cross-section of 2.5 m^2; if differencing can cancel the background to the 5% level, or 0.13 m^2, the mover (which has gone from one pixel to another) will be about 10 dB stronger than the differenced background.

The foveal SAR certainly needs to be a software-defined cognitive radar, since it does adaptive dynamic imaging. It will have a heavy processing load and might well make good use of sophisticated CS techniques. The resemblance of the foveal approach to CS is fairly clear, and could possibly be considerably improved by CS experts. Here one sacrifices resolution initially, saving radar resources, but ultimately applies the full power of SAR imaging to the movers.

6.6   CS without CS

There are several circumstances where techniques different from those of conventional CS could be used to enhance CS or could be very detrimental to the applications of CS. We mention a few:

1. **Power management:** Some space-based and even aircraft-based radars and SARs are, in a sense, power-limited. They need a certain power to reach a certain SNR (with Nyquist-compliant transmissions), but they may only be able to use this power for a relatively small fraction of the time. A space-based SAR, for example, may be able to make good Nyquist-rate images for 10% of its

orbit, using the rest of the orbit to recharge its batteries through solar panels. A software-defined radar could save on power, in principle, by sparsifying the number of pulses it transmits so as to preserve Doppler resolution when it flies over scenes of (approximately) known sparsity, using power at the Nyquist rate only when the scene structure or importance of capturing full data warrant. Similarly, it could be possible to save on power during the chirp compression of range pulses, using chirp signals of the full bandwidth needed for range resolution but sparsifying with the help of code sequences that do better than linear FM chirp on bandwidth. A factor of two saving in transmit power will pay several times over for the extra processing power needed onboard.

2. **Downlink mitigation:** Reducing the downlink bandwidth necessary for image transmission is often cited as an advantage for CS with SARs, which are prodigious producers of bits, perhaps gigabits per image. But there are other ways to handle this problem. A SAR always has the capability to transmit its images to a distant receiver at least at the rate at which it accumulates images, using the full bandwidth of its T/X antenna, and CS could lead to useful compression of these images and savings in bandwidth or time or both. A high-resolution (~ 10—20 cm or even better) SAR has a bandwidth of a GHz or more, and it is a relatively small penalty to use some part of this bandwidth to transmit received SAR data directly from the SAR rather than on a low-rate downlink.

3. **Cooperative CS for radar:** A previous JASON report (Brenner *et al.*, 2008) [12] deals with the problem that some FAA or military radars whose lines of sight overlook wind turbine farms are seriously impacted by the moving turbine blades. The report suggests that the wind turbines be equipped with simple equipment to sense the turbine blades' instantaneous position, angular speed, pitch angle, and axis of rotation. These relatively few bits of information would be sent to the affected radar, which could generate a model image of

the turbine and coherently subtract it from the radar returns. This method requires a certain amount of processing power on the radar.

4. **Cooperative sparsity:** In certain circumstances a SAR will need to communicate with friendly ground forces. There are measures available to be carried out by the ground forces that amount to CS for such cooperative transmissions.

5. **Autofocus and phase retrieval:** Arguing that standard autofocus techniques are degraded by sparse sampling in SAR, Kel (2012) [2] propose what they claim is a better method. For certain SAR image types, there are algorithms (Dyson, 1992) [22] that average over nearby range bins to recover slow-time phases with only two or three iterations. The fact that the method converges so rapidly and successfully for certain images suggests that these images are in fact quite sparse and that CS algorithms can be very successful. Further work might suggest a quantitative connection between sparsity and recovery of slow-time phases.

6. **Coherent countermeasures:** DRFM (Digital Radio Frequency Memory) techniques are widely known. A red force asset, desiring to thwart detection by blue forces, receives the blue SAR output, digitizes it, and stores it in a buffer (short-term memory). The blue signal is then re-transmitted by the red target with a time delay that offsets the target in azimuth. For further confusion the re-transmitted signal can be modified. Studies need to be made of what would be needed for a DRFM to thwart a blue radar known to be using CS; in particular, to determine whether specific CS SAR algorithms are unusually sensitive to DRFM techniques.

6.7   Summary

6.7.1   Findings

Our findings include not only what emerges from the above detailed considerations but also several issues not discussed in detail, yet certainly worthy of intensive consideration, such as speckle and the need to quantify sparsity of various SAR images.

1. **CS, resolution, and SNR:** Without major changes to the radar pulse and power protocols, resolution-preserving sparse sampling means loss of SNR. This loss can be made up with additional peak power at a lower duty factor, provided that the required changes are not too large, or with degraded resolution in proportion to the sampling compression. Most CS-SAR examples are worked with an undersampling ratio (usually called δ) of 1/2 or so (see, for example, Potter *et al.* (2010) [39]), requiring a power increase by a factor of $1/\delta \approx 2$ to preserve SNR at a fixed resolution.

2. **Sub-sampling and sidelobes:** Sparse antennas generate sidelobes, as does sparse sampling and reconstruction. How small the sidelobes are depends on the cleverness of the algorithm used for the point-spread function. One can do better than standard sinc functions, for example, by using Alltop sequences (Alltop, 1980) [5], essentially quadratic chirp functions; these are highly-incoherent, a desirable property of the atoms of a CS dictionary (Herman and Strohmer, 2009) [27].

3. **Sub-sampling algorithms especially useful for SAR:** SAR can compress ranges pulses with a variety of algorithms. Particular A/D and D/A algorithms can work very well indeed on well-chosen chirp protocols, such as chirp pulses that are locally Fourier sparse, in this case frequency-hopping with the frequency fixed for a short period of time. Such CS sub-sampling algorithms

106

run at much less time (and less power) than conventional Nyquist-sampling A/D technology (Pfetsch *et al.*, 2008) [38]. This can be a first-order enabler for broadband SAR.

4. **Processing loads:** These vary greatly with the algorithms employed. One paper compares matching pursuit and basis pursuit algorithms (Tropp and Gilbert, 2007a) [49], observing that an orthogonal matching pursuit algorithm took a processing time of order $NK^2 \ln(N/K)$ for sparsity K in an N-dimensional signal, but an ℓ_1-minimization algorithm took more than 10 times longer. Neither CS algorithm was nearly as fast as a simple threshholding algorithm, but both were much more successful in recovering sparse signals with sparse measurements. The empirical observation of Baron *et al.* (2005) [9] is that the processing load for "good" CS algorithms varies as $N \log_2(1 + (N/K))$ for an N-pixel scene of sparsity K. We were told by CS/radar workers who should know that as a rule of thumb for CS processing with which they were familiar, this CS processing used about an order of magnitude more flops than standard matched-filter processing would need for a given scene. But things could be much worse, since it could take as many as 10^3 iterations to make a particular algorithm converge at a desired accuracy. A SAR operating conventionally can generate gigabits of data for a single scene at high resolution, and it may take 100 or perhaps a great deal more flops per bit to deal with the data.

5. **Speckle:** Speckle arises when a pixel of a coherently-illuminated target is rough on the wavelength scale so that when the target image is processed coherently interference causes random variations in brightness from pixel to pixel. It is particularly serious for SAR because it is *multiplicative* noise, not additive. Over the decades, radar workers have used numerous methods to mitigate speckle, the simplest of which is to take a number of images of the same scene and average them. The higher the resolution the less the speckle, which works

in the wrong direction for many CS applications where the resolution may have to be reduced to save transmit power. In CS, some workers (Patel *et al.*, 2010) [37] have found success in reducing speckle by including a total variation (TV) penalty to the CS cost function. (The TV of a function is essentially a measure of how rapidly the function varies; usually, TV is defined as $||\nabla x||_1$). We do not know whether such CS methods are better than multi-look or other traditional means of beating down speckle.

6. **Understanding sparsity:** The briefings and articles available to JASON during the Summer Study did not make us comfortable that generic SAR images are necessarily very sparse, easy to quantify, or straightforward to exploit. There are exceptions to this: Identifying a man-made target, such as a truck, may make good use of CS because the actual image is a small number of glint points. An algorithm proposed in Dyson (1992) [22], and related algorithms by others, show that for certain SAR imagery it is possible to make an excellent high-resolution reconstruction even though the slow-time phases are, for some reason, unknown.

7. **CS for real-world radar:** In this early stage, most applications of CS to radar use post-processing on data acquired quite conventionally. It will be critical to know how each CS application affects the real-world performance of a radar using specific CS-like techniques, and in particular how it changes the receiver operating characteristic (ROC) curve (giving the probability of detection v. the probability of false alarm). Possible benefits include power-saving (in most cases, at the cost of poorer SNR); getting higher bandwidth performance for A/D converters in specific applications, such as compressing SAR range pulses; and using smaller downlink bandwidths for SAR signals. The greatest potential for benefits will come from software-defined radar.

6.7.2 Recommendations

1. **CS should be an option, not a requirement:** Future SARs should be software-defined (thus ready for a wide range of CS options) and built for their highest and best use (matched filter; Nyquist sampling), but ready to operate optionally in a CS mode when the penalties such as lowered SNR are acceptable.

2. **Specific uses of CS-SAR:** Several aspects of CS seem promising for developing to enhance SAR:

   (a) Applying known CS algorithms to construct hardware for broadband A/D converters that can be used with compressed SAR range pulses,

   (b) Compressing sparse glint-point images of manmade targets,

   (c) Recovering phases using the algorithm proposed in Dyson (1992) [22], and

   (d) Characterizing applications where loss of SNR through CS can be tolerated.

3. **Quantifying sparsity:** a study of the sparsity of various SAR scenes, based on specific imagery and not just on statistics, to be summarized as a new kind of NIIRS (National Image Interpretability Rating Scale) that quantifies the sparsity and the sparse recoverability of these specific targets. A NIIRS assigns a number characterizing the interpretability of a specific target at various scales, *e. g.*, an aircraft; its make and model;...; the rivets on the wings. This CS NIIRS scale would acknowledge that for radar the sparsity of a target image changes with the number of pixels in the target image.

4. **CS-SAR countermeasures:** CS-SAR has specific vulnerabilities that must be studied, including vulnerabilities from lowered SNR. We recommend an electronic warfare program study of how coherent SAR jammers, such as DRFMs,

can be enhanced to exploit the vulnerabilities associated with sub-sampling and loss of processing gain that might come from use of CS-SAR.

5. **CS without CS:** We recommend a study on CS alternatives leading to results comparable to those that would be achieved by CS, in particular for cooperative communications and interference mitigation.

7 SUMMARY

During the last decade, rapid advances from applied mathematics in the reconstruction of sparse signals have produced intense efforts to apply these techniques to reduce data sampling to the minimum needed for particular applications. Most commonly termed Sparse Sensing (CS), these endeavors have deep roots in some fields, particularly radio astronomy and coastal radar, but how profoundly DoD systems will be affected is not yet clear. Some early claims seem extravagant, but, nonetheless, both DoD's needs and the potential benefits of CS are so large that these issues must be resolved as soon as practical. To aid DoD's efforts, below, we repeat our principal findings and recommendations from the Executive Summary and also include ones from report sections that are not included in the principal results.

7.1 Principal Findings

1. In general, the sparsity or compressibility of scenes of interest to the DoD is not well studied. The CS literature often deals with idealized situations, e.g., a few bright objects against a dark background. Many scenes, however, have lesser contrasts, and it is not clear what fraction can be treated as sparse versus compressible.

2. The CS literature provides quantitative performance guarantees for a variety of sparse reconstruction techniques, stated in terms of the minimum number of data samples that are needed for successful reconstruction and the magnitude of the reconstruction errors. In addition, there has also been much practical work on the development of faster, more reliable reconstruction algorithms. Both the philosophy and specific algorithms are likely to benefit many DoD programs, warranting reexamination of older deconvolution approaches as well as incorporation into new projects.

3. Compressive sensing is not a 'free lunch' but always involves a tradeoff; reduced data may save measurement resources, but it also means a lower signal-to-noise ratio (SNR) and possibly other artifacts, such as side lobes or false alarms. Less mature than sparse reconstruction, compressive sensing research is looking for 'sweet spots' where tradeoffs enable measurements that could not be made otherwise.

4. The single-pixel camera (Duarte *et al.*, 2008) [21] trades signal-to-noise ratio (SNR) and sampling speed for cost, using a single, high-quality sensor in lieu of a more expensive focal plane array (FPA). Commercial infrared single-pixel cameras are being developed, but to date there is no independent evaluation to understand the tradeoffs that are being made.

5. Compressed sensing may be an attractive option for small remote systems with limited power and bandwidth, e.g., satellites, drones, and unmanned underwater vehicles (UUVs). Investigation of radar applications is at an early stage, and to date most studies are academic analyses of idealized cases that may not apply to DoD.

6. As an additional tradeoff factor, compressed sensing may increase flexibility in designing and operating radars, but other traditional approaches should also be investigated. In many cases, CS will be most effective as an option rather than a requirement.

7. CS research is fully international and could influence design and operation of systems by potential adversaries.

7.2 Secondary Findings

1. Overall, it is likely that CS algorithms can find useful radar applications when the target space is known to be sparse and stable. Before recent CS developments, both radio astronomy and coastal radars demonstrated successful

applications of compressed sensing, and similar results should be possible with military radars, under at least some conditions.

2. Thinned conventional P-RD and CS can reduce transmit power, decrease search time, and possibly processing time. This could be a strong advantage for power-limited radars on isolated platforms, such as drones and satellites. In both cases, reduced SNR is the principal disadvantage, which may be severe for weak targets.

3. CS carries an additional disadvantage, increased processing time. In addition, there are issues about how sparse signals really are, as demonstrated by simulations with off-grid targets.

4. With most results coming from theory or simulations, application of CS to P-RD radar is at a very early stage of development, precluding firm conclusions. These studies, however, where work is needed to better understand the possibilities.

5. Owing to the significant disadvantages, CS algorithms are likely going to be successful only when targets are sparse. Consequently, CS algorithms should be considered as supplements to optimized techniques developed for difficult targets.

6. Without major changes to the radar pulse and power protocols, resolution-preserving sparse sampling means loss of SNR in proportion. This loss can be made up with additional peak power at a lower duty factor, provided that the required changes are not too large, or with degraded resolution in proportion to the sampling compression. Most CS-SAR examples are worked with an undersampling ratio (usually called δ) of $1/2$ or so (see, for example, Potter *et al.* (2010) [39]), requiring a power increase by a factor of $1/\delta \approx 2$ to preserve SNR at a fixed resolution.

7. Sparse antennas generate sidelobes, as do sparse sampling and reconstruction. How small the sidelobes are depends on the cleverness of the algorithm used for the point-spread function. One can do better than standard sinc functions, for example, by using Alltop sequences (Alltop, 1980) [5], essentially quadratic chirp functions; these are highly-incoherent, a desirable property of the atoms of a CS dictionary (Herman and Strohmer, 2009) [27].

8. SAR can compress ranges pulses with a variety of algorithms. Particular A/D and D/A algorithms can work very well indeed on well-chosen chirp protocols, such as chirp pulses that are locally Fourier sparse, in this case frequency-hopping with the frequency fixed for a short period of time. Such CS sub-sampling algorithms run at much less time (and less power) than conventional Nyquist-sampling A/D technology (Pfetsch *et al.*, 2008) [38]. This can be a first-order enabler for broadband SAR.

9. Processing loads vary greatly with the algorithms employed. One paper compares matching pursuit and basis pursuit algorithms (Tropp and Gilbert, 2007A) [49], observing that an orthogonal matching pursuit algorithm took a processing time of order $NK^2 \ln(N/K)$ for sparsity K in an N-dimensional signal, but an ℓ_1-minimization algorithm took more than 10 times longer. Neither CS algorithm was nearly as fast as a simple threshholding algorithm, but both were much more successful in recovering sparse signals with sparse measurements. The empirical observation of Baron *et al.* (2005) [9] is that the processing load for "good" CS algorithms varies as $N \log_2(1 + (N/K))$ for an N-pixel scene of sparsity K. We were told by CS/radar workers who should know that as a rule of thumb for CS processing with which they were familiar, this CS processing used about an order of magnitude more flops than standard matched-filter processing would need for a given scene. But things could be much worse, since it could take as many as 10^3 iterations to make a particular algorithm converge at a desired accuracy. A SAR operating conventionally can generate gigabits

of data for a single scene at high resolution, and it may take 100 or perhaps a great deal more flops per bit to deal with the data.

10. Speckle arises when a pixel of a coherently-illuminated target is rough on the wavelength scale so that when the target image is processed coherently interference causes random variations in brightness from pixel to pixel. It is particularly serious for SAR because it is *multiplicative* noise, not additive. Over the decades, radar workers have used numerous methods to mitigate speckle, the simplest of which is to take a number of images of the same scene and average them. The higher the resolution the less the speckle, which works in the wrong direction for many CS applications where the resolution may have to be reduced to save transmit power. In CS, some workers (Patel *et al.*, 2010) [37] have found success in reducing speckle by including a total variation (TV) penalty to the CS cost function. (The TV of a function is essentially a measure of how rapidly the function varies; usually, TV is defined as $||\nabla x||_1$). We do not know whether such CS methods are better than multi-look or other traditional means of beating down speckle.

11. The briefings and articles available to JASON during the Summer Study did not make us comfortable that generic SAR images are necessarily very sparse, easy to quantify, or straightforward to exploit. There are exceptions to this: Identifying a man-made target, such as a truck, may make good use of CS because the actual image is a small number of glint points. An algorithm proposed in Dyson (1992) [22], and related algorithms by others, show that for certain SAR imagery it is possible to make an excellent high-resolution reconstruction even though the slow-time phases are, for some reason, unknown.

12. In this early stage, most applications of CS to radar use post-processing on data acquired quite conventionally. It will be critical to know how each CS application affects the real-world performance of a radar using specific CS-like techniques, and in particular how it changes the receiver operating charac-

teristic (ROC) curve (giving the probability of detection v. the probability of false alarm). Possible benefits include power-saving (in most cases, at the cost of poorer SNR); getting higher bandwidth performance for A/D converters in specific applications, such as compressing SAR range pulses; and using smaller downlink bandwidths for SAR signals. The greatest potential for benefits will come from software-defined radar.

7.3 Principal Recommendations

1. DoD can and should play a major role in exploring where and how compressed sensing can be applied, particularly to radar and optical systems. These efforts should include applying new sparse reconstruction algorithms to old deconvolution problems as well exploring new systems.

2. To find where and how CS can benefit DoD radar applications, DoD should develop a strongly guided program of 6.1/6.2 research to:

   - Develop a sparsity library for important types of targets

   - Quantify how CS degrades target identification through Receiver Operating Characteristic (ROC) curves

   - Create performance metrics for evaluating reconstructed signals

   - Develop operational experience with CS-radar with test beds on different types of radars

   - Perform regular reviews and provide guidance from people experienced in military radars

3. If attractive CS radar applications are found, they should be developed in conjunction with software-defined, cognitive radars to provide the needed flexibility in choosing when and how sparse illumination is used.

4. Although this is not necessarily an example of compressed sensing, DoD should consider consolidating GMTI (Ground moving target indicator) and SAR (Synthetic aperture radar) functions in a 'Foveal Radar' that subdivides the coherent processing interval to obtain coarse identification of movers and then switches to full SAR for high-resolution images. Pulses are not skipped in this mode; nor is resolution compromised in the final images.

5. The use of compressed sensing for visible or infrared imaging, as in the single-pixel camera, involves tradeoffs between cost, sensitivity, resolution, and speed. When commercial models of such cameras become available, we recommend than an independent investigator be tasked to evaluate these devices to assess these tradeoffs. In addition to assessing the utility of these devices for DoD, the information will be useful as a case study of pluses and minuses of compressed sensing.

7.4 Secondary Recommendations

1. Potential benefits warrant further research to determine when CS can benefit military P-RD radars. This work should be closely tied to observations with real systems, which can begin with software modifications rather than designing new hardware.

2. Because sparsity is the central issue in applying CS, development should begin with situations known to be sparse, such as a few aircraft against the sky, and proceed to more complicated situations.

3. **CS should be an option, not a requirement:** Future SARs should be software-defined (thus ready for a wide range of CS options) and built for their highest and best use (matched filter; Nyquist sampling), but ready to operate optionally in a CS mode when the penalties such as lowered SNR are acceptable.

117

4. **Specific uses of CS-SAR:** Several aspects of CS seem promising for developing to enhance SAR:

   (a) Applying known CS algorithms to construct hardware for broadband A/D converters that can be used with compressed SAR range pulses,

   (b) Compressing sparse glint-point images of manmade targets,

   (c) Recovering phases using the algorithm proposed in Dyson (1992) [22], and

   (d) Characterizing applications where loss of SNR through CS can be tolerated.

5. **Quantifying sparsity:** a study of the sparsity of various SAR scenes, based on specific imagery and not just on statistics, to be summarized as a new kind of NIIRS (National Image Interpretability Rating Scale) that quantifies the sparsity and the sparse recoverability of these specific targets. A NIIRS assigns a number characterizing the interpretability of a specific target at various scales, *e. g.*, an aircraft; its make and model;...; the rivets on the wings. This CS NIIRS scale would acknowledge that for radar the sparsity of a target image changes with the number of pixels in the target image.

6. **CS-SAR countermeasures:** CS-SAR has specific vulnerabilities that must be studied, including vulnerabilities from lowered SNR. We recommend an electronic warfare program study of how coherent SAR jammers, such as DRFMs, can be enhanced to exploit the vulnerabilities associated with sub-sampling and loss of processing gain that might come from use of CS-SAR.

7. **CS without CS:** We recommend a study on CS alternatives leading to results comparable to those that would be achieved by CS, in particular for cooperative communications and interference mitigation.

References

[1] (2010). *Software defined RADAR a state of the art*, volume Cognitive Information Proc. (CIP), 2010 2nd Intl. Workshop on, 14-16 June 2010. IEEE.

[2] (2012). *Auto-focus for compressively sampled SAR*, volume First International Workshop on Compressed Sensing Applied to Radar, Bonn, Germany, May 2012.

[3] Abrial, P., Moudden, Y., Starck, J.-L., Fadili, J., Delabrouille, J., and Nguyen, M. (2008). CMB data analysis and sparsity. *arXiv:0804.1295v1 [astro-ph]*.

[4] Ackaya, M. and Tarokh, V. (2007). On sparsity, redundancy and quality of frame representation. In *Proc. IEEE International Symposium on Information Theory*, pages 951–955.

[5] Alltop, W. (1980). Complex sequences with low periodic correlations. *IEEE Trans. Inform. Theory*, **26**(3), 350–354.

[6] Arias-Castro, E. and Eldar, Y. (2011). Noise folding in compressed sensing. *IEEE Sig. Proc. Lettr.*, **18**(8), 478–481.

[7] Bajwa, W., Gedalyahu, K., and Eldar, Y. (2011). Identification of parameteric underspread linear systems and super-resolution radar. *IEEE Trans. on Signal Proc.*, **59**(6), 2548–2561.

[8] Baraniuk, R. and Steeghs, P. (2007). Compressive radar imaging. *IEEE Radar Conf., Waltham, Mass., April 2007*.

[9] Baron, D., M.B.Wakin, Duarte, M., Sarvotham, S., and Baraniuk, R. (2005). Distributed compressed sensing of jointly sparse signals. Technical report.

[10] Beck, A. and Teboulle, M. (2009). A fast iterative shrinkage-thresholding algorithm for linear inverse problems. *SIAM J. Imaging Sciences*, **2**(1), 183–202.

[11] Bhatnagar, S. (2006). Presentation at the 10th synthesis imaging workshop, Albuquerque, NM.

[12] Brenner, M., Cornwall, M., Dyson, F., Eardley, D., Horowitz, P., Long, D., Sullivan, J., Vesecky, J., Weinberger, P., and Cazares, S. (2008). Wind farms and radar. Technical Report JSR-08-126, JASON.

[13] Burq, N., Dyatlov, S., Ward, R., and Zworski, M. (2011). Weighted eigenfunction estimates with applications to compressed sensing. *arXiv:01111.2383v1 [math.NA]*.

[14] Candés, E. and Wakin, M. (2008). An introduction to compressive sampling. *IEEE Sig. Proc. Mag.*, **21**(3), 21–30.

[15] Candés, E., Rombert, J., and Tao, T. (2006). Robust uncertainty principles: Exact signal reconstruction from highly incomplete frequency information. *IEEE Trans. Inform. Theory*, **52**(2), 489–509.

[16] Candes, E. J. and Wakin, M. B. (2008). An Introduction To Compressive Sampling. *IEEE Signal Processing Magazine*, **25**, 21–30.

[17] Chi, Y., Scharf, L., Pezeshki, A., and Calderbank, A. (2011). Sensitivity to basis mismatch in compressed sensing. *IEEE Trans. on Signal Proc.*, **59**(5).

[18] Davenport, M., Duarte, M., Eldar, Y., and Kutyniok, G. (2012). Introduction to compressed sensing. In Y. Eldar and G. Kutyniok, editors, *Compressed sensing*, chapter 1, pages 1–64. Cambridge Univ. Press.

[19] Donoho, D. (2006a). Compressed sensing. *IEEE Trans. Inform. Theory*, **52**(4), 1289–1306.

[20] Donoho, D. (2006b). For most large underdetermined systems of linear equations, the minimal l_1 norm solution is also the sparsest solution. *Comm. Pure Appl. Math.*, **59**(6), 797–829.

[21] Duarte, M., Davenport, M., Takhar, D., Laska, J., Sun, T., Kelly, K., and Baraniuk, R. (2008). Single-pixel imaging via compressive sampling. *IEEE Sig. Proc. Mag.*, **25**(2), 83–91.

[22] Dyson, F. e. a. (1992). Recovery of SAR images with one dimension of unknown phases. Technical Report JSR-91-175, JASON.

[23] Ender, J. (2010). On compressive sensing applied to radar. *Signal Proc.*, **90**, 1402–1411.

[24] Gedalhayu, K. and Eldar, Y. (2010). Time delay estimation from low rate samples: the union of subspaces approach. *IEEE TRANSACTIONS ON SIGNAL PROCESSING*, **58**(6), 3017–3031.

[25] Haspert, K. (2012). OSD perspective on JASON investigations of compressive sensing (cs). Briefing to JASON.

[26] Hazard, C., Shimmins, A. J., and Mackey, M. B. (1963). Investigation of radio source 3C 273 by method of lunar occultations. *Nature*, **197**(487), 1037.

[27] Herman, M. and Strohmer, T. (2009). High-resolution radar via compressed sensing. *IEEE Trans. Signal Processing*, **57**(6), 2275–2284.

[28] Högbom, J. A. (1974). Aperture Synthesis with a Non-Regular Distribution of Interferometer Baselines. *Astron. and Astrophys. Suppl.*, **15**, 417.

[29] Hua, Y. and Sakar, T. (1990). Matrix pencil method for estimating parameters of exponentially damped/on damn sinusoids in noise. *IEEE Trans. Acoust. Speech, Sig. Proc.*, **38**(5), 814–824.

[30] Kay, S. and Demeure, C. (1984). The high resolution spectrum estimator: A subjective entity. *Proc. of the IEEE*, **72**, 1815–1816.

[31] Kellerman, K. I. and Moran, J. M. (2001). The development of high-resolution imaging in radio astronomy. *Annu. Rev. Astron. Astrophys.*, **39**, 457–509.

[32] Kim, J., Lee, O., and Ye, J. (2012). Compressive MUSIC: Revisiting the link between compressive sensing and array signal processing. *IEEE Trans. Inform. Theory*, **58**, 278–301.

[33] Krim, H. and Vigberg, M. (1996). Two decades of array signal processing research: the parametric approach. *IEEE Sig. Proc. Mag.*, **13**(4), 67–94.

[34] Li, F., Cornwell, T. J., and de Hoog, F. (2011). The application of compressive sampling to radio astronomy I. Deconvolution. *Astron. and Astrophys.*, **528**, A31.

[35] Norton, N., Williams, N., Williams, H., Spurlock, G., and Kirov, G. (2002). Universal robust highly quantitative SNP allele frequence measurements in DNA pools. *Human Genetics*, **110**(5), 471–478.

[36] Parker, J., Ferrara, M., and Potter, L. (2012). Radar applications of sparse reconstruction and compressed sensing. In W. Melvin, editor, *Principles of Modern Radar*, volume 2, chapter 6. SciTech.

[37] Patel, V., Easley, G., Jr., D. H., and Chellappa, R. (2010). Compressed synthetic aperature radar. *IEEE J. Selected Topics in Signal Proc.*, **4**(244-254).

[38] Pfetsch, S., Ragheb, T., Laska, J., Nejati, H., Gilbert, A., Strauss, M., Baraniuk, R., and Massoud, Y. (2008). On the feasililily of hardware implementation of sub-Nyquist random-sampling based analog-to-information conversion. *IEEE Intl. Symp. Circuits and Systems*, pages 1480–1483.

[39] Potter, L., Ertin, E., Parker, J., and Çetin, M. (2010). Sparsity and compressed sensing in radar imaging. *Proc. of the IEEE*, **98**.

[40] Prabhu, H. and Pe'er, I. (2009). Overlapping pools for high-throughput targeted resequencing. *Genome Res.*, **19**(7), 12541261.

[41] Raginsky, M., Willett, R., Harmany, Z., and Marcia, R. (2010). Compressed sensing performance bounds under Poisson noise. *IEEE Trans. on Signal Proc.*, **58**, 3990–4002.

[42] Rauhut, H. and Ward, R. (2011). Sparse recovery for spherical harmonic expansions. In *Proc. SampTA*.

[43] Roy, R. and Kailath, T. (1989). ESPIRIT = estimation of signal parameters via rotational invariance techniques. *IEEE Trans. Acoust. Speech, Sig. Proc.*, **37**(7).

[44] Scharf, L. (1991). *Statistical Signal Processing*. Addison-Wesley, Reading, MA.

[45] Schmidt, M. (1963). 3c 273 - a star-like object with large red-shift. *Nature*, **197**(487), 1040.

[46] Schmidt, R. (1986). Multiple emitter location and signal parameter estimation. *IEEE Trans. Antennas & Propagat.*, **SP**(34), 276–280.

[47] Shental, N., Amir, A., and Zuk, O. (2010). Identification of rare alleles and their carriers using compressed sensing. *Nucl. Acids Res.*, **38**(19).

[48] Skolnik, M. (2008). *Radar Handbook*. McGraw-Hill, 3rd edition.

[49] Tropp, J. and Gilbert, A. (2007a). Signal recovery from random measurements via orthogonal matching pursuit. *IEEE Trans. Inform. Theory*, **53**(12), 4655–4666.

[50] Tropp, J. and Gilbert, A. (2007b). Signal recovery from random measurements via orthogonal matching pursuit: The Gaussian case. Technical Report 2007-01, Appl. and Comput. Math, Calif. Inst. Tech.

[51] Tropp, J. A. and Wright, S. J. (2010). Computational Methods for Sparse Solution of Linear Inverse Problems. *Proc. of the IEEE*, **98**(6), 948–958.

[52] Wilner, D. (2012). Presentation at the 13th Synthesis Imaging Workshop, Socorro, NM.